FOIA Number: 2012-0769-F

# FOIA MARKER

**This is not a textual record. This is used as an administrative marker by the William J. Clinton Presidential Library Staff.**

---

**Collection/Record Group:** Clinton Presidential Records

**Subgroup/Office of Origin:** Council on Environmental Quality

**Series/Staff Member:** Kathleen (Katie) McGinty

**Subseries:**

---

**OA/ID Number:** 2896

**FolderID:**

---

**Folder Title:**
Clouds

| Stack: | Row: | Section: | Shelf: | Position: |
|---|---|---|---|---|
| S | 61 | 6 | 3 | 2 |

File - Richard Lindzen file w/ Cloud heating [illegible]

**UNITED STATES DEPARTMENT OF COMMERCE**
**National Oceanic and Atmospheric Administration/ERL**
GEOPHYSICAL FLUID DYNAMICS LABORATORY
Princeton University
Forrestal Campus, US Route 1
Post Office Box 308
Princeton, New Jersey 08542

PHONE: FTS: 298-6502
FAX: 298-5070
COMM: 609-452-6502
FAX: 609-987-5070

November 14, 1991 R/E/GF

Ms. Katie McGinty
U.S. Senate
SR 393 Russell Building
Washington, DC 20510

Dear Katie,

This is in response to your request for input on Dick Lindzen's letter to the New York Times. I can certainly understand why he is upset that he was characterized as having "withdrawn the complex hypothesis that was an important element of his skepticism". Since the "Gore Hearing" both Syukuro Manabe and I have had public encounters with him (Manabe in Italy and myself at the House Science Subcommittee Hearing the following day) that offered no indication that he had changed any views whatsoever.

Concerning the content of Lindzen's letter: His first paragraph makes it clear that he is searching for <u>any</u> negative feedback that is currently not well characterized in today's models. That, by itself is perfectly reasonable. What is disturbing is his nearly theological assertion that these magic feedbacks will be discoverd if only we are clever enough to find them. Unfortunately, that is a fundamentally unscientific assertion which seems to be offered in the name of science.

Concerning the 4 points of his testimony in paragraph 2:

1. The models do indeed all show a large positive feedbackdue to water vapor. A number of observational studies are now quite consistent with that result. Oddly, if Lindzen were making "defense lawyers" choices of things to attack the credibility of models, he would look a lot less foolish to his scientific peers if he had chosen clouds, rather than water vapor for his "magic negative feedback" mechanism. That is well known to be more difficult to refute.

2. Such models do not depend crucially upon behavior of water vapor in the 6-16 km region. The largest effect is well-known to be the total water vapor in the atmospheric column. Roughly 99% of that water vapor is below 6 km. Significantly, the atmospheric data show persistent moistening of the 5-10 km region when convective systems are present and in the warmer times of the year. If these facts had gone the other way, the water vapor part of his hypothesis would have been credible, even though its impact on the total greenhouse opacity would be far less than he asserts.

3. It is true that current models do commit computational errors that are locally troubling. My own model is the result of considerable effort to reduce those errors substantially. I see no evidence that correction of such errors has any reasonable possibility of changing the model sensitivity to water vapor feedback in any significant way.

4. I agree with him completely that we do not adequately know the physical processes whch determine water vapor at these upper tropospheric levels. Again, those uncertanties are far more likely to play a central role in the cloud-radiative feedback part of the climate sensitivity problem, than in the water vapor feedback part.

I must note that Linzen's inductive leap to infer that Mr. Wicker is urging "allegiance to the results of computational errors" is superb theater but a severe distortion of current reality.

Finally, I confess a certain amazement that the political community has, in effect, legitimized Linzen's unscientific, untestable, unrefereed, and unpublished assertions. In Washington, it seems that that "Lindzen Brain" model has equal credibility to that of the IPCC Report. Clearly, the greenhouse effect is real, it won't go away by any combination of arguments or good luck, and the world doesn't have a clue about how to deal with it. Nothing that either Dick Lindzen or the doomsayers say have any effect whatsoever on those realities.

Best regards,

Jerry D. Mahlman, Director

# SENATE COMMERCE COMMITTEE MEETING ON ROLE OF CLOUDS IN CLIMATE CHANGE

October 7, 1991

Statement by:

ALAN K. BETTS
Atmospheric Research
RD2, Box 3300, Middlebury, VT 05753

Subject: **GLOBAL WARMING AND THE TROPICAL WATER BUDGET**

## 1. Background

I was born and educated in England, with a BA (and MA) in Natural Sciences (Theoretical Physics) from the University of Cambridge in 1967, and a PhD in Meteorology from Imperial College, of the University of London, in 1970. I came to the Department of Atmospheric Science at Colorado State University in 1970 to work on the analysis of a tropical field experiment in Venezuela (VIMHEX: the Venezuelan International Meteorological and Hydrological Experiment), in which I had participated in 1969. I remained on the academic faculty at CSU until 1978, when I moved to Vermont to continue my research work independently. For the past 13 years, I have lived and worked in Vermont, supported by direct grants and contracts from the National Science Foundation and the National Aeronautics and Space Administration.

My research has dealt with atmospheric convection and clouds; their description by observations and theory, and the representation of their energy and water transports in global models, both numerical weather prediction and climate models. In the 1970s my research concentrated on convection in the tropics, and I helped plan and execute the Global Atmospheric Research Program Atlantic Tropical Experiment in 1974 (GATE) (Betts, 1974, Houze and Betts, 1978), as well as a second VIMHEX Experiment in 1972. For this research, I was awarded the Richardson Prize of the Royal Meteorological Society in 1974, the Meisinger Award in 1977 and a Special Award in 1978 by the American Meteorological Society. I co-ordinated the convection research for GATE for the National Academy of Science panel. In the past decade my research has broadened to cover as well the analysis of clouds and convective boundary layer processes over land and the oceans, both in the tropics and mid-latitudes, and the representation of convective processes in global models. I am currently a member of the National Academy panel for the International Satellite Cloud Climatology Project.

## 2. Water vapour and the climate system

The earth's climate system, which involves not only the atmosphere, but the ocean circulations and the biosphere, is exceedingly complex. As a result of theoretical studies, a global observing system, and the development of computers fast enough to model the global atmosphere at sufficiently high resolution, we have made remarkable progress in our understanding in the past 20 years. Yet our present models are still extremely simple, when compared with the complexity of the real climate system of the earth. As a result our global climate models are only as good as the conceptual components of which they are made.

I wish to discuss the links in the chain between the known global increase of the gases such as $CO_2$, $CH_4$ and the CFC's, which are due to anthropogenic activity, and the changes of temperature, water vapour and clouds in the tropics; which in turn primarily control the surface equilibrium temperature of the earth. I will focus my discussion on water vapour: others here will discuss the radiative effects of the clouds themselves. Water vapour is the major absorber in the infrared contributing to the greenhouse effect. Unlike the other greenhouse gases, whose global concentrations are slowly increasing because of anthropogenic activity, the concentration of water vapour is controlled by the transport and precipitation processes in clouds. Generally the water vapour content increases with temperature, because the saturation vapour pressure increases with temperature. In the tropics, water evaporates primarily from the oceans, which are heated directly by incoming solar energy, rises in cumulonimbus clouds (thunderstorms), where it condenses, releasing the latent heat of condensation and freezing. This latent heat release both drives the vertical circulation and balances the net infrared cooling of the atmosphere. The air which flows out of these storms in the upper troposphere is full of ice, which forms the extensive picturesque anvils so characteristic of thunderstorms. In the tropics, clusters of thunderstorms produce extensive anvil clouds, which are readily visible on satellite pictures. These anvils, which are often 400 mb thick, last for many hours, sometimes even a day, since they are maintained by dynamical, convective and radiative processes. As they decay and their ice crystals evaporate, they are responsible for most of the water vapour input to the upper troposphere. Estimates from GATE (Gamache and Houze, 1983) have suggested that up to 10% of the water which is evaporated at the ocean surface is injected into these thick anvils. Away from convective disturbances where air sinks as it slowly cools radiatively, the relative humidity in the tropical upper troposphere is around 30 - 40% up to about 350 mb, where routine rawinsonde measurements become unreliable. At higher levels, the data from the Stratospheric Aerosol and Gas Experiment (SAGE-II) suggest that the relative humidity (away from deep convection) is about 20-25% at 200 mb. The annual variation is small, with higher values on the summer side of the equator.

## 3. Lindzen's argument

Lindzen (1990) has argued that there is a possibility that deep convection might dry the upper troposphere. This is important because absolute decreases of water vapour at high levels can offset the effect of increases at low levels in their greenhouse effect.

His argument is as follows. *Boundary layer temperature and moisture increase with increasing sea surface temperature, so that the tops of the deep convective clouds in the tropics will go higher.* This is correct. If the temperature at the tropopause falls, then the highest outflows from these clouds will be at colder temperatures. Since the saturation mixing ratio over ice decreases with temperature, Lindzen argues *that the cumulonimbus outflow will therefore inject drier air at the highest outflow level; and then the subsidence of this dry air between clouds will produce a drier upper troposphere.*

This idea is wrong (Betts, 1990), because deep convective clouds inject water (as ice and vapour) into the upper troposphere at all levels above their freezing level (this is near the middle troposphere in the tropics; about 550 mb), not just at their tops. Near their highest outflow levels, most of this water is in the form of ice (the anvil clouds), so that the comparatively small value of the saturation mixing ratio plays a relatively insignificant role in the water budget at the highest levels. If Lindzen's model were right, the present upper troposphere would be very dry. In fact, the relative humidity near the freezing level in the deep tropics is about 40%. This is consistent with a subsidence of order 20 mb/day (which is roughly in thermal balance with the radiative cooling rate), and the injection of 10% of the surface evaporation as ice into the upper troposphere (mentioned above).

Lindzen's model is implausible on more general grounds. If the sea surface temperature rises in the tropics, the troposphere as a whole is warmed to a higher temperature, so that, at any given pressure, the saturation mixing ratio increases significantly. For the absolute mixing ratio to decrease at any level, the relative humidity must therefore decrease significantly (by 12 - 15% for a 2°C rise in sea surface temperature). The theoretical evidence is to the contrary. If the temperature warms (towards a warmer "moist adiabat") the stability of the atmosphere increases proportionally more than the increase in the radiative cooling rate, so that the mean sinking motion between the convective systems decreases (Betts and Ridgway, 1989). This reduced subsidence would tend to increase (not decrease) the relative humidity at any level (Betts and Albrecht, 1987). In this simple coupled model of Betts and Ridgway (1989), doubling $CO_2$ increased the tropical surface temperature by 2 to 3°C, consistent with the increase shown by global circulation models.

Clearly, we need better observations of water vapour in the tropical upper troposphere, but the evidence we have is consistent with a relatively tight coupling of water vapour to temperature in which the relative humidity changes rather little.

## 4. Conclusion

I have concentrated on the role of water vapour in the tropics on the greenhouse effect. It is probable that water vapour, because it is coupled thermodynamically to the temperature, will increase as the temperature of the troposphere increases. This coupling leads to an important amplification of the greenhouse effect, as is shown by both global climate models (e.g. Cess et al., 1990) energy balance models (e.g. Betts and Ridgway, 1989) and observational studies (e.g. Raval and Ramanathan, 1989). The radiative role of clouds is more complex, and others here will discuss this in more detail.

As a society we have many choices, but one basic dilemma concerning climate change. The waste products of our civilization are significantly modifying the atmosphere, making it more opaque to infrared radiation. The coupling of temperature and water vapour amplify this effect, while the effects of changes in cloudiness are more complex. Modelling studies suggest that a warming of the atmosphere of several degrees will result if present trends continue. Because of the natural fluctuations of the climate system, it may be a decade or more before we can have confidence that the recent climate warming reflects a long-term trend. Because of the complexity of the earth system, our relatively simple models might mislead us, but again the improvement of our models is a steady incremental process which also takes decades.

If we wait a decade or two for increased certainty, the climate impact will be much larger, harder to reverse, and the impact on the earth's natural ecosystem may be severe. A wise society would take action now to reduce emissions to the atmosphere, in order to limit and delay the long-term impact on our climate. Much can be done at little incremental cost. The scientific community can present the evidence, but political resolve and global co-operation are clearly needed. Changing the direction of our industrial society towards one which is more respectful of its impact on our global environment will take time, probably decades, even if we begin now.

References:

Betts, A.K., 1974: The scientific basis and objectives of the US Convection Subprogram for the GATE. Bull. Amer. Meteor. Soc., 55, 304-313.

Betts, A.K., 1990: Greenhouse warming and the tropical water budget. Bull. Amer. Meteor. Soc., 71, 1464-1465.

Betts, A.K., and B.A. Albrecht, 1987: Conserved variable analysis of boundary layer thermodynamic structure over the tropical oceans. J.Atmos. Sci. 44, 83-99.

Betts, A.K., and Ridgway, 1989: Climatic equilibrium of the atmospheric convective boundary layer over a tropical ocean. J. Atmos. Sci. 46, 2621-2641.

Cess et al., 1990: Intercomparison and interpretation of climate feedback processes in 19 atmospheric general circulation models. J. Geophys. Res., 95, 16601-16615. (32 authors).

Gamache, J.F., and R.A. Houze, 1983: Water budget of a mesoscale convective system in the tropics. J. Atmos. Sci. 40, 1835-1850.

Houze, R. A., and A.K. Betts, 1981: Convection in GATE. Rev. Geophys. and Space Phys. 19, 541-576.

Lindzen, R.S., 1990: Some coolness concerning global warming. Bull. Amer. Meteor. Soc. 71, 288-299.

Raval, A., and V. Ramanathan, 1989: Observational determination of the greenhouse effect. Nature, 342, 758-761.

# THE ROLE OF CLOUDS IN CLIMATE CHANGE

**Testimony of**

Dr. Kevin E. Trenberth*
National Center for Atmospheric Research**

before

The U. S. Senate Committee on Commerce, Science, and Transportation
The United States Senate
SR-253 Russell Senate Office Building
9:30 a.m., October 7, 1991

* Any opinions, findings, conclusions, or recommendations expressed in this publication are those of the author and do not necessarily reflect those of the National Science Foundation.
** The National Center for Atmospheric Research (NCAR) is sponsored by the National Science Foundation.

## Introduction

My name is Kevin Trenberth. I am the Head of the Climate Analysis Section and Deputy Director of the Climate and Global Dynamics Division at NCAR, the National Center for Atmospheric Research. In my work, I am especially interested in global-scale climate dynamics; the observations, processes and modeling of climate changes from monthly to interannual to decadal time scales. I am from New Zealand and I believe that I have unique experience and expertise on the Southern Hemisphere and global atmospheric circulation. I was one of the instigators of the International Tropical Oceans Global Atmosphere (TOGA) programme (under the World Climate Research Programme) and I have served in the U.S. and still serve internationally on TOGA advisory panels. I have served on many National Academy of Science committees, panels and/or boards, and I serve on the NOAA Climate and Global Change Advisory Panel. I have been involved in the global warming debate and the Intergovernmental Panel on Climate Change (IPCC) scientific assessment activity.

With regard to the subject of clouds, I will first summarize the state of knowledge concerning basic water vapor observations in the atmosphere and briefly comment on the relevance of these observations to simulating climate with general circulation models. Water vapor is the most important greenhouse gas in the atmosphere. It is fairly transparent to solar radiation but modulates the outgoing longwave radiation (OLR). Good measurements of water vapor exist throughout the troposphere, but not with global coverage. The climate models indicate that convective clouds play a vital role in moistening the upper troposphere.

A debate has developed over the Ramanathan-Collins (1991) hypothesis concerning the role of clouds as a thermostat on the climate system. They suggested that in the region of high sea surface temperatures, deep convection develops that produce clouds which block out the sun and thus limits further sea surface warming. However, there are examples where this does not work, and the mechanism should not be applied locally because there are nearby regions of compensating effects. The hypothesis does not have general applicability and there are other known limiting mechanisms.

A focus of the impacts of clouds on climate has been their radiative effects, but I am concerned that the role of atmospheric flow in determining patterns of clouds should not be overlooked. Recently, a very useful construct called "cloud forcing" has been introduced. It deals with the radiative effects of clouds, and so can be divided into shortwave (solar) cloud forcing and longwave (infrared) cloud forcing. However, it often tends to ignore other aspects of clouds, such as where the moisture comes from to form the clouds, why clouds occur where they do, why they have the form that they take, and the fact that in forming precipitation latent heat is realized in the clouds, thereby heating the atmosphere. All these factors mean that the atmospheric dynamics are critical in forming patterns of clouds. At the same time the atmospheric flow is strongly affected by the radiative cloud forcing and the latent heating. As a result, there is a strong coupling between clouds, the atmospheric dynamics, and the underlying surface of the ocean or land that can only be properly approached by studies that address these interactions. For example, TOGA is concerned with tropical ocean-atmosphere coupling. Interannual variations in the climate system, which are also a subject of central interest to TOGA, have been used as an indication of what may happen in longer-term climate change. However, clouds have not been a principle concern in the El Niño studies because they are of secondary importance in that phenomenon. This may not be the case in global change.

## Atmospheric water vapor: What do we know?

The main **measurements** of atmospheric water vapor are from *radiosondes*, which consist of a package of instruments flown through the atmosphere on a balloon twice daily at many hundreds of stations all around the world. The package is expendable, so the instrumentation is as cheap as possible. Over the years, the radiosonde itself has evolved, different countries use different instruments with differing accuracy and precision. For water vapor, the sensor measures relative humidity (RH) and has changed with time. Special problems occur at low humidity measurements and these continue unnecessarily. In the U.S. a lithium chloride element was introduced in 1943 but was incapable of making any measurements for relative humidities less than 20%. About 1965, a new carbon element was gradually introduced to measure humidity. In 1973 the housing of the radiosonde was changed and this affects the radiative and ventilation characteristics of the instrument, thereby changing the readings. Recently, in 1989, a second manufacturer was added in the U.S. that currently supplies about 20 western U.S. stations. However, problems with the new instrument continue. For example, the black paint used in the air intake to the instrument turned out to be hygroscopic (water attracting) and comparisons between radiosondes from the two manufacturers reveal differences.

There are some **problems** with the instrument. There is a time lag response in both temperature and relative humidity measurements. There is some hysteresis in the moisture sensor (it remembers moisture), creating differences in readings of up to about 3%. There have long been errors in the treatment of RH for values <20%, a heritage of the early sensor. In the U.S. this is coded as "30" dew point depression, which the National Meteorological Center (NMC) interprets as 15% RH, while the National Climate Data Center uses 19%. Neither is correct. The actual sensor works fine but simply has not had a calibration curve supplied. Overseas, fairly widespread use is now made of a Väisälä radiosonde instrument that measures low humidities.

Aside from the low humidity problems, the **accuracy** of the humidity sensor on the U.S. radiosonde is 4 to 7% RH (high end because of hysteresis effects). With uncertainties in other instruments and balloon location drift, the net uncertainty (assigned by the European Centre for Medium Range Weather Forecasts (ECMWF)) is : 10% from 1000 to 500 mb (lower troposphere) and 20% from 500 to 300 mb (upper troposphere).

What area of the globe is one measurement representative of? One fundamental problem in using the measurements is that water vapor is not well mixed in the atmosphere, so that there are large spatial gradients (e.g. clouds, fronts), and there are rapid changes in time. The **representativeness** of one measurement is difficult to assess. ECMWF uses an influence radius of 250 km at 1000 mb and 300 km in upper troposphere (Illari, 1989). Thus there are too few radiosonde measurements to determine global fields.

Another form of measurement of water vapor is from **satellite** sensing in the infrared and microwave. These measurments have the advantage of global coverage, but at present give poor vertical resolution. Also, the retrieval algorithms make assumptions, and there are several different algorithms. The microwave results are sensitive to surface emissivity, so that the method can only be applied over the ocean and the algorithms must remove the influence of surface wind. Comparisons between radiosonde and infrared (TOVS, the TIROS Operational Vertical Sounder) retrieval measurements indicate errors of 15% in tropics, and 35% in mid latitudes (biggest errors where RH is small) (Illari, 1989). Recently, new measurements have been reported from the SAGE II instrument of RH from 6 to 12 km altitude at 1 km vertical resolution are accurate to 10% (Rind et al., 1991).

Given the basic data, how do we get global fields of relative humidity **analyses**? The method used is through a process called four-dimensional data assimilation at major centers like NMC and ECMWF. The analyses are univariate for RH, which means RH is analyzed by itself as a combination of measurements and information from the numerical weather prediction model used to provide a "first guess" as to what the field looks like. This first guess is actually a forecast from the previous analysis and is subject to errors of perhaps 20%. Global RH analyses have not compared well with observations (Illari, 1989) and have changed erratically with time as the numerical weather prediction model used in the data assimilation has changed, see Fig. 1 (Trenberth and Olson, 1988). Use has been made of satellite data in recent years. However, because of low humidities in the upper troposphere there is no RH analysis above 300 mb at ECMWF.

In **summary**, reasonably good RH information is available from radiosondes, although information in the upper troposphere is mostly confined to local or special measurements. Mean values are better known than daily and monthly time series, and the evolution of global fields is not well enough known for climate purposes.

**Climate models** have not been able to simulate observed moisture levels in the mid to upper troposphere without including effects of vertical transport of moisture by convective clouds. Specifically, in developing the Community Climate Model at NCAR, my colleagues have found it necessary to include a convective parameterization that detrains moisture into the upper troposphere. Any model convection scheme that "rains out" all the moisture in these clouds and which does not detrain a fraction fails to come close to reproducing observed moisture concentrations (Fig. 2). The vertical moisture transport by convection is vital in forming the observed tropical moisture concentrations in the atmosphere which, in turn, has a strong greenhouse effect.

## The Dynamics of Cloud Forcing

The cloud radiative forcing method for analyzing the effects of clouds on the earth's radiation budget was developed by Charlock and Ramanathan (1985). It contrasts the radiation composites for clear sky conditions with the total observed, and the difference is a direct measure of the effects of clouds on the radiation balance of the earth. In this section, it is emphasized that these are not the only effects of clouds and that there are several issues linked to cloud forcing.

Firstly, the tropical convective regions where optically thick upper level clouds occur require a supply of **moisture**, since precipitation exceeds evaporation in these regions.

Secondly, the latent heating from precipitation in the convective regions requires **upward motion** and an export of heat in the atmosphere. This heating helps drives large-scale overturning in the atmosphere.

Because atmospheric mass is conserved, the rising motion in the convective regions must be balanced by **sinking motion** elsewhere. This can be seen by the divergent flow in the upper troposphere which changes with season (Fig. 3). The dominant patterns in Fig. 3 constitute what is known as the Hadley (north-south) and Walker (east-west) cells of large-scale overturning. In practice, the compensating sinking motion occurs over fairly warm water in the tropics and subtropics.

The large-scale subsidence creates a strongly stable atmosphere which **suppresses cloud** development and the vertical transport of free-atmosphere water vapor, and produces the dry zones in the tropics, some of which have high sea surface temperature. This is where the top-of-the-atmosphere outgoing longwave radiation is largest and the absorbed solar radiation at the surface is increased.

In view of the above, it is clear that an increase in shortwave cloud forcing and greenhouse effect, due to increased water vapor, in one location in the tropics necessarily means a **compensating** decrease in these factors someplace else in the tropics. While it appears that cloud forcing has one effect in convective areas, it has the opposite effect nearby and the two regions are closely coupled through the atmospheric dynamics. Therefore the net cloud forcing should not be considered locally, but should be averaged over the regions coupled through the dynamics (Hartmann and Michelsen, 1991).

## Sea Surface Temperature (SST) controls in the tropics

Ramanathan and Collins (1991) proposed that optically thick clouds in the tropics act as a thermostat in controlling high SST (above about 31°C). They hypothesize that in high SST regions, deep convection develops and creates such clouds that block out the sun ("shortwave cloud forcing") and thus limit further sea surface warming.

**Discussion:**

Several points relevant to this mechanism and its possible general applicability need to be made:

1) Locations of convective cloud do not depend solely on SST but also on SST gradients, and on land heating (land-sea contrasts and monsoons) from more remote regions, as well as on atmospheric dynamics (Trenberth, 1991). Consequently, spatial patterns of cloud do not closely follow those of SST, see for example see Fig. 4, for March, April, May (MAM) 1987, from Hartmann and Michelsen, 1991).

Over the Indian Ocean, where the influence of the Asian landmass cannot be ignored, regions of high SST (in MAM 1987 the highest, of over 31°C, Fig. 4) occur but often with subsiding air aloft, so that the atmosphere becomes stable and suppresses convection.

Because regions of upward motion must be balanced by regions of downward motion in the atmosphere, cloud and convection cannot occur everywhere (even if SST is high everywhere). Convection is organized by atmospheric dynamics into "convergence zones" (see Fig. 5) and monsoons; (cf. the Hadley and Walker Circulations, Fig. 3). The upward motions are concentrated into small regions where there are collections of convective clouds, whereas the subsiding motions are more gradual and widespread.

Because of the atmospheric dynamics involved in generating cloud from deep convection (moisture supply, export of heat, conservation of mass) an increase in shortwave cloud forcing in one area must be compensated by a decrease somewhere else, and radiative cloud forcing is inherently not a local problem, as noted above.

2) Ramanathan and Collins (1991) did not fully discuss the role of evaporation, and thus surface latent heat loss, as a further controlling mechanism. In general this appears to be the dominant controlling mechanism for SST in the tropics, with increases in latent heat loss from the surface of $\sim 10$ W m$^{-2}$ per °C change in SST. In the tropics, this partly arises simply from the fact that warmer air can hold much more water vapor (the Clausius-Clapeyron equation). But, in addition, in regions of convection, gusty winds and cooler drier downdrafts can greatly enhance surface evaporation to twice this value (Moncrieff, 1990). Typical surface heat losses from evaporation in warm pool regions are 100 to 150 W m$^{-2}$.

3) Surface thermal radiation toward space also contributes significantly to controlling SST (higher SST, higher radiation) with a heat loss of $\sim 6$ W m$^{-2}$ per °C increase in SST in the tropical warm pools. Typical surface thermal radiative heat losses in warm pool regions are 60 W m$^{-2}$.

4) In general, when there are changes in SST, as in an El Niño event, there are strong compensations between changes in shortwave cloud (Fig. 6) and longwave cloud plus water vapor (greenhouse) effects. The increased cloudiness blocks the sun, but is more than compensated for by the increased greenhouse effect of increased water vapor plus the trapping of heat by the clouds. In regions of higher SST convective cloud typically increases, but in nearby regions there are decreases in convective cloud, so that opposite effects take place. The sum of the changes in the two radiation components (short- and longwave) with changes in SST indicates heat increases of $\sim 6$ W m$^{-2}$ per °C change in SST which virtually offsets the surface thermal radiation effects (in 3)), so that the change in net radiation terms in the tropics sums close to zero. This is very robust over many areas in which there are increases and/or decreases in cloud (Hartmann and Michelsen, 1991).

5) It is likely, however, that the distribution in the vertical atmospheric column of the long- and shortwave radiative heating is different. Changes in solar radiation are more apt to be felt at the surface, whereas the longwave heating is distributed throughout the atmosphere. Therefore changes in cloudiness should have a direct effect on heating at the surface. Over the ocean, this can impact SSTs, as suggested by Ramanathan and Collins, but the effect is complicated by changes in the ocean currents and upwelling induced by changes in the atmospheric winds.

6) There is no good reason for a "magic" number such as 31°C for SST maxima, and higher SSTs could occur under global warming. There are good reasons why SSTs and air temperatures are fairly uniform over large areas of the tropics and the upper limit should be fairly well defined (Wallace, 1991). Wallace argues that the distribution of SSTs in the tropics should be skewed to an absence of hot spots (i.e. large warm pools should form) because of

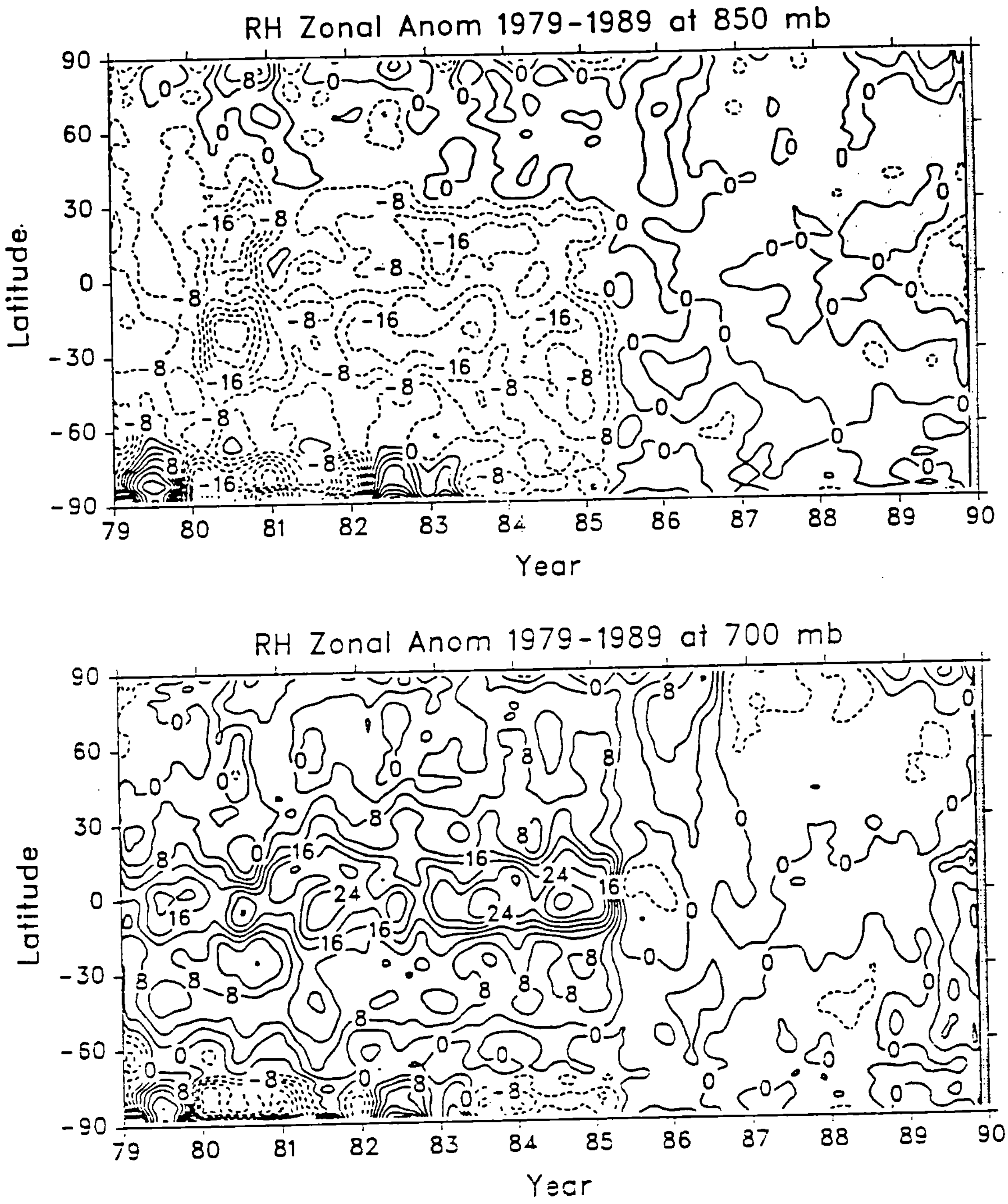


Fig. 1 Latitude-time series for several quantities from the ECMWF WMO archive. Shown are departures from the mean annual cycle from May 1985 to May 1989 of the relative humidity at 850 and 700 mb, in %. Most changes seen here are spurious and associated with changes in the data assimiiation system.

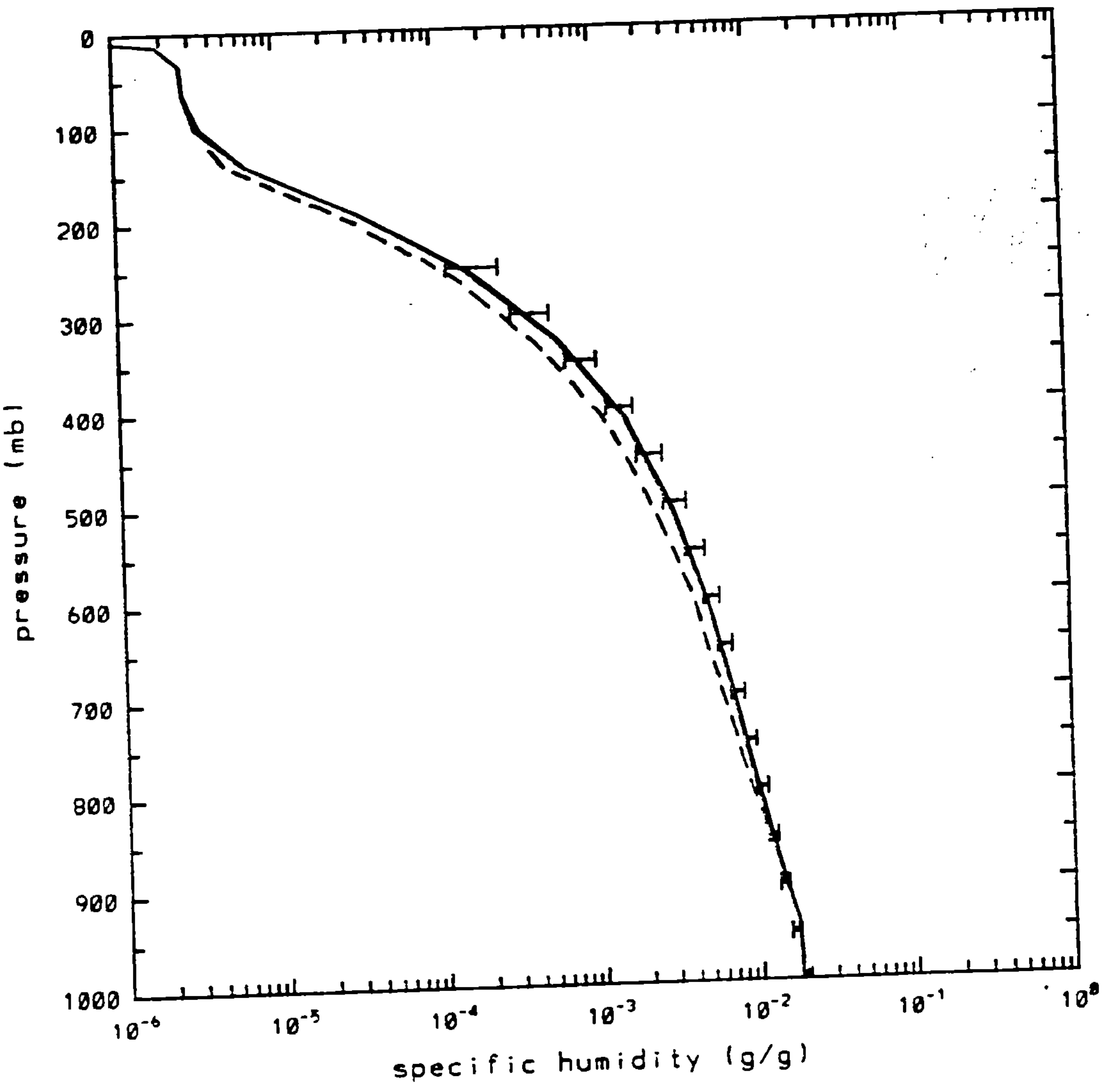


Fig. 2 The vertical profile of specific humidity at the location of Truk island (7.5°N 151°E) in the tropical west Pacific. The horizontal bars show the range (as given by plus and minus one standard deviation) of monthly mean observations from radiosondes at the island for the month of July. Note the horizontal scale is logarithmic and water vapor amounts (in grams of water vapor per gram of air) decrease rapidly with height. The solid profile is the result for the monthly mean from a simulation with the NCAR CCM2 climate model in which a mass flux convection scheme is included which features an overshoot of clouds and detrainment of moisture into the troposphere at cloud top. The dashed profile is the model simulated result when all the condensation in clouds is forced to precipitate out. The result in the latter case is a deficit of moisture in the troposphere compared with observations, which leads to temperatures that are too cold because of the reduced greenhouse effect. (Courtesy J. Hack, NCAR).

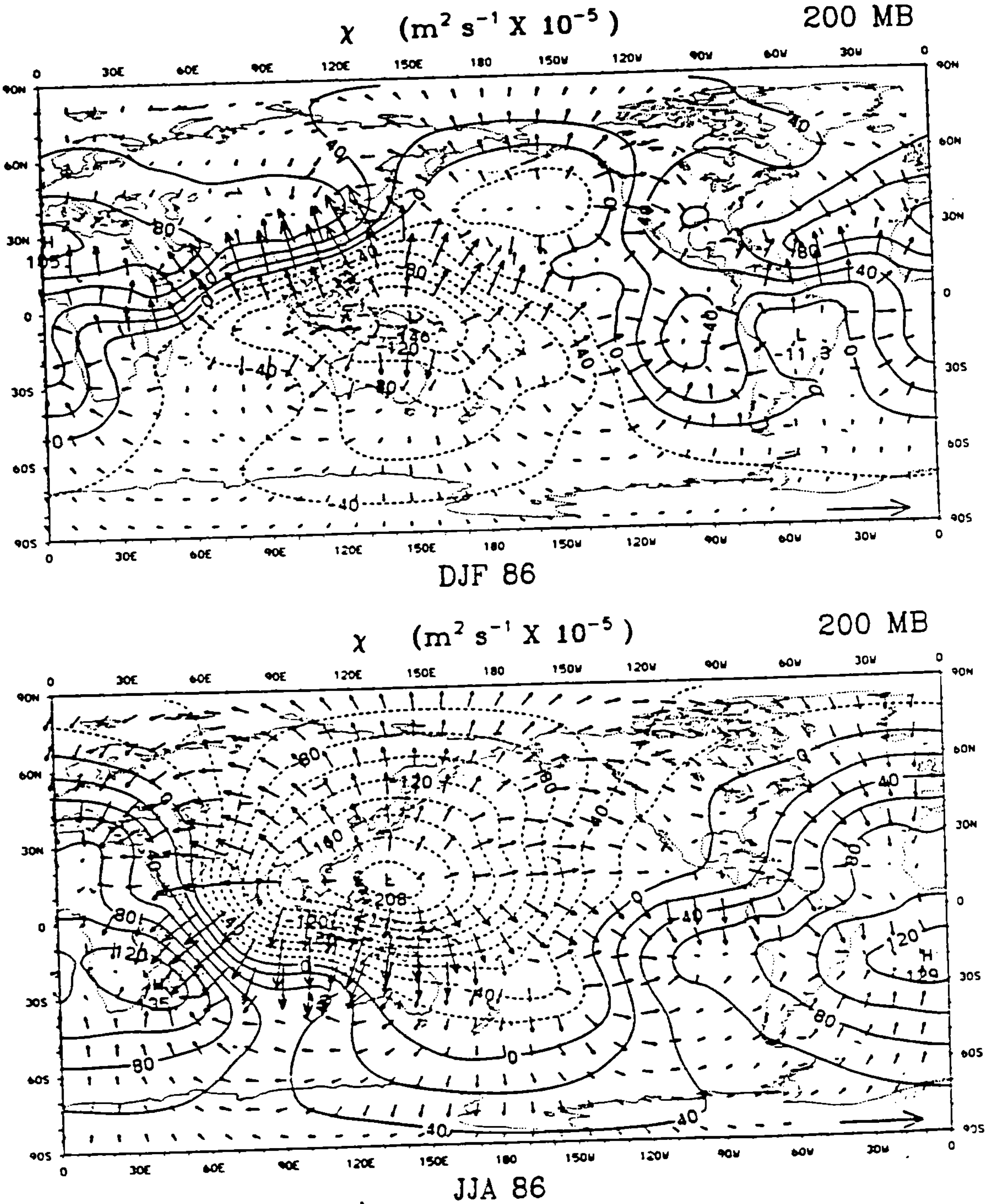


Fig. 3 Seasonal mean velocity potential and the divergent component of the wind vectors at 200 mb for (a) December–February 1985–86, and (b) June–August 1986. The vector plotted at lower right depicts 10 m $s^{-1}$. From Trenberth (1991). The arrows depict the upper tropospheric flow from regions of intense upward motion in convective areas to regions of more gradual downward motion.

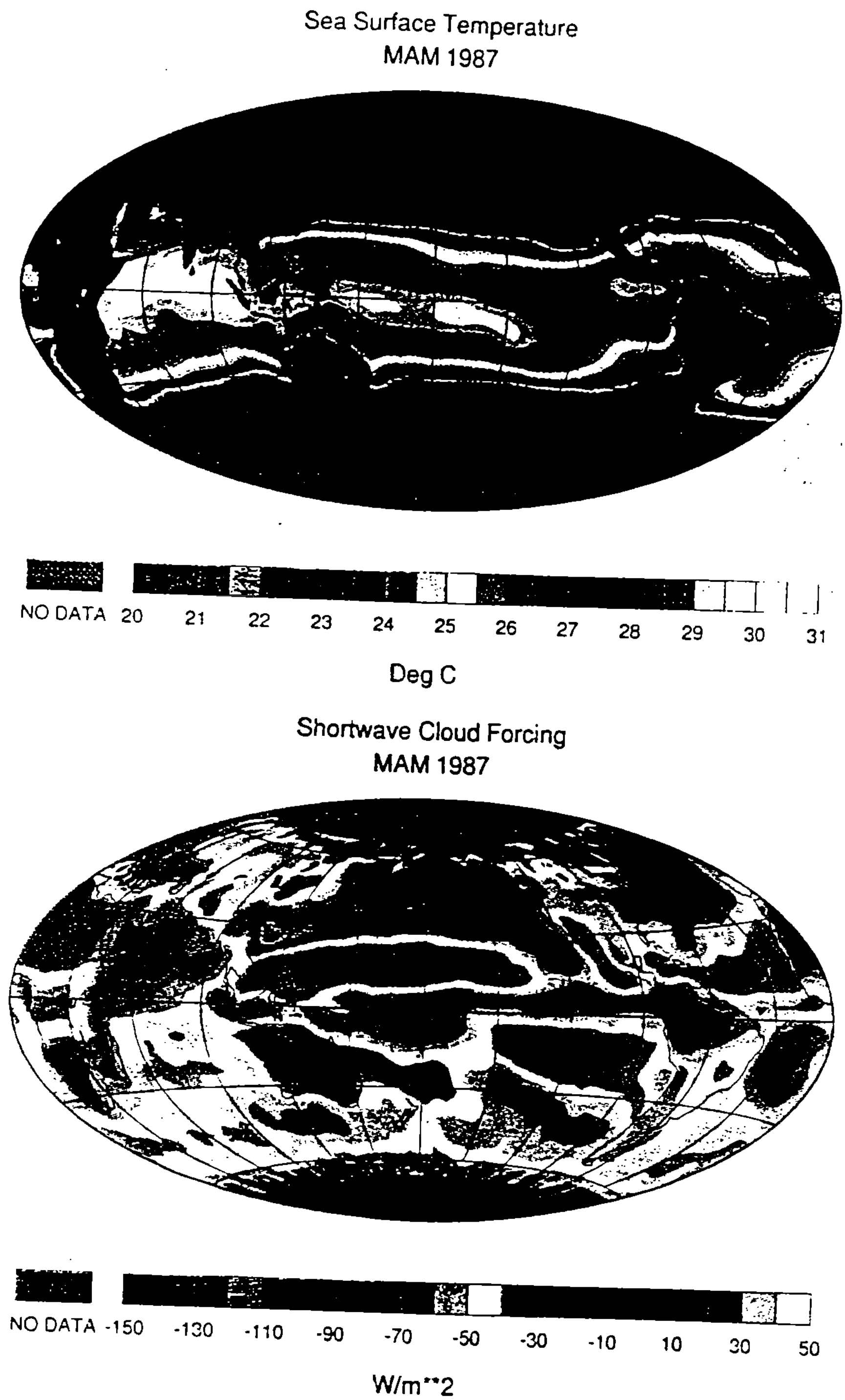


Fig. 4 a) Sea surface temperature (°C) and b) shortwave cloud forcing (W $m^{-2}$) for March–May 1987 mapped on a Hammer equal area projection. The originals are in color and the SST map colors were chosen to emphasize the tropics. From Hartmann and Michelsen (1991).

Mercator Satellite Relative Cloud Cover, 1400 Local, 40°N to 40°S, Mean Octas, October 1967-1970.

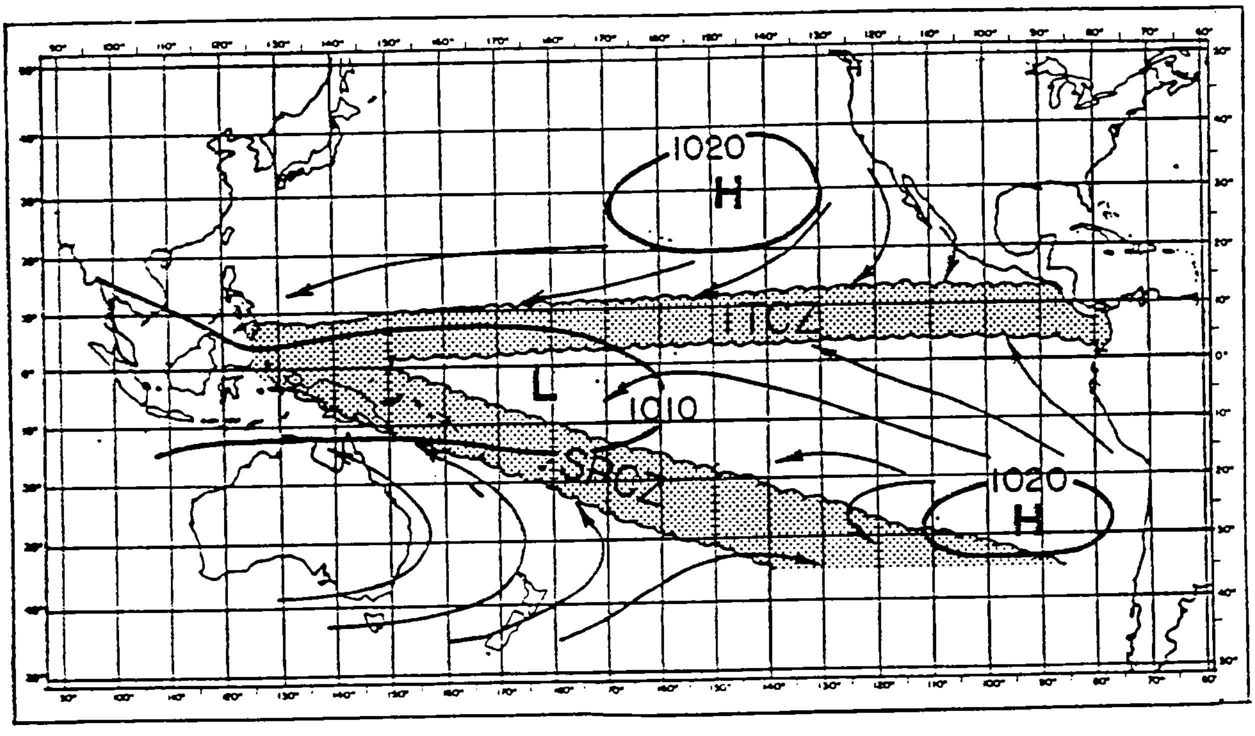


Fig. 5 a) Mercator satellite picture of cloud cover 40°N to 40°S for October 1967 to 1970; and b) pictorial representation of the key features in a) showing the Intertropical Convergence Zone (ITCZ) and South Pacific Convergence Zone (SPCZ), with the annual mean sea level pressure field superposed along with schematic surface wind streamlines.

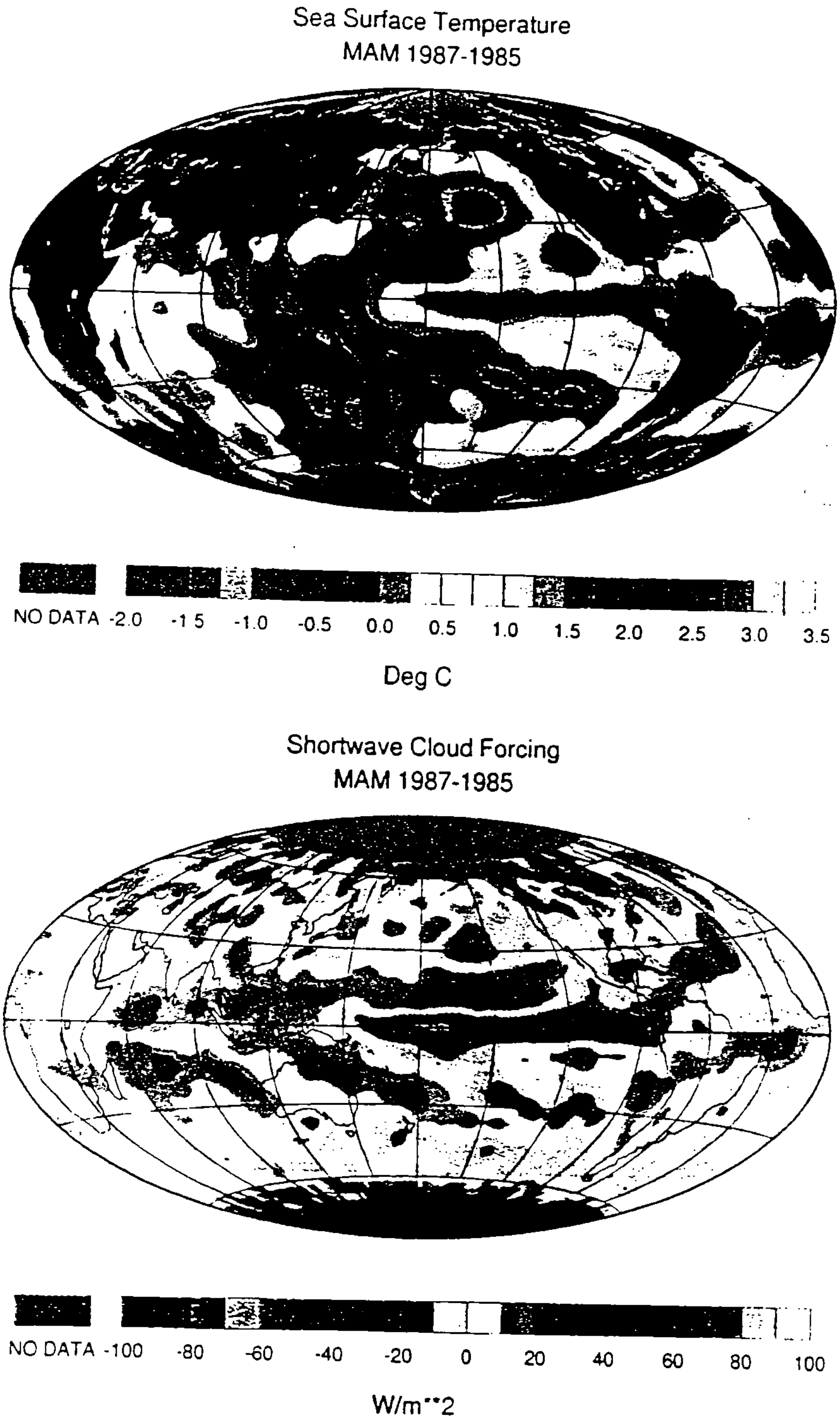


Fig. 6 a) Sea surface temperature (°C) and b) shortwave cloud forcing (W $m^{-2}$) differences between March–May 1987 – 1985 mapped on a Hammer equal area projection. The originals are in color. From Hartmann and Michelsen (1991).

RIND/SATELLITES

# Positive water vapour feedback in climate models confirmed by satellite data

**D. Rind*, E.-W. Chiou†, W. Chu†, J. Larsen†, S. Oltmans‡, J. Lerner*, M. P. McCormick† & L. McMaster†**

* NASA/Goddard Institute for Space Studies, New York, New York 10025, USA
† NASA/Langley Research Center, Hampton, Virginia 23665-5225, USA
‡ NOAA CMDL, Boulder, Colorado, 80302, USA

**CHIEF among the mechanisms thought to amplify the global climate response to increased concentrations of trace gases is the atmospheric water vapour feedback. As the oceans and atmosphere warm, there is increased evaporation, and it has been generally thought that the additional moisture then adds to the greenhouse effect by trapping more infrared radiation. Recently, it has been suggested that general circulation models used for evaluating climate change overestimate this response, and that increased convection in a warmer climate would actually dry the middle and upper troposphere by means of associated compensatory subsidence[1]. We use some new satellite-generated water vapour data to investigate this question. From a comparison of summer and winter moisture values in regions of the middle and upper troposphere that have previously been difficult to observe with confidence, we find that, as the hemispheres warm, increased convection leads to increased water vapour above 500 mbar in approximate quantitative agreement with the results from current climate models. The same conclusion is reached by comparing the tropical western and eastern Pacific regions. Thus, we conclude that the water vapour feedback is not overestimated in models and should amplify the climate response to increased trace-gas concentrations.**

? = what geographical regions??

Studies with the Goddard Institute for Space Studies (GISS) general circulation model (GCM) show that, of the 4.2 °C warming that results from doubling atmospheric $CO_2$, ~1.7 °C is contributed by the increase in water vapour[2]. In this regard, Lindzen[1] believes that the increased convection associated with the projected warming would act to dry the middle and upper troposphere. In his hypothesis, air rising in cumulus convective towers would cool and saturate, producing rain, which would fall out of the column. To balance the upward air-mass flux, there would have to be compensating downward motion, or subsidence, which would dry the atmosphere above ~5 km, thereby leading to a negative water vapour feedback.

In the vicinity of warmer sea surface temperatures, there will be greater convection; indeed, satellite observations have been used to verify that the greenhouse effect is larger over warmer ocean regions[3], suggesting that a positive feedback arises from increased convection. Here we address the question more directly by using satellite-derived water vapour observations to test the water vapour response to increased convection in regions of the middle and upper troposphere that have previously been difficult to observe with other methods.

The water vapour data set has been generated by the SAGE II (Stratospheric Aerosol and Gas Experiment) instrument aboard the Earth Radiation Budget Satellite[4] (ERBS). SAGE II has been collecting data continuously since its launch in October 1984. It is a solar occultation instrument measuring attenuated sunlight through the Earth's limb with a path length of ~200 km and a vertical resolution of 1 km. Each sunrise and sunset experienced by the spacecraft results in a solar occultation measurement yielding ~900 opportunities to retrieve gas-concentration profiles. The path length is small enough to isolate individual areas, but large enough to encompass most of the observed vertical motions associated with convection[10]. Water vapour is retrieved by determining the extinction of the solar signal at 0.94 μm. The instrument is self-calibrating as it observes the unattenuated sun above the atmosphere before or after each event. The water vapour observations have been validated by comparison with radiosonde data, frost point hygrometer, Lyman-α and LIMS satellite observations[5], and have been shown to produce realistic values, with an estimated accuracy of ~10%.

We compared the relative humidity calculated using the SAGE II water vapour data with that calculated using radiosonde observations with the Vaisala water vapour sensor, an instrument now in widespread use. The temperature data needed for the SAGE relative humidity calculations were provided by the National Weather Service of the National Oceanographic and Atmospheric Administration. The estimated radiosonde sensor accuracy is 2–3%, but this value becomes more uncertain with increasing altitude[6]. A comparison was made whenever the satellite and *in situ* measurements were within 250 km and 6 h during 1987.

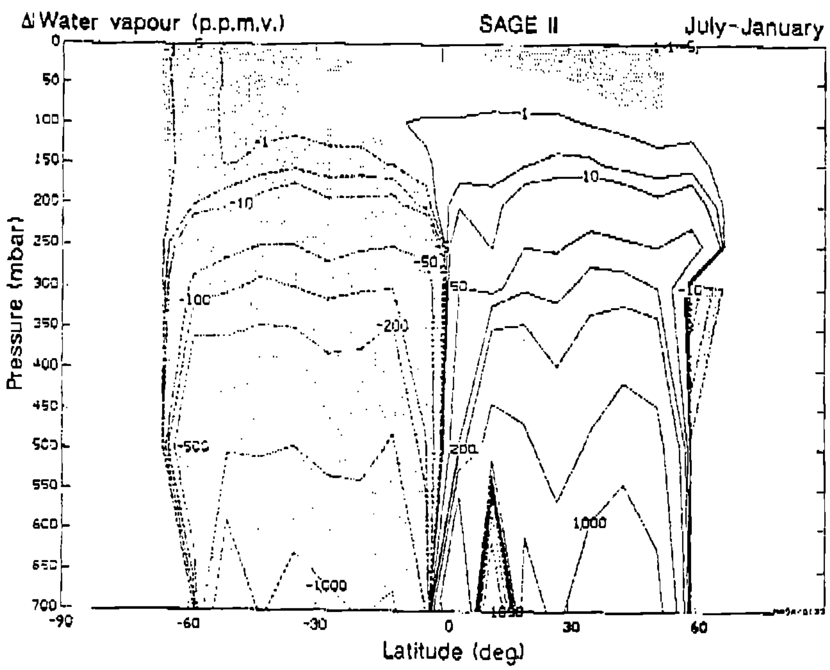


FIG. 1 Change in water vapour between July and January from SAGE II observations for January 1985 to July 1989.

• 19 GCM's – "excellent" agrmt re water vapor
• corroborated by satellite & SST measurements by Raval & Ram. } different geograph location as surrogate!

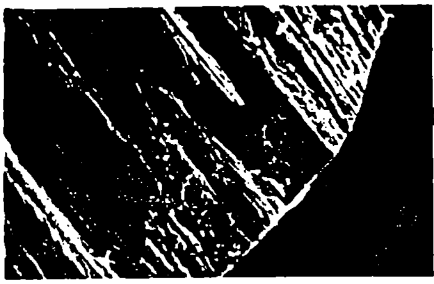

FIG. 2 Detail of a clinopyroxene microkrystite from the K/T boundary of DSDP site 577. The mafic glass between the pyroxene has been etched away by sea water. Similar forms are seen in all other known altered microkrystites.

siderophile ('iron-loving') elements, associated with Solar System objects. Models of the dispersion of ejecta clouds also indicate that much of the high-energy material should be deposited on the other side of the globe from the impact. This explains the high levels of iridium and shocked quartz found in the Southern Pacific (at DSDP site 596; F. T. Kyte, University of California at Los Angeles), in New Zealand and on the Kerguelen Plateau (ODP site 738c), if North America was the site of the impact.

Identifying the impact site, whether it is Chicxulub or not, is not the same as unravelling the mechanism that actually caused the extinctions. The original simple picture — a suppression of photosynthesis resulting from a darkening of the skies by ejecta — has been supplanted by a plethora of complex schemes. Oblique impacts may be more efficient in transferring a larger proportion of the impact energy to the atmosphere than vertical collisions (P. H. Schultz, Brown University, Rhode Island), and fast ejecta re-entering the atmosphere may radiate off their energy and ignite global wildfires (Melosh). Shock heating of the atmosphere may lead to $NO_x$ production, and thus to acid rain. Trapped natural gas (clathrates), principally methane, may have been released in large volumes, following disruption of submarine sediments (M. Max, Naval Research Lab, Washington DC). This would contribute to a greenhouse atmosphere, as would the release[6] of $10^{18}$ moles of $CO_2$ through impact with carbonate rocks as found at Yucatan. Carbon and oxygen isotope data from southern Spain[7] suggest a rise in sea surface temperatures of at least 8 °C. Identifying the impact site may help to tie down the details of the extinction. □

Jan Smit is at the Institute of Earth Sciences, Free University, PO Box 7161, 1007 MC Amsterdam, The Netherlands.

1. Sigurdsson, H. et al. Nature 349, 482–487 (1991)
2. Sheenan, P. M. et al. Geol. Soc. Am. Abs Prog A, 356 (1990)
3. Grieve, R.A.F. Nature 340, 428–429 (1989)
4. Hildebrand, A. R. & Boynton, W. V. Science 248, 843–847 (1990)
5. Officer, C. B. et al. Nature 326, 143–149 (1987)
6. Ross, I. R. et al. Tectonophysics 155, 139–168 (1988)
7. Smit, J. Geologie Mijnb 69, 187–204 (1990)

GREENHOUSE WARMING

# Positive about water feedback

• corroborated by Rind satellite measurements in different seasons.

Robert D. Cess

INTERACTIVE feedback mechanisms constitute the greatest uncertainty in projecting future climate change associated with increasing greenhouse gases. The change can be either amplified (positive feedback) or reduced (negative feedback). One mechanism, involving water vapour, has long been regarded as being positive[1], but recently it was suggested[2] that it is instead negative. On page 500 of this issue[3], however, Rind et al. present combined observational and model results which are strongly supportive of the conventional interpretation that water vapour indeed provides positive feedback.

The customary explanation of water-vapour feedback is that if the Earth were to warm, for example as the result of increasing greenhouse gases, then (owing to increased evaporation) the warmer atmosphere should contain more water vapour which, itself a greenhouse gas, would amplify the warming. The most straightforward way of studying this specific feedback is to restrict attention to clear-sky conditions, so as to eliminate the multitude of complexities associated with the additional feedback due to clouds, for which the sign is in doubt[4]. Even with this restriction, in all likelihood water-vapour feedback also includes climate-induced changes in atmospheric lapse rate[5], the temperature drop with altitude, although little effort has been made at separating this from feedback due solely to water vapour. It is emphasized that lapse-rate feedback is implicit in what is commonly referred to as water-vapour feedback.

To place the study by Rind et al.[3] in perspective, it is useful to review recent developments in our understanding of water-vapour feedback. A comparison last year[4] of the global-warming simulations from 19 general circulation models (GCMs) of the atmosphere, found excellent agreement among their depictions of positive water-vapour feedback. This is significant with respect to the issue addressed by Lindzen[2] and by Rind et al.[3]; namely, does the increased convection expected in a warmer climate produce positive or negative water-vapour feedback? Lindzen's contention is that convection will cause water-vapour feedback to be negative, because sinking air in regions surrounding deep cumulus clouds will dry the upper troposphere. The point is that the 19 GCMs used several very different parameterizations of convection, so that their agreement over water-vapour feedback is not an artefact of this parameterization.

In an observational evaluation of water-vapour feedback based on satellite infrared and surface-temperature data, Raval and Ramanathan[6] used measurements over different oceanic locations as a surrogate for global climate change; their results concur well with the 19 GCMs[4]. One could, of course, argue that for this purpose a change of location is not a proper surrogate for a change of global climate, and that the agreement is coincidental. A recent study, however, makes this unlikely. A.D. Del Genio and coworkers (private communication), using the same GCM as Rind et al.[3], predict correctly the changes in radiative fluxes with geographical location observed by Raval and Ramanathan. Furthermore, their model is one of the 19 used in the GCM intercomparison[4], so that it is producing comparable water-vapour feedback for both geographical and global climate change, suggesting that changed location, at least for inferring water-vapour feedback, is a useful surrogate for global change.

• Corrob by RIND by Comparing Convective West Pacific w/ non-convective East.

Still, one might argue that this agreement also is merely a model artefact. But the new contribution by Rind et al. to our overall picture of positive water-vapour feedback wouldn't support this. The authors first demonstrate that for $CO_2$-induced global warming, their model predicts an increase in the amount of water vapour in the middle and upper troposphere; this should be expected for a GCM that produces positive water-vapour feedback. Their next step is the important one. To validate their model, they consider the effect of seasonal climate changes on middle- and upper-tropospheric water-vapour content, and show, through comparison with satellite-generated data, that the GCM produces realistic results. This reinforces our confidence that the GCM is also producing realistic predictions for the feedback for the $CO_2$-induced warming. It is important to recognize that, in this context, seasonal climate change is used as a validation tool rather than as a surrogate for climate change.

Nevertheless, one can argue that this validation constitutes only a necessary, but not a sufficient, test of the GCM. Rind et al.[3], however, provide a further and intriguing comparison which specifically addresses the effect of enhanced convection on middle- and upper-tropospheric water-vapour levels. They do this by com-

1. Manabe, S. & Wetherald, R.T. J. atmos. Sci. 24, 241–259 (1967).
2. Lindzen, R.S. Bull. Am. Met. Soc. 71, 288–299 (1990)
3. Rind, D. et al. Nature 349, 500–503 (1991)
4. Cess, R.D. et al. J. geophys. Res. 95, 16601–16615 (1990)
5. Wetherald, R.T. & Manabe, S. J. atmos. Sci. 45, 1397–1415 (1988).
6. Raval, A. & Ramanathan, V. Nature 342, 758 (1989)
7. Cess, R.D. Nature 342, 736–737 (1989)

paring satellite data for atmospheric moisture over the convective western Pacific with that over the largely non-convective eastern Pacific. The data clearly show that convection moistens the middle- and upper-troposphere over the western Pacific relative to the eastern Pacific. This runs right against Lindzen's argument[2] that convection drys the atmosphere.

As with the other comparisons discussed in this article, one can probably add a caveat to the trans-Pacific comparison. But it is difficult to believe that the agreements found in all of these comparisons are collectively coincidental. Instead they collectively make a compelling case that water-vapour constitutes a positive feedback mechanism, although as previously discussed there is a need to understand better the lapse-rate component of this feedback. Nor does this imply that we necessarily understand other feedback mechanisms. Cloud feedback is a prime example of a crucial feedback that is poorly understood'. □

*Robert D. Cess is in the Institute for Terrestrial and Planetary Atmospheres, State University of New York, Stony Brook, New York 11794, USA.*

RNA SPLICING

# Alive with DEAD proteins

*David A. Wassarman and Joan A. Steitz*

It has been known for many years that splicing of nuclear pre-messenger RNA (pre-mRNA) requires ATP hydrolysis. Yet the phosphates of ATP are incorporated into neither the intermediates nor the products of the splicing reaction, from which it would seem that the catalytic mechanism itself is independent of ATP — as is the case for the self-splicing of group II introns, which proceeds by way of identical reaction intermediates[1]. Instead, it has seemed likely that ATP facilitates the assembly of myriad *trans*-acting factors onto the pre-mRNA as a prerequisite to splicing. The resulting 'spliceosome' is known to include four distinct small RNA–protein complexes, as well as several less well characterized protein factors.

## Evidence

Many lines of evidence have hinted at dynamic transitions as the spliceosome proceeds through the reaction pathway, ultimately releasing ligated exons and excised intron. On pages 494 and 487 of this issue, Schwer and Guthrie[2] and Company *et al.*[3] describe the characterization of two essential splicing factors from the yeast *Saccharomyces cerevisiae* as members of a family that includes RNA helicases and RNA-dependent ATPases; the factors concerned are PRP16 and PRP22, PRP standing for precursor RNA processing. Finding ATP-driven switch proteins not only sheds light on splicing's ATP requirement but also promises insights into the pathway, mechanism and fidelity of the process.

Yeast genetics has been exploited to identify over 20 proteins which contribute directly to pre-mRNA splicing[4]. Some are integral components of the small nuclear ribonucleoprotein particles (snRNPs, which contain U1, U2, U4/U6 and U5 RNAs); others (designated 'factors') can be identified only in the spliceosome. PRP16 is a factor required *in vitro* for the second cleavage–ligation step of the splicing reaction (see figure). Schwer and Guthrie[2] show that stalled spliceosomes pre-formed in a PRP16 immunodepleted extract can be complemented with the purified protein and ATP to yield mature mRNA; PRP16 then dissociates from the spliceosome. PRP22 acts at a late step, release of the spliced mRNA, one that might have not been expected to require a factor. In a heat-inactivated PRP22 extract *in vitro*, Company *et al.*[3] find that the mature messenger is retained in the spliceosome.

Sequence analysis of PRP16 and PRP22 — as well as of three other yeast splicing factors, PRP2 (ref. 5), PRP5 (ref. 4) and PRP28 (ref. 6) — shows that they are related to a rapidly expanding family dubbed the 'DEAD box' proteins[7] (DEAD standing for Asp-Glu-Ala-Asp in the single-letter amino-acid code). Gene products containing the DEAD motif plus six other shared sequence segments come from the whole range of organisms and are implicated in a variety of cellular processes (see table). Among the seven conserved regions are two that make up part of the ATP-binding site in proteins whose structure is known. The eukaryotic protein synthesis initiation factor eIF4A is the prototype[7] and the member of the DEAD-box family that is the best characterized biochemically[8]. In combination with other initiation factors, it is believed to use the energy generated from ATP hydrolysis to unwind mRNA secondary structure upstream of the initiation codon, thereby facilitating attachment of the 40S ribosome. It should be noted that this unwinding is not of the irreversible type accomplished by covalent base modification, as described for some RNA helicase activities[9]. Only two other members of the DEAD-box family, human p68 (ref. 10) and *Escherichia coli* SrmB (ref. 11), have been biochemically examined and shown to exhibit RNA-dependent ATPase activity (and helicase activity in the case of p68).

As the roster of related proteins grows, the story becomes more complex. In fact, PRP2, 16 and 22 are not literally DEAD-box proteins, but 'DEAH-box' proteins (H for His). They also share several other sequence features that distinguish them as a novel subclass of the family. In an age when attributing function to a protein based merely on sequence similarity raises few eyebrows, it is particularly gratifying that the biochemical activity of PRP16 has been investigated. Schwer and Guthrie[2] isolated the protein and directly demonstrated its ability to hydrolyse ATP in the presence of RNA. Whether helicase activity will be found remains to be seen. Admittedly, doing decisive biochemistry on most of the proteins listed in the table is not easy because their exact RNA substrates are unknown.

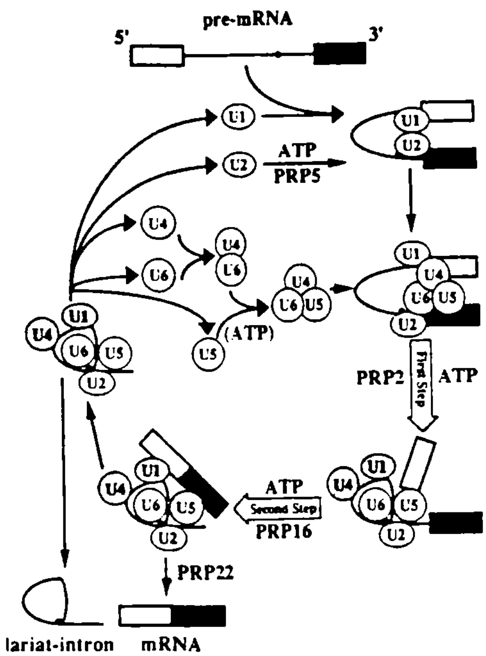


The roles of DEAD and DEAH proteins in pre-mRNA splicing. The branch point is indicated by ●; shading of the U1 and U4 snRNPs indicates weak interactions with the spliceosome. Note that it is uncertain whether ATP hydrolysis facilitates assembly or dissociation (or both) of the U4/U6 and U5 snRNPs. A more complete model and description of pre-mRNA splicing in yeast can be found in ref. 4.

## Speculation

Nonetheless, we can speculate on how a variety of RNA helicases or RNA-dependent ATPases might feed into the splicing pathway. Steps currently known to require factors assigned to the family are shown in the figure. Additional yeast proteins possessing signature sequences of the DEAD (ref. 12) or DEAH (ref. 3) types have already been identified

 

To: Al
From: Katie
Re: Lindzen rebuttal to Tom Wicker's piece in the Times
Date: 11-14-91

I have a copy of a letter that Lindzen has written to the Times in response to Tom Wicker's piece of 24 October. Lindzen repeats his claim in the letter that "My hypothesis has been that water vapor, at altitudes of 6-16 km, might very well decrease in a warmer climate, and act to effectively cancel warming due to increasing greenhouse gases. Such an effect would constitute what is known as a negative feedback." Lindzen admits that he withdrew his suggested mechanism for accomplishing this -- namely that "deep clouds might rise to greater heights and deliver less water vapor to the environment." He insists, however, that the bottom line that we will see decreased water vapor in a warmer climate is still correct. The new theory that he offers is that "a similar negative feedback would arise if deep clouds produced more ice in a colder climate and less ice in a warmer climate." Evidence produced at the hearing and subsequent personal communications I have had with scientists completely refute this idea. Indeed, the best Lindzen can do is to say that it is "a not implausible possibility."

To get at the heart of Lindzen's argument-----Is there less water vapor in the atmosphere (either from deep clouds or the new reduced ice theory) as the planet warms? The experts say no and so does the data.

THE EXPERTS:

o Allen Betts' testimony: "Lindzen argues that the cumulonimbus outflow will therefore injuect drier air at the highest outflow level; and thne the subsidence of this dry air between clouds will produce a drier upper troposphere. This idea is wrong .... If Lindzen's model were right, the present upper troposphere would be very dry. In fact, the relative humidity near the freezing level in the deep tropics is about 40%." Betts then continues with further refutation of the idea: "Lindzen's model is implausible on more general grounds...."

o Kevin Trenberth's testimony: "Any model convection scheme [like Lindzen's] that 'rains out' all the moisture in these clouds ... fails to come close to reproducing observed moisture concentrations. The vertical moisture transport by convection is vital in forming the observed tropical moisture concentrations in the atmosphere which, in turn, has a strong greenhouse effect."

THE DATA:

Recall that Lindzen has absolutely no data to support his theories. His ideas are merely "thought experiments." The problem is that the "real world" data is directly contrary to his hypotheses.

o The models: Robert Cess: "A comparison last year of the global warming simulations from 19 general circulation models (GCMs) of the atmosphere found excellent agreement among their depictions of <u>positive</u> water vapor feedback. This is significant with respect to the issue addressed by Lindzen....The point is that the 19b GCMs used several very different parameterizations of convection so that their agreement over water vapour feedback is not an artefact of this parameterization."

o Satellites and Sea Surface Temps:

o Raval and Ramanathian used satellite and sea surface temperements over different oceanic locations as a surrogate for global climate change: their results confirm the GCM predictions.

o Del Genio used satellite data to compare water vapor over different geographical locations. Results: warmer geographical regions have more moisture in the troposphere than colder regions.

o David Rind used satellite data to compare the effect of seasonal climate changes and geographical changes on middle and upper tropospheric water vapour content. Results: confirmed the positive feedback predicted by their models and refuted Lindzen. "Increased convection leads to increased water vapour ... in approximate quantitative agreement with the results from current climate models. The same conclusion is reached by comparing the tropical western and eastern Pacific regions."

Lindzen raises an additional argument is his letter. Namely -- that "In current models, the behavior of water vapor in this altitude range (6-16 km) is largely determined by identifiable computational errors." On this, Lindzen is again, dead wrong.

First, as indicated above, actual measurements of water vapor in the troposphere indicate that the models are right on on this.

Second, Lindzen is NOT a modeler, and this statement demonstrates that he is out of touch with the science. The expert on this is Philip Rasch at NCAR. I spoke to him today and he indicated that, while it was once true that the models did not do a good job simulating the effect of water vapor in a greenhouse environment, three years ago he and his colleague David Williamson, developed a new computational system that corrected the earlier problems. This is the system that models in the United States and in Europe use; the accuracy of the new system is validated by the satellite measurements of the actual role of water vapor. Rasch has published profusely on this -- obviously, Lindzen is simply out of touch. (Note Jerry Mahlman's note on this point, too. He also has worked to remove water vapor errors from his model -- local errors may persist, but even then, Jerry says that "I see no evidence that correction of such errors has any reasonable possibility of changing the model sensitivity to water vapor feedback in any significant way.")

OFF THE RECORD: Jerry Mahlman is a member of the Global Change Research Committee at the National Academy. He confided in me that the Academy is deeply troubled by the negative impact Lindzen is having on the Academy's credibility. The Academy has 2 members that are experts on climate -- Dickinson and Manabe. Lindzen has no expertise in climate (his background is atmospheric dynamics). The Academy had a meeting on this recently where concern was expressed that Lindzen was jeopardizing the Academy's ranking in the world scientific research community on the issue of climate change. International groups such as the IPCC are the authorities; the Academy's work has been marginalized. The Academy is considering doing a position paper to set the record straight on this and to make clear the Lindzen does NOT speak for the Academy on this.

SENT BY:Xerox Telecopier 7021 ;11- 4-91 ; 1:24PM ; 18049822137→ #3
R.S.LINDZEN TEL:1-617-964-3953 NOV 05.91 19:47 NO.002 P.03

Contar
202 224 0580

Letters to the Editor
The New York Times
229 West 43d Street
New York, NY 10036

To the Editor:

Tom Wicker, in his Op-Ed piece, *Time for Action* (NYT, October 24, 1991) refers to my having '"withdrawn" the complex hypothesis that was an important element of his skepticism.' His reference is profoundly misleading and completely out of context. His conclusion that my 'changed position' seems to 'justify a heightened urgency in responding to threatening atmospheric developments' is totally unwarranted. My hypothesis has been that water vapor, at altitudes of 6-16 km, might very well decrease in a warmer climate, and act to effectively cancel warming due to increasing greenhouse gases. Such an effect would constitute what is known as a negative feedback. I have had no reason to alter this hypothesis. Two years ago, I offered as an *example* of a mechanism that would be consistent with this hypothesis, the fact that in a warmer environment, deep clouds might rise to greater heights and deliver less water vapor to the environment. While this mechanism is qualitatively correct, my colleagues and I found early this year that the mechanism was quantitatively inadequate. This did not (and does not) overly concern us since there are other mechanisms that are potentially more effective. For example, a similar negative feedback would arise if deep clouds produced more ice in a colder climate and less ice in a warmer climate -- a not implausible possibility.

These seemingly arcane matters were not, however, at the heart of my testimony before Senator Gore. The main points I made in my testimony were: 1) No current model would predict large warming without strong positive feedback from water vapor; 2) Such feedbacks depend crucially on the behavior of water vapor in the altitude range 6-16 km; 3) In current models, the behavior of water vapor in this altitude range is largely determined by *identifiable computational errors*; and 4) Even if these computational errors were corrected, we do not adequately know the physical processes which do determine water vapor at these levels. It is my personal feeling that computational errors hardly constitute a sound basis for economically profound policy. This may be considered by some to be a political position. I hope, however, that I may be forgiven, as a scientist, for feeling that the alternative politics, which lead Mr. Wicker to urge allegiance to the results of computational errors, to be both peculiar and deeply worrisome.

RICHARD S. LINDZEN
Cambridge, MA, Oct. 24, 1991

*The writer is Alfred P. Sloan Professor of Meteorology, Massachusetts Institute of Technology.*

**Address:** Building 54 Room 1720, Massachusetts Institute of Technology
Cambridge, MA 02139
**Phones:** office: 617-253-2432 home: 617-332-4342 fax: 617-964-3953

202 333 7790
Tuesday

pls. make file -
Clouds.

Please note cirrus clouds are in
the upper troposphere around 10-15 km
altitude.
They indicate presence of ~~high~~ humidity.
Preferentially they are associated
with warm ocean waters.

C-P

Reprinted from JOURNAL OF APPLIED METEOROLOGY, Vol. 27, No. 4, April 1988
American Meteorological Society

# Thin Cirrus Clouds: Seasonal Distribution over Oceans Deduced from Nimbus-4 IRIS

C. PRABHAKARA, R. S. FRASER, G. DALU,* MAN-LI C. WU AND R. J. CURRAN†

*NASA/Goddard Space Flight Center, Greenbelt, MD 20771*

T. STYLES

*Applied Research Corporation, Landover, MD 20785*

(Manuscript received 25 February 1987, in final form 24 September 1987)

ABSTRACT

Spectral differences in the extinction between the 10.8 and 12.6 $\mu$m bands of the infrared window region, due to optically thin clouds, are observed in the measurements made by a broad-band infrared aircraft radiometer. Similar spectral properties are also revealed by the measurements made by the high-resolution infrared interferometer spectrometer (IRIS) aboard the Nimbus-4 satellite, which had a field of view of ~95 km. These observations show that the extinction due to cloud particles at 12.6 $\mu$m is appreciably larger than that at 10.8 $\mu$m. Both water or ice particles in the clouds can account for such spectral difference in extinction provided that the particles are smaller than the wavelength of radiation. This spectral effect is demonstrated with the help of multiple scattering radiative transfer calculations. As the IRIS data reveal this spectral feature, about 100 to 200 km away from the center of high altitude cold clouds (~230 K), it is inferred that this feature is related to the spreading of cirrus clouds. Based on this hypothesis, we have deduced mean seasonal maps of the distribution of thin cirrus clouds over the oceans from 50°N to 50°S from the IRIS data. These maps reveal that, over the oceans, such clouds are often present over the convectively active areas such as ITCZ, SPCZ, and the Bay of Bengal. These results have application to studies of earth radiation balance and climate.

## 1. Introduction

Over the tropical oceans, cirrus clouds in the atmosphere are largely produced by convectively active rain cells that penetrate deep into the troposphere. The cirrus anvils or shields associated with such convective cells in the upper troposphere extend over a wide area. The ice crystals in such clouds have a lifetime of several hours and can spread by diffusion and advection over distances of a few hundred kilometers. Persistent cirrus cloud layers are known to exist over large regions of the globe (Appleman, 1961; Welch et al., 1980) ranging from thin wisps to a few kilometers in thickness. These cirrus clouds can significantly affect the radiation balance of the earth–atmosphere system and can thus play an important role in the climate of the earth (e.g., Platt, 1981; Liou, 1986). Moreover, since these clouds can spread into thin semitransparent layers, they can lead to significant errors in remote sensing investigations of surface and atmospheric properties.

Satellites can be used to obtain the global distribution of cirrus clouds. Barton (1983) deduced the frequency of occurrence of high-level clouds globally with the help of the near-infrared reflected solar radiation measurements around 2.7 $\mu$m made by the Selective Chopper Radiometer (SCR) on Nimbus-5 satellite. These high-level clouds in the upper troposphere were inferred to be cirrus clouds. Global distribution of high clouds, considered to be cirrus clouds, was also derived from extinction measurements of visible radiation made by the Stratospheric Aerosol and Gas Experiment (Woodbury and McCormick, 1986).

Over the tropical oceans the spectral signature indicating a stronger extinction near 12.6 $\mu$m, as compared to that close to 10.8 $\mu$m, was observed in the data obtained by an Infrared Interferometer Spectrometer (IRIS), having a field of view of ~95 km, on board the Nimbus-4 satellite (Hanel et al., 1972; Curran, 1972). Such data are observed about 100 to 200 km away from the center of thick cold high-altitude clouds. The brightness temperature, near 11 $\mu$m, of such cold clouds was quite often less than 230 K. The ice particles at the top of such cold clouds could spread into thin cirrus layers. In the subtropical subsidence oceanic regions, where primarily low-level warmer clouds occur, this spectral signature is not noticed. Inoue (1985) pointed out the spectral signature described above in the NOAA-7 AVHRR data at 11 and 12 $\mu$m and attributed it to ice crystals in cirrus clouds.

Recent aircraft measurements made by a scanning multichannel radiometer, the Ocean Temperature Scanner (OTS), revealed the same spectral property while flying over thin edges of low-level clouds during a cold air outbreak in winter over the Atlantic Ocean near Wallops Island.

* Present affiliation: C.N.R., Instituto di Fisica dell' Atmosfera, Rome, Italy.

† Present affiliation: NASA Headquarters, Washington D.C.

*Corresponding author address:* Dr. C. Prabhakara, Code 613, Climate & Radiation Branch, Laboratory for Atmospheres, Goddard Space Flight Center, Greenbelt, MD 20771.

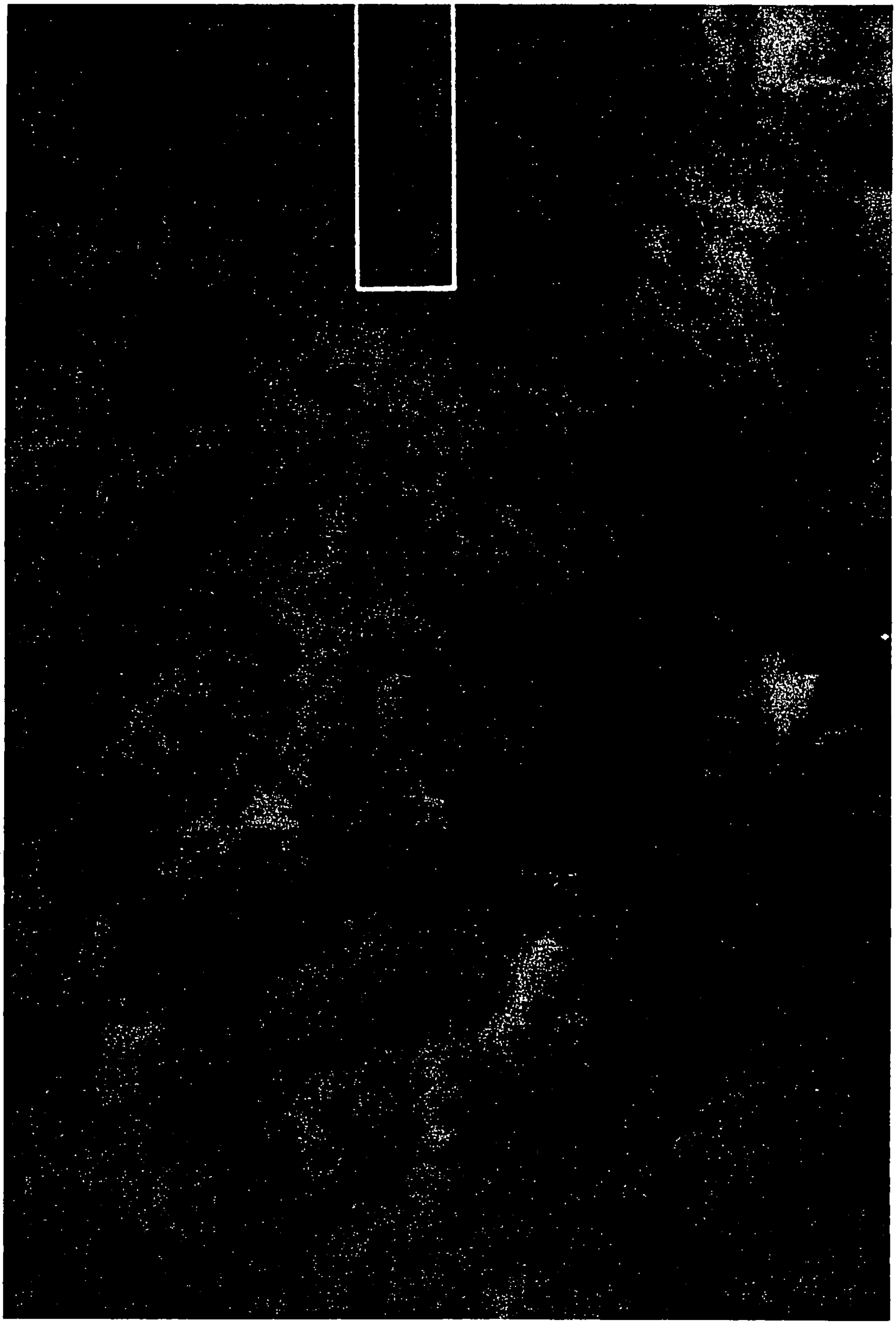

FIG. 1a. Visible image (12 km × 7 km) of clouds over the Atlantic Ocean near 37°N, 73°W on 1400 EST 16 January 1983. Aircraft flight path is from top to bottom along the middle of the image and radiometer scans left to right. The sun is in the south which corresponds to the left of the image. The small inset at the top (∼1600 m × 600 m) of the figure is examined in detail in Figs. 3a, b, c.

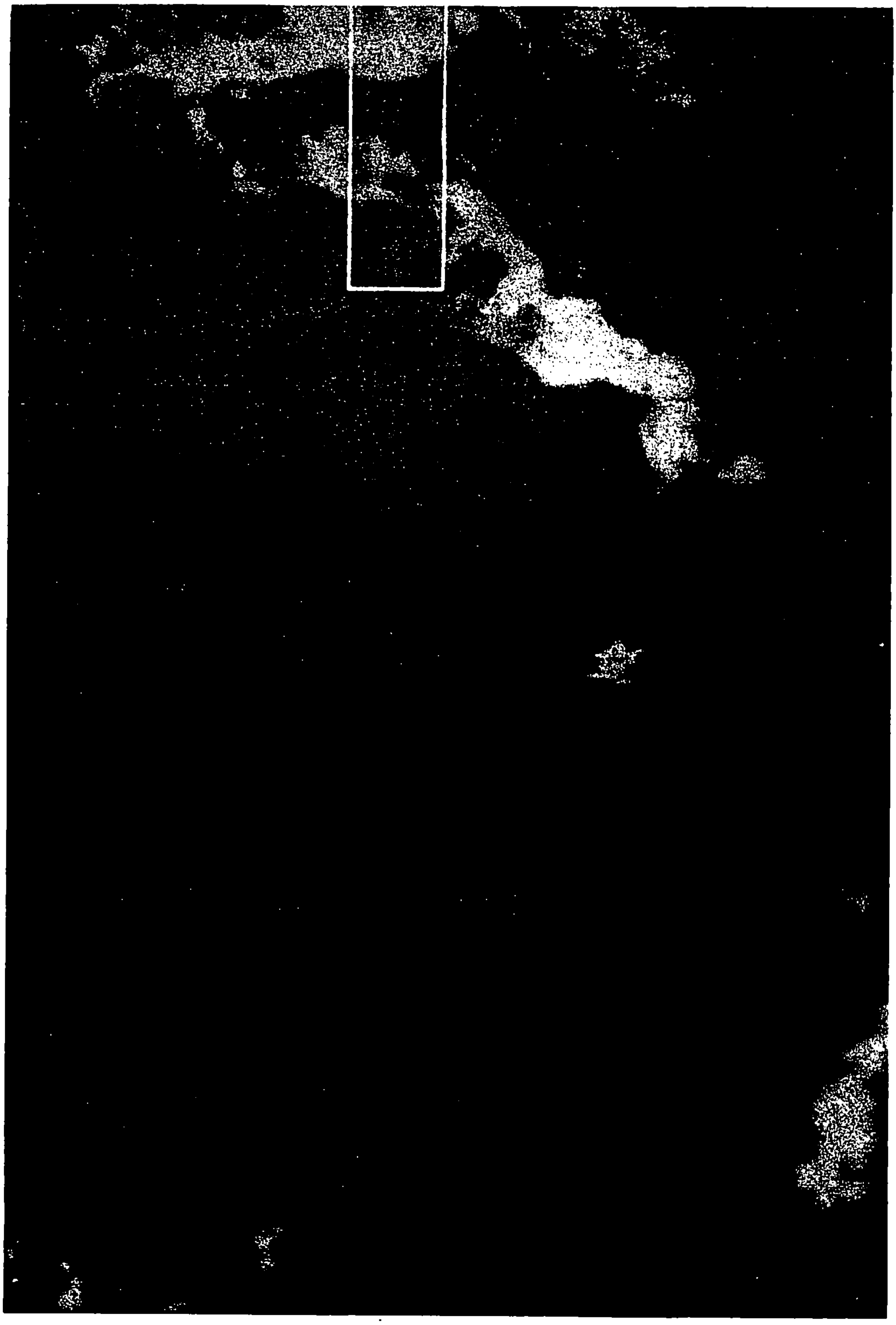

FIG. 1b. Infrared image corresponding to Fig. 1a in the 10.8 $\mu$m channel. The small inset at the top is the same as Fig. 1a.

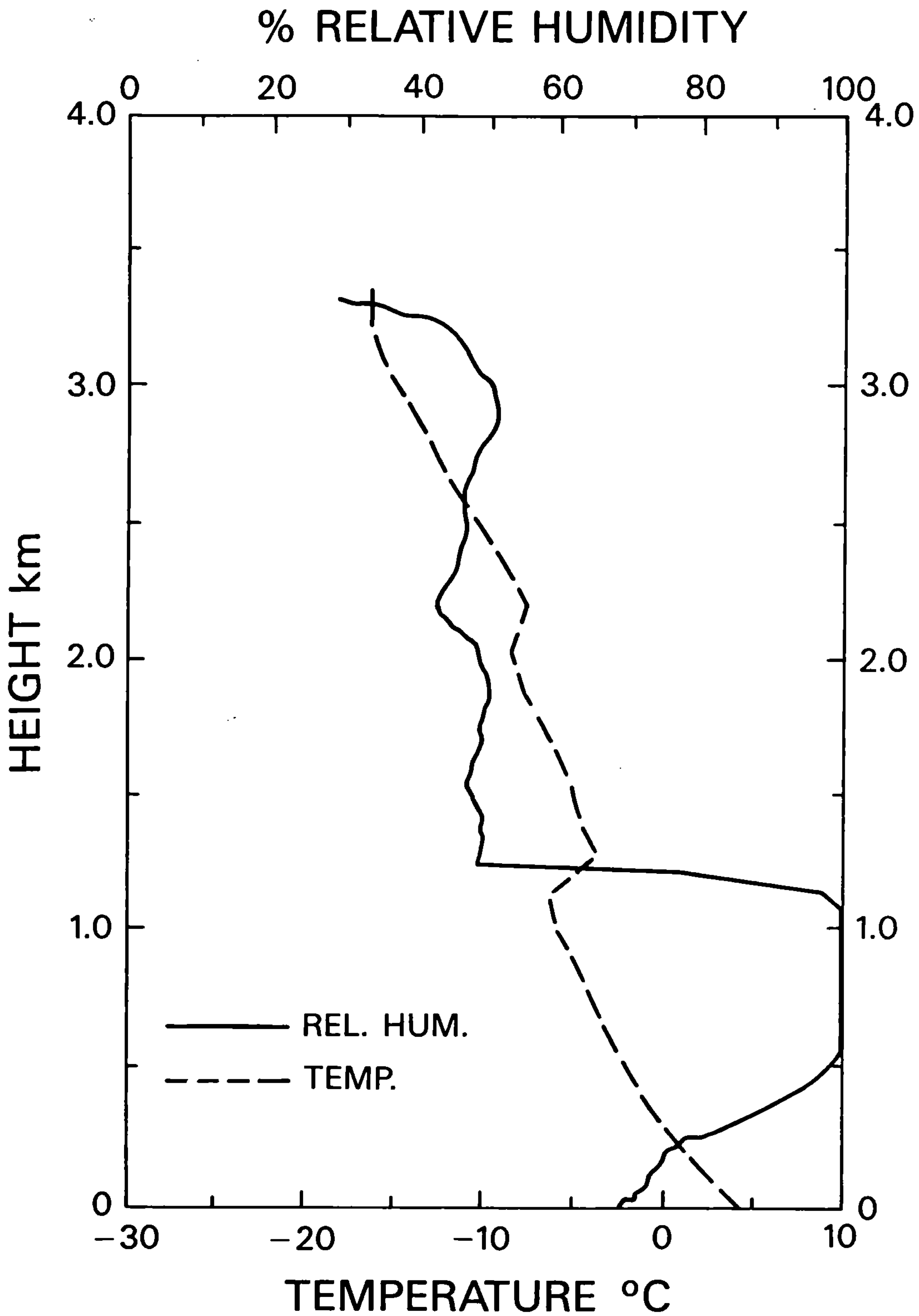


FIG. 2. Vertical soundings of temperature and relative humidity near 37°N nad 73°W on 16 January 1983.

In order to explain the spectral characteristics of these clouds, the volume and, hence, the mass extinction and scattering coefficients of the water and ice particles, as a function of size, are calculated for the two wavelength bands at 10.8 and 12.6 $\mu$m. As both the water and ice particles show similar spectral dependence of extinction, this optical effect could be explained by either water or ice particles as long as the

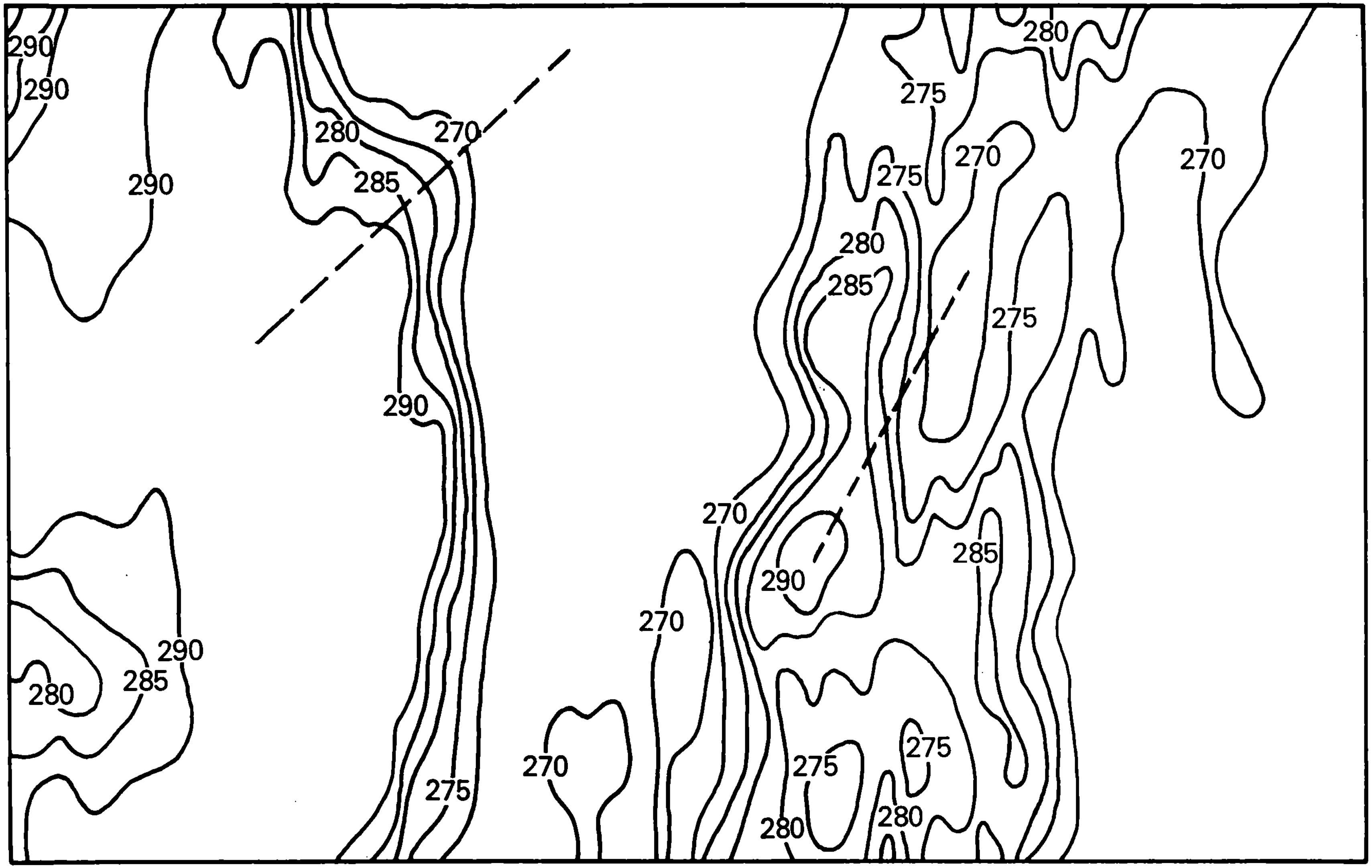


FIG. 3a. The 10.8 $\mu$m brightness temperature distribution in the area corresponding to the inset shown in Fig. 1a.

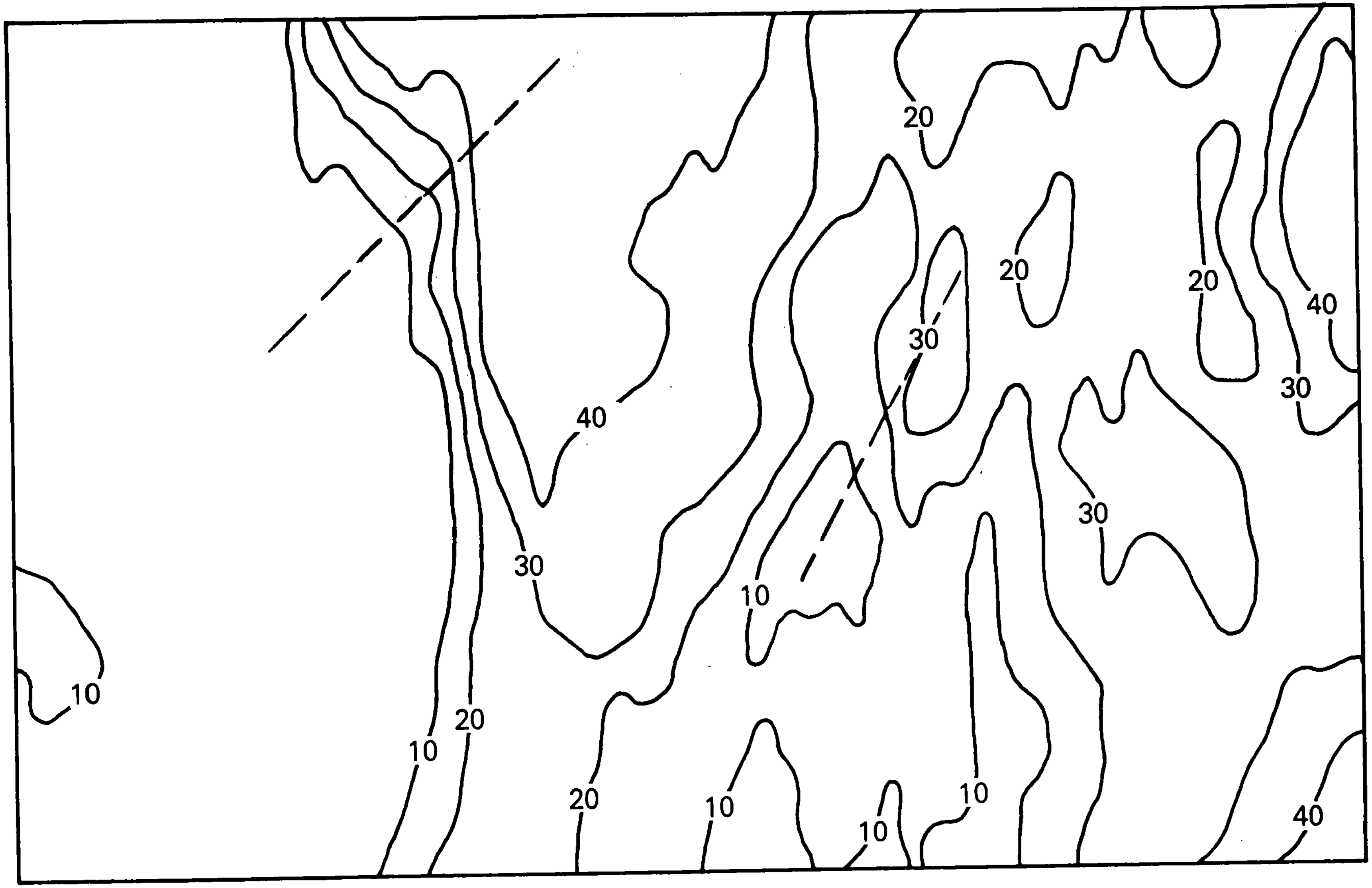


FIG. 3b. As in Fig. 3a but for the visible reflectivity.

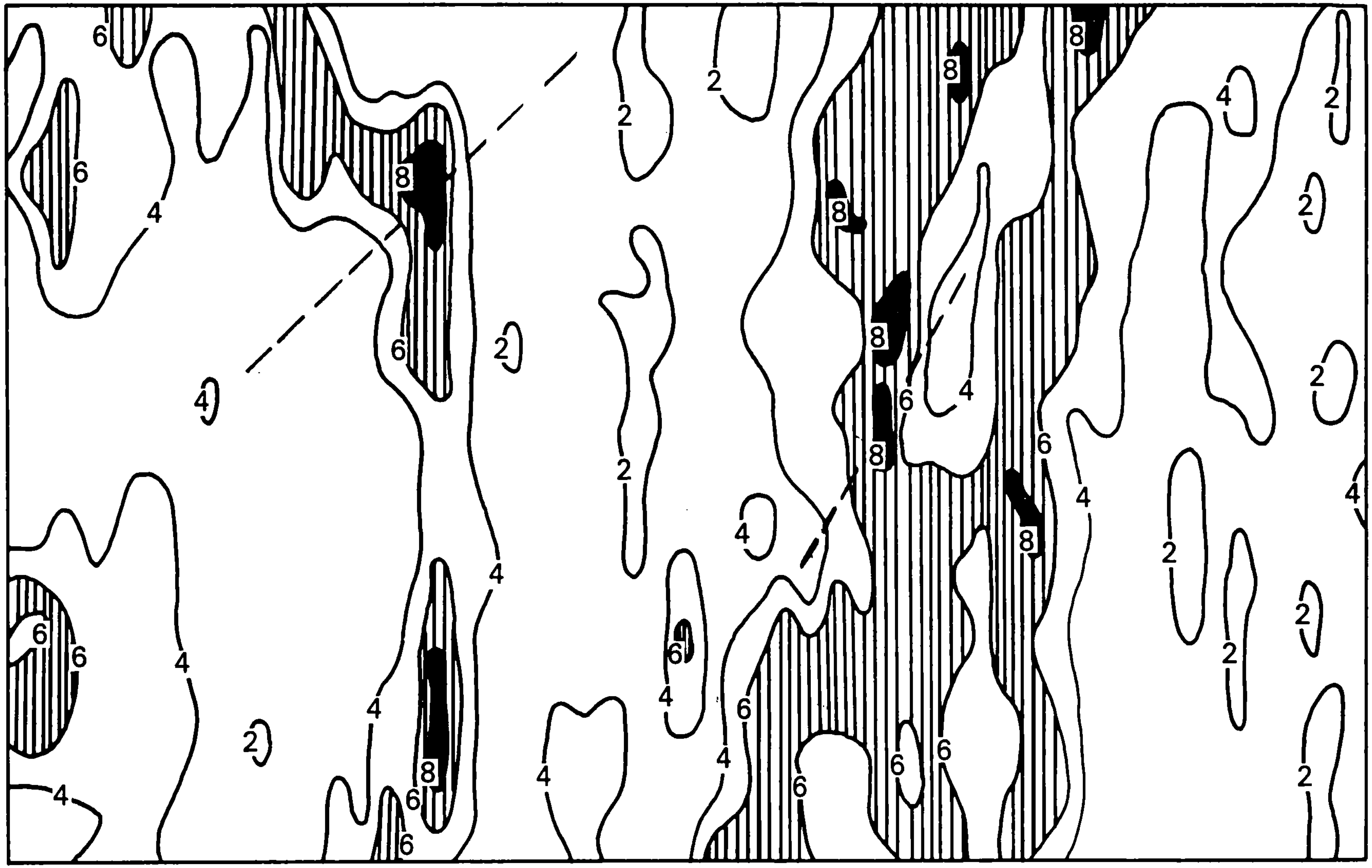

FIG. 3c. As in Fig. 3a but for the brightness temperature difference $\Delta T$ ($= T_{10.8} - T_{12.6}$).

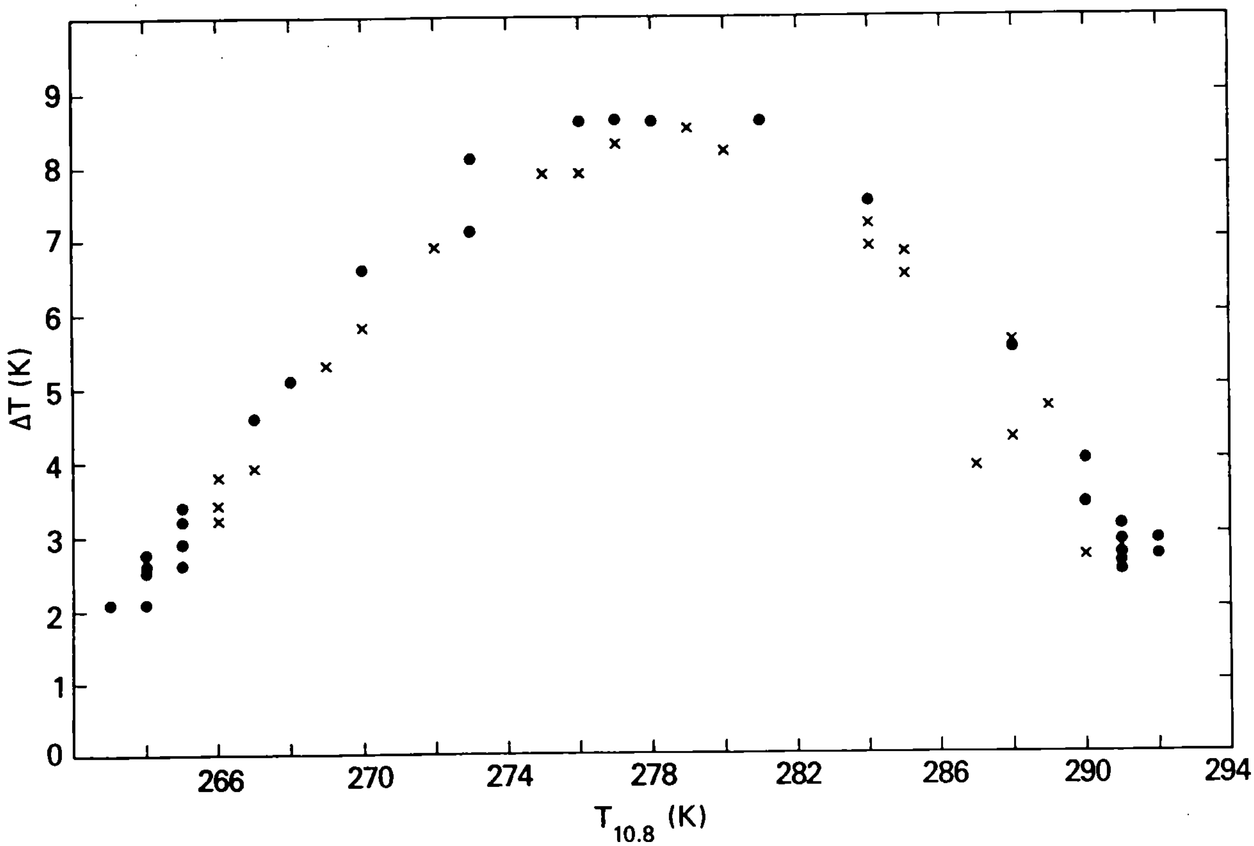


FIG. 4a. Brightness temperature difference, $\Delta T$, vs $T_{10.8}$ along the two cross sections (dashed lines) shown in Figs. 3a, c. Two symbols distinguish the data from two cross sections.

size is smaller than the wavelength of radiation. In the present study, we are demonstrating this spectral feature with the help of radiative transfer calculations to simulate the upwelling brightness temperature at 10.8 and 12.6 $\mu$m as a function of the optical depth and cloud particle size. With this understanding we are utilizing the IRIS window measurements, over the global oceans, to derive mean seasonal maps of optically thin cirrus clouds.

## 2. Aircraft observations

The Ocean Temperature Scanner (OTS) was flown on board an aircraft over the Atlantic Ocean off Wallops Island, Virginia, for the purpose of remote sensing of sea surface temperature (SST). These data were collected as a part of the Mesoscale Air–Sea Interaction Experiment (MASEX) (Melfi et.al., 1985).

The OTS radiometer (Barnes, 1977) had two infrared channels, about 1 $\mu$ wide, centered at 10.8 and 12.6 $\mu$m. In addition, a broad visible channel, 0.5 to 0.9 $\mu$m, was present to observe clouds. The radiometer scanned 30° on either side of nadir and had a spatial resolution of about 25 m at nadir from an altitude of 7 km. The noise equivalent temperature of OTS was about 0.2 K in the infrared channels. In the visible channel, it had a precision of about 0.1% with about 3% uncertainty in absolute value. The instrument was calibrated before the aircraft experiment was conducted and the calibration was checked after the flight.

The OTS data were obtained over the coastal water in the vicinity of 72.7°W and 36.4°N near Wallops Island, which is close to the edge of the Gulf Stream. On the day the data were collected (1400 EST 16 January 1983), there was a cold air outbreak with prevailing winds from the northwest to north over land onto the Atlantic Ocean. Starting from about 50 km away from the coast, cloud streets were present along the direction of the wind. These cloud streets existed at intervals of about 10 km with relatively clear areas separating the adjacent cloud bands.

Figures 1a, b show the visible and infrared (10.8 $\mu$m) images of the OTS data taken near the Gulf Stream from an altitude of about 7 km. The dimensions of the images are about 12 km along the flight path and 7 km across the path. In the visible image, the bright clouds appear white, and clear-sky sea surface appears dark, while in the IR, the warm sea surface appears white and the cold clouds appear dark. These clouds have a wide range in size. They are forming and dissipating in response to rising and sinking motions. The OTS resolution permits us to resolve some of the details

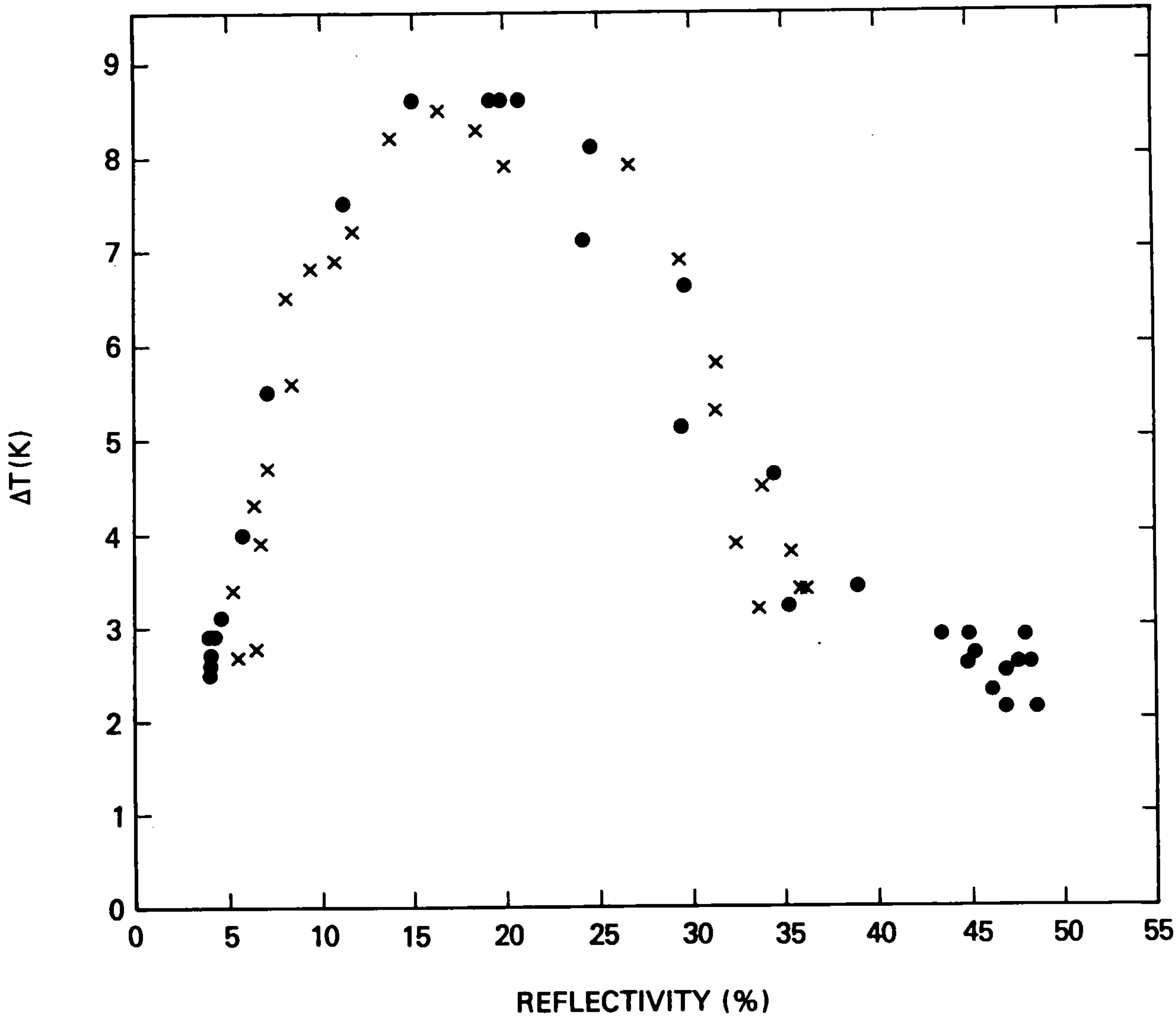


FIG. 4b. Brightness temperature difference $\Delta T$ vs reflectivity along the two dashed lines shown in Figs. 3b, c.

in the clouds. The dropsonde observations made during the MASEX experiment revealed saturated layers of air as shown in Fig. 2, corresponding to the cloud layer, from about 0.6 km to 1.2 km above the sea surface. The vertical temperature profile showed an inversion at the cloud top level with a temperature minimum of about 264 K, while at the cloud bottom the temperature was about 270 K. Knollenberg 2D-C and 2D-P probes flown on the aircraft detected particles larger than 50 $\mu$m, which were essentially snow flakes with some graupel (personal communication, Black)[1] in the clouds. However, from these observations we can not conclude that cloud particles smaller than 50 $\mu$m are ice particles. Water droplets in the small size range could be present.

[1] Robert Black, NOAA, Miami, Florida.

In Figs. 1a, b a small segment, close to nadir view, is identified for more detailed examination of cloud properties. The details of the 10.8 $\mu$m brightness temperature and visible reflectivity corresponding to these segments are shown in Figs. 3a, b. From these figures we see a marked increase in brightness temperature from about 270 to 290 K going from cloudy to clear sky areas, while the reflectivity drops from 40% to about 5%. In order to appreciate the importance of the other window channel at 12.6 $\mu$m, we have constructed Fig. 3c in which the brightness temperature difference $\Delta T$ ($\Delta T = T_{10.8} - T_{12.6}$) of the two infrared channels is shown for the same area.

From Fig. 3c we notice that the difference, $\Delta T$, systematically has large values near the edges of the clouds, sometimes exceeding 8 K. On the other hand, in the warm clear areas as well as cold cloudy areas, the difference is as low as 2 K. This range in $\Delta T$ within short

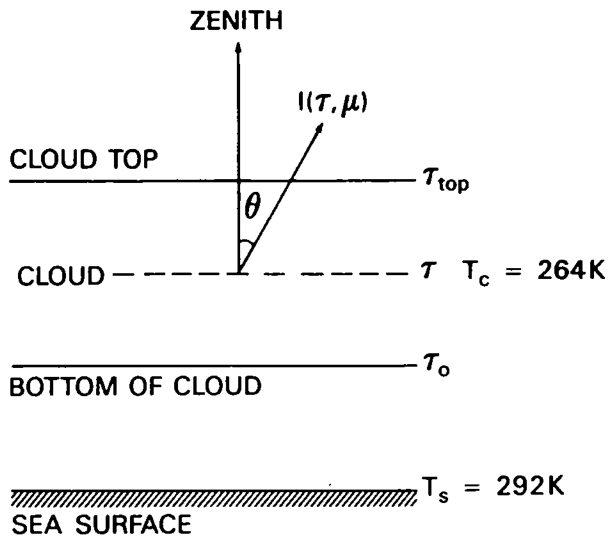


FIG. 5. Schematic diagram of the optical depth $\tau$ and the distribution of the intensity $I$ in the cloud.

distances, of the order of 100 m, cannot be explained in terms of water vapor absorption. This leaves the spectral properties of the cloud particles as a probable cause for this differential absorption.

In order to further illustrate the nature of this phenomenon, plots of $\Delta T$ versus $T_{10.8}$ and $\Delta T$ versus reflectivity are shown in Figs. 4a, b. The plotted data were taken along the cross section indicated by the dashed lines in Figs. 3a–c. From Fig. 4a we notice that $\Delta T$ initially increases as $T_{10.8}$ drops by about 15 K. From Fig. 4b we see that the maximum in $\Delta T$ occurs when the reflectivity has reached a value of about 15%, and this happens in the transition region between clear sky and thick cloud. In this transition region, cloud particles are dissipating rapidly and as a result we expect a decrease in their size and concentration.

## 3. Radiative transfer simulations

Optical properties of ice and water particles as function of particle size, at 10.8 and 12.6 $\mu$m, are similar. Because of this similarity, radiative transfer calculations through water or ice clouds give similar results at these wavelengths. For the reasons given in section 2, the MASEX cloud edges could be composed of ice or water particles smaller than 50 $\mu$m. Although the clouds observed by aircraft are finite in horizontal extent, a plane-parallel atmosphere is assumed in the radiative transfer model. The vertical profiles of temperature and water vapor that are needed for this purpose are shown in Fig. 2. To simplify the problem, the cloud situated between 0.6 and 1.2 km above the sea surface is assumed to be isothermal. The particles in the cloud are assumed to be spherical and in local thermodynamic equilibrium.

The radiative transfer equation may be expressed as (Chandrasekar, 1960)

$$\mu \frac{dI(\tau, \mu)}{d\tau} = I(\tau, \mu) - \frac{\tilde{\omega}}{2} \int_{-1}^{1} I(\tau, \mu') \times P(\mu, \mu') d\mu' - (1 - \tilde{\omega}) B(T_c) \quad (1)$$

where $I(\tau, \mu)$ is the azimuthally averaged intensity at optical depth $\tau$ in the cloud and in a direction $\theta$ with respect to the zenith ($\mu = \cos\theta$), as shown in Fig. 5; $B$ is the Planck function; $T_c$ is the temperature of the cloud, assumed isothermal; $\tilde{\omega}$ is the single scattering albedo; and $P(\mu, \mu')$ is the azimuthally averaged scattering phase function. The optical depth $\tau$ of the cloud is expressed as $\tau = e^{-\int k_e dm}$ where $k_e$ (cm$^2$/g) is the mass extinction cross section and $m$ is the mass of the particles per unit volume.

In solving Eq. (1) we need to specify the mass extinction cross section as well as the single scattering albedo and the phase function. All these parameters depend on the size and shape of the particles. As a first step the volume extinction and scattering coefficients are calculated assuming that there are 100 particles per cm$^3$, spherical in shape, having a size distribution as given by Hansen and Travis (1974). The effective radius $r_{eff}$ ($=\Sigma r_i^3 n_i / \Sigma r_i^2 n_i$, where $n_i$ is the number density in interval $i$) and the effective variance $v_{eff}$ of the drop size determine this distribution. In this study, $v_{eff}$ is assumed to be 0.113. With this information, together with the values of the refractive indices for ice, the parameters stated above are calculated using Mie theory according to a scheme developed by Wiscombe (1980). The volume extinction coefficient $\beta_e$ (km$^{-1}$), the volume scattering coefficient $\beta_s$ (km$^{-1}$), and the single scattering albedo $\tilde{\omega}$ computed in this manner are listed in Table 1 as a function of the effective radius of the particles. Similar calculations are also made for water droplets and are shown in the table for comparison. Then, from these $\beta$s, the mass extinction $k_e$ (cm$^2$/g) and scattering $k_s$ (cm$^2$/g) cross sections, that do not depend on the concentration of the particles, are calculated and are presented in Fig. 6. These coefficients are used in the radiative transfer calculations. Figure 6 shows that when the particles are small compared to wavelength the mass extinction cross section tends to be independent of the size of the particles while for large particles it decreases as $1/r$. Furthermore, the extinction cross sections for the two wavelengths converge for large particles. For small particles, the extinction at 12.6 $\mu$m is about two times as large as that at 10.8 $\mu$m. (See also Table 1.) The extinction curves presented by Bohren and Huffman (1983) for water droplets at 10 and 12.5 $\mu$m vividly reveal these properties for large and small particles.

The other information that is needed to solve (1) for $I(\tau, \mu)$ between the cloud bottom at $\tau = 0$ to cloud top where $\tau = \tau_{top}$, is the upward intensity reaching the bottom of the cloud and the downward intensity incident on the top of the cloud.

The upward intensity reaching the bottom of the cloud $I(0, \mu^+)$ is approximated as follows:

$$I(0, \mu^+) = B(T_s)e^{-k_w w/\mu^+} + B(\bar{T})(1 - e^{-k_w W/\mu^+}) \quad (2)$$

where $T_s$ is the sea surface temperature, $w$ (g/cm$^2$) the total amount of water vapor in a vertical column below the cloud, and $k_w$ (cm$^2$/g) the water vapor absorption coefficient. Based on a study by Prabhakara et al. (1974), the value of $k_w$ at 10.8 and 12.6 $\mu$m is taken as 0.1 and 0.2 cm$^2$/g respectively. Here $\bar{T}$ is the mean radiative temperature of the atmosphere below the cloud, and $\mu^+$ means $0 < \mu < 1$, or $0 < \theta < \pi/2$. It is assumed that the downward intensity $I(\tau_{top}, \mu^-)$ incident at the top of the cloud in the window region is negligible as there is very little water vapor or any other absorbing constituent above the cloud.

With the above boundary conditions, (1) is solved by the method of successive orders of scattering. This method involves the computation of the source function and the intensity using the recursion relationship between them (see e.g., Liou, 1980) for each successive order of scattering. The intensity contributed by a given order of scattering is smaller by a factor of about $\tilde{\omega}$ as compared to that of the preceding order. As $\tilde{\omega}$ is significantly smaller than unity for the particles considered here (see Table 1), the intensity decreases rapidly with increase in order. It is found that after seven orders of scattering, the error in neglecting higher orders amounts to less than 0.5 K in the brightness temperature emerging from the top of the cloud.

With this radiative transfer scheme, the brightness temperature at the top of the cloud for the two wavelength bands, 10.8 and 12.6 $\mu$m is calculated over a range of the effective radius $r_{eff}$ of the particles and the cloud optical depths. To illustrate the results, as an example, the brightness temperatures at nadir calculated for $r_{eff} = 3$ $\mu$m is plotted in Fig. 7 as a function of the optical depth at 10.8 $\mu$m. From this figure we see that when the cloud is optically thin, warm radiation from the surface ($T_s$ = 292 K) and the atmosphere below the cloud emerges through the cloud with very little extinction. However, when the cloud is optically thick, this warm radiation is quenched and what is seen on the top of the cloud is essentially the emission of the cloud at a temperature of 264 K. Furthermore a significant detail emerges from the calculations. When the cloud particles are small and also the cloud optical depth is small, the difference between the brightness temperatures ($\Delta T = T_{10.8} - T_{12.6}$) increases linearly

TABLE 1. Volume extinction cross section $\beta_e$, volume scattering cross section $\beta_s$ and the single scattering albedo $\tilde{\omega}$ ($=\beta_s/\beta_e$) as a function of the effective radius $r_{eff}$ for the two wavelengths 10.8 and 12.6 $\mu$m. For each $r_{eff}$, two values of $\beta_e$, $\beta_s$, $\tilde{\omega}$ are given. The values in the upper line refer to ice and those in the lower line to water.

| | 10.8 $\mu$m | | | 12.6 $\mu$m | | |
|---|---|---|---|---|---|---|
| $r_{eff}$ $\mu$m | $\beta_e$ km$^{-1}$ | $\beta_s$ km$^{-1}$ | $\tilde{\omega}$ | $\beta_e$ km$^{-1}$ | $\beta_s$ km$^{-1}$ | $\tilde{\omega}$ |
| 0.375 | 2.91 (−3)* | 5.02 (−6) | .0017 | 5.18 (−3) | 2.18 (−5) | .0042 |
| | 1.39 (−3) | 4.69 (−6) | .0034 | 3.95 (−3) | 6.77 (−6) | .0017 |
| 0.750 | 2.36 (−2) | 2.83 (−4) | .012 | 4.41 (−2) | 1.32 (−3) | .0299 |
| | 1.16 (−2) | 2.74 (−4) | .024 | 3.20 (−2) | 3.96 (−4) | .0124 |
| 1.500 | 1.89 (−1) | 1.09 (−2) | .058 | 4.03 (−1) | 5.59 (−2) | .138 |
| | 1.05 (−1) | 1.17 (−2) | .111 | 2.59 (−1) | 1.66 (−2) | .0643 |
| 3.000 | 1.43 | 2.19 (−1) | .153 | 3.20 | 9.63 (−1) | .301 |
| | 1.000 | 2.71 (−1) | .271 | 1.921 | 3.38 (−1) | .176 |
| 6.000 | 9.64 | 2.69 | .28 | 1.81 (1) | 7.52 | .42 |
| | 8.952 | 3.941 | .44 | 1.21 (1) | 3.74 | .309 |
| 12.000 | 5.45 (1) | 2.14 (1) | .39 | 7.61 (1) | 3.55 (1) | .47 |
| | 6.28 (1) | 3.40 (1) | .54 | 6.22 (1) | 2.57 (1) | .41 |
| 24.000 | 2.54 (2) | 1.17 (2) | .46 | 2.90 (2) | 1.45 (2) | .50 |
| | 2.93 (2) | 1.57 (2) | .54 | 2.68 (2) | 1.27 (2) | .47 |

* Numbers in parentheses correspond to exponent of 10. Real and imaginary parts of the refractive index are as follows:

$$\text{ice}\begin{cases}10.8\ \mu\text{m}, & n = 1.09 - i0.168\\ 12.6\ \mu\text{m}, & n = 1.40 - i0.415\end{cases}$$

(Warren, 1984)

$$\text{water}\begin{cases}10.8\ \mu\text{m}, & n = 1.168 - i0.0828\\ 12.6\ \mu\text{m}, & n = 1.136 - i0.2710\end{cases}$$

(Downing & Williams, 1975)

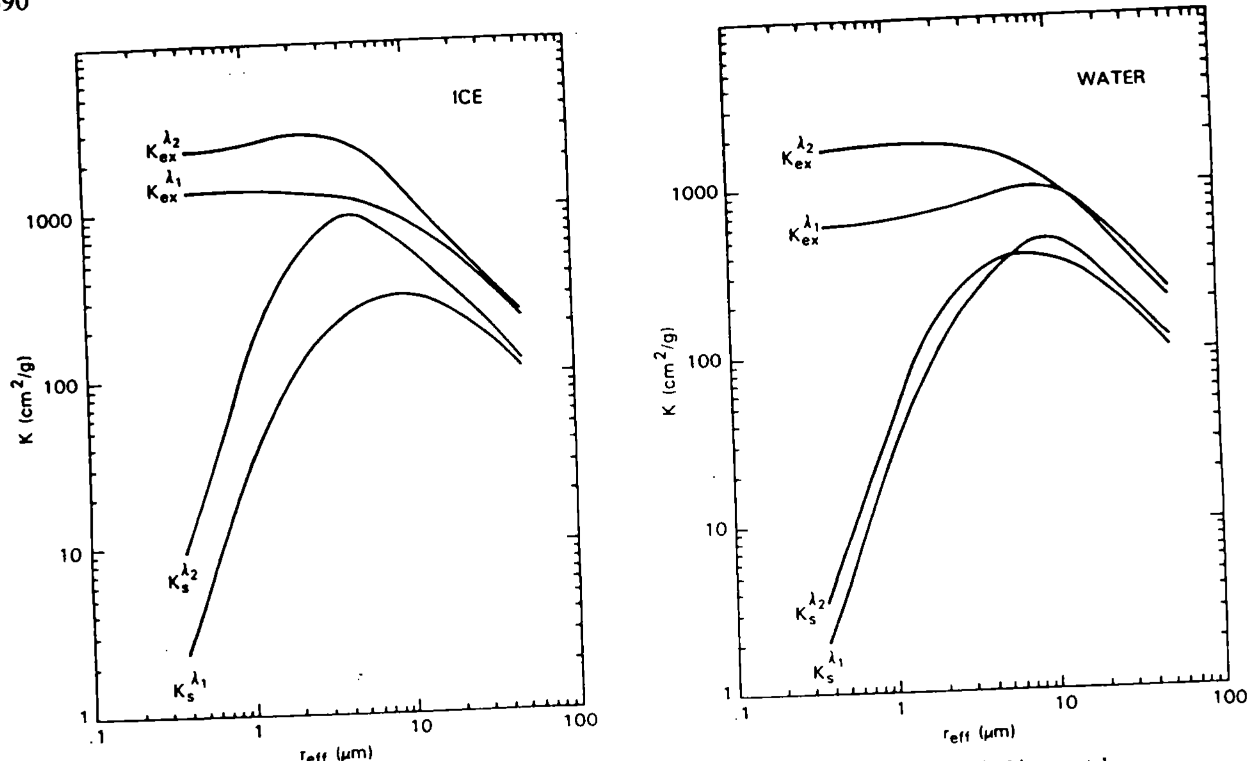


FIG. 6. Extinction cross section $k_e$ and scattering coefficient $k_s$ vs effective radius $r_{eff}$ of spherical ice crystals for the wavelengths $\lambda_1$ = 10.8 and $\lambda_2$ = 12.6 μm.

with the optical depth. This is mainly because the extinction at 12.6 μm is significantly larger for small particles. For these small particles, when the optical depth at 10.8 μm is about unity, $\Delta T$ reaches a maximum value. At larger depths, $T_{10.8}$ and $T_{12.6}$ approach one another and $\Delta T$ decreases.

It is readily noticed from Fig. 7a that the nature of the particles, namely ice or water, does not make a significant difference. This is mainly because the brightness temperature, for each channel, depends strongly on the optical depth and only weakly on the parameter $\tilde{\omega}$ (see Eq. 1) as the scattering and emission by the cloud tend to compensate. Since $\Delta T$ (see Fig. 7b) does not depend critically on the phase of the particles but on the differential opacity between the 10.8 and 12.6 μm channels, from this point on the discussion is limited to spherical ice particles. The nonspherical nature of ice particles modifies the extinction cross section (see e.g., Mugnai and Wiscombe, 1986). Such a modification affects the opacity in these two channels alike. For this reason $\Delta T$, which depends on the differential opacity, is also not significantly altered by the shape of the particles.

The results presented in Fig. 7b can be plotted as a function of $T_{10.8}$ in order to compare with the aircraft results shown in Fig. 4a. This is done in Fig. 8 for various values of the particle size, i.e., $r_{eff}$. It is seen from this figure that when $r_{eff}$ is in the range of 1 to 4 μm, $\Delta T$ approaches a maximum value of about 8.5 K and the corresponding $T_{10.8}$ is 278 K. These values are in reasonable agreement with the aircraft radiometer observations near the edge of the clouds, as shown in Figs. 4a, b.

For particles in the size range of 1 to 4 μm, Mie calculations suggest that the optical depth in the visible region, ~0.75 μm, is about four times larger than the optical depth in the 10.8 μm band (see e.g., Bohren and Huffman, 1983). The reflectivity values as a function of $\Delta T$, shown in Fig. 4b, can be explained with estimates of such visible optical depth (Arking and Childs, 1985). From this figure we see that as $\Delta T$ increases, corresponding to an increase in the infrared optical depth, the reflectivity is increasing. When $\Delta T$ is near maximum, i.e., $\tau_{10.8} \approx 1$, as stated above, $\tau_{vis} \approx 4$. The value of reflectivity of 15% obtained at that point is consistent with $\tau_{vis} = 4$. From this reasoning it appears that small particles, water or ice, in the range of about 1 to 4 μm can explain the infrared and visible measurements made by the aircraft radiometer at the edge of clouds. Large particles could not account for the infrared and visible optical properties in a consistent manner.

## 4. Cirrus observations over oceans from IRIS

An Infrared Interferometer Spectrometer (IRIS) was flown on the Nimbus-4 satellite, which produced spectral data in the 5 to 25 μm range with a resolution of 2.8 cm$^{-1}$ and a noise equivalent temperature of 0.5 K

(Hanel et al., 1972). In Fig. 9 a typical IRIS spectrum over the cloud-free tropical ocean near Guam is shown. These IRIS data can be degraded, by spectral averaging, to simulate the two broadbands of the aircraft radiometer. The position of these two bands is shown in the figure. The difference in brightness temperature between these two bands, namely $\Delta T$, can be examined in the IRIS data.

In Fig. 10, $\Delta T$ deduced from IRIS spectra over the tropical oceans between 10°N to 10°S is shown as a function of $T_{10.8}$. In spite of a large spread in the data we notice that there is a trend indicating a broad maximum in $\Delta T$ around $T_{10.8}$ = 255 K. The observations shown in this figure are qualitatively similar to those shown in Fig. 4a corresponding to low-level clouds of midlatitudes associated with a cold air outbreak. A detailed examination of the IRIS data revealed that generally large $\Delta T$ values occur about 100 to 200 km away from cold (~230 K) high-altitude clouds. When we see a cold brightness temperature at 11 $\mu$m, over a large field of view of 95 km, we can infer the presence of thick cirrus cloud associated with severe convective motions and composed of ice crystals. As these ice particles spread out of the cloud due to wind and diffusion, the large particles settle down soon, gravitationally, leaving the small particles to drift aloft to distances beyond the region of low-level convection. With this background we infer that the large $\Delta T$ values observed in the IRIS data, correspond to outer regions of cirrus. The 11 $\mu$m brightness temperature in these outer regions can be substantially warmer.

In order to understand the IRIS data, radiative transfer calculations were made for the case of an ice crystal cirrus cloud in the upper troposphere. A tropical atmosphere having a sea surface temperature of 300 K and 4 g/cm$^2$ of total water vapor in the atmosphere with a 1 km thick cloud near 9 km altitude at a temperature of 240 K is assumed. The $\Delta T$ obtained from these calculations for different ice particle sizes is shown in Fig. 11. Also, in this figure, $T_{10.8}$ is used as the abscissa instead of the optical depth. From this figure, we notice that $\Delta T$ is much larger for all particle sizes as compared to that of low-level cloud shown in Fig. 8. This is mainly because of the larger contrast in temperature between the surface and the cloud.

When the IRIS data shown in Fig. 10 is compared to the calculations shown in Fig. 11 we notice some disagreement. The computations indicate that the maximum $\Delta T$ occurs when $T_{10.8} \approx 270$ K while the observations suggest a broad maximum near about 255 K. Secondly, the observed $\Delta T$ maximum is considerably smaller than the computed one. Both these features suggest that in the tropics there are often low-level clouds below the cirrus which results in reducing both $\Delta T$ and $T_{10.8}$. Furthermore, the data on $\Delta T$ shown in Fig. 10 suggest that several of the clouds involved were thin cirrus clouds in the tropics that had large $\Delta T$ with $T_{10.8}$ greater than 270 K. According to these calculations, optically thin cirrus clouds, having an optical depth of about 1 at 10.8 $\mu$m contain ice particles in a vertical column amounting to ~$10^{-3}$ g cm$^{-2}$. If we assume the thickness of the clouds is ~1 km, the ice water content is ~$10^{-2}$ g m$^{-3}$, which is reasonable for cirrus clouds (e.g., Heymsfield and Platt, 1984).

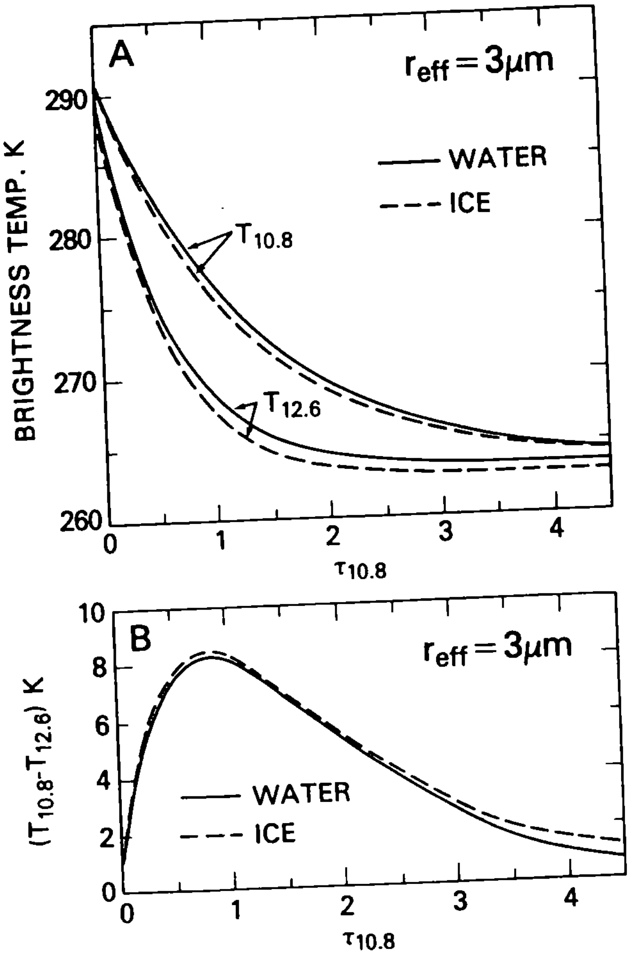


FIG. 7. (a) Upwelling brightness temperature, at 10.8 and 12.6 $\mu$m, through the cloud in the zenith direction as a function of optical depth $\tau_{10.8}$. The effective radius of the water or ice particles in the cloud is 3 $\mu$m. (b) The difference in the brightness temperatures, $\Delta T$, shown in (a) as a function of $\tau_{10.8}$.

In a recent study, Sassen et al. (1985) show that the lower part of cirrus clouds could contain supercooled (~235 K) water droplets, having concentration of about 30 particles per cm$^3$ and mean radius of about 5 $\mu$m. Furthermore, Heymsfield and Platt (1984) find that in the cirrus clouds the contribution to the visible extinction by ice particles in the 2–20 $\mu$m size range could be as much as 53%. Based on these studies, it is plausible to explain the IRIS observations of $\Delta T$, about 100 to 200 km away from high cold clouds, in terms of ice or water particles smaller than the wavelength of radiation.

With this understanding of the IRIS window data, we have produced seasonal maps of thin cirrus clouds

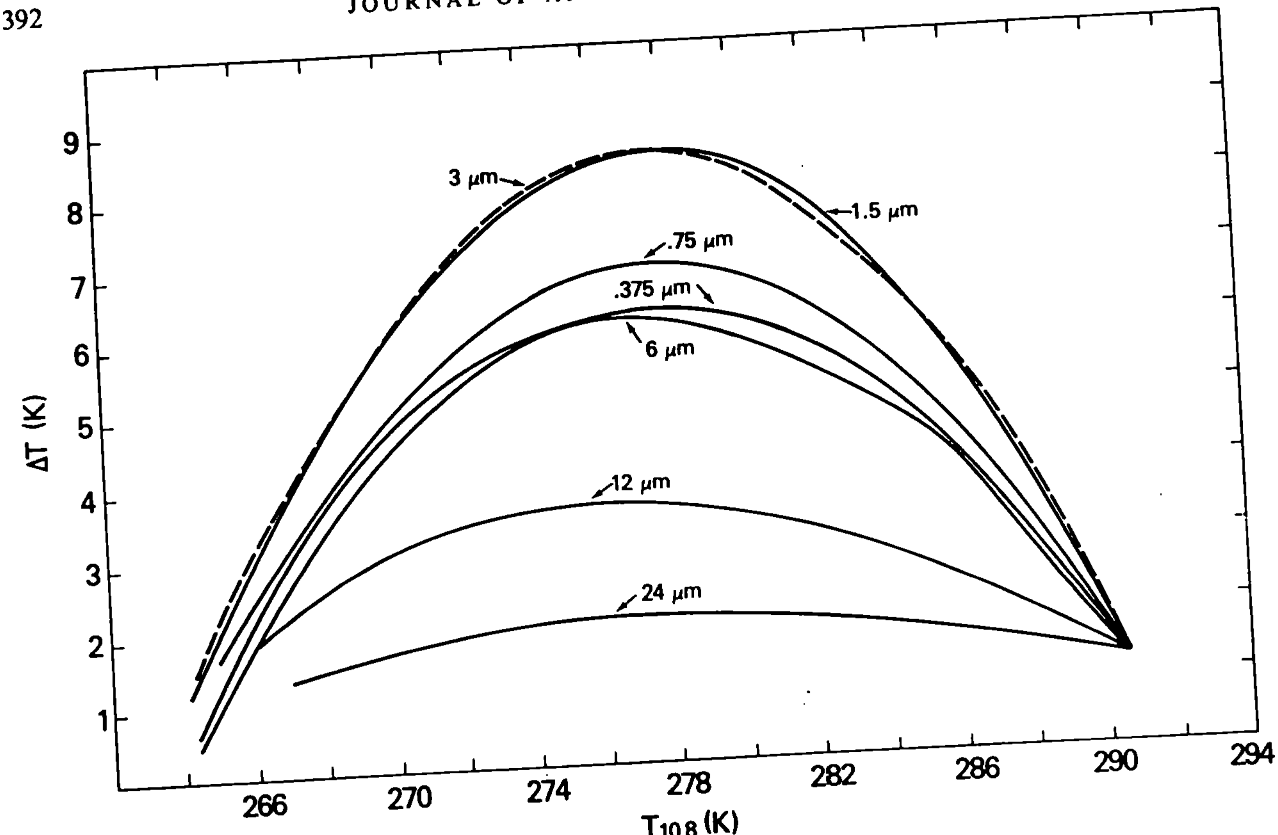


FIG. 8. Theoretical values of $\Delta T$ vs $T_{10.8}$ for low-level spherical ice crystal clouds as a function of particle size.

over the global oceans between 50°N to 50°S with the help of measured $\Delta T$ values. The IRIS is not a scanning instrument and so we have only a limited number of observations to make such maps. Typically, there are about 30 observations in a grid box of 2° lat × 3° long during a period of about 3 months. In order to highlight the effect of thin cirrus clouds, we have selected one of these observations that yields the highest value for $\Delta T$ in a grid box during a season. Four seasonal maps of $\Delta T$ covering the entire life of IRIS from April 1970 to January 1971 are thus produced. These four maps are displayed in Figs. 12a–d. We have noticed in the data selected to produce these maps, that the $T_{10.8}$ was generally warm and only about 10 to 20 K below the expected local sea surface temperature, suggesting that the clouds are optically thin. The magnitude of $\Delta T$ shown in Figs. 12a–d is reduced to about 60% when all available IRIS data for each season are averaged. However, the salient features contained in the maps are not lost.

Interpretation of these seasonal maps in terms of thin cirrus cloud amount is not unequivocal. The $\Delta T$ shown in the maps depends on the cloud amount, its optical thickness and height, and the particle size. Clouds at lower levels may also affect $\Delta T$. However, when we examine the maps it is clear that the convectively active areas, such as the ITCZ, SPCZ, and the Bay of Bengal during the summer monsoon, show a relatively large value of $\Delta T$. The convective storms in such regions are associated with cirrus anvils which could spread into a thin cloud exceeding 100 km in size. From this reasoning the $\Delta T$ shown in the maps is like an index of the optically thin cirrus clouds. In fact the geographic distribution and seasonal variation of the thin cirrus clouds shown in these figures compares well with that of high-level clouds shown by Barton (1983), and Woodbury and McCormick (1986).

## 5. Discussion and conclusions

In the cirrus clouds, large particles can settle down gravitationally in a short time, leaving smaller particles to be dispersed, over a few hours, to distances of about 100 to 200 km. The cirrus that spreads out from the dense storm center thins down toward the edge where the low- and midlevel cloud amount associated with the storm also decreases substantially. The IRIS data that showed appreciable $\Delta T$ are apparently coming from these cirrus cloud edges.

A significant inference from this study is that small particles, ice or water, with an effective radius less than 10 μm are largely present near the edges of the high-altitude clouds such as cirrus. These particles are responsible for the window optical effects discussed in

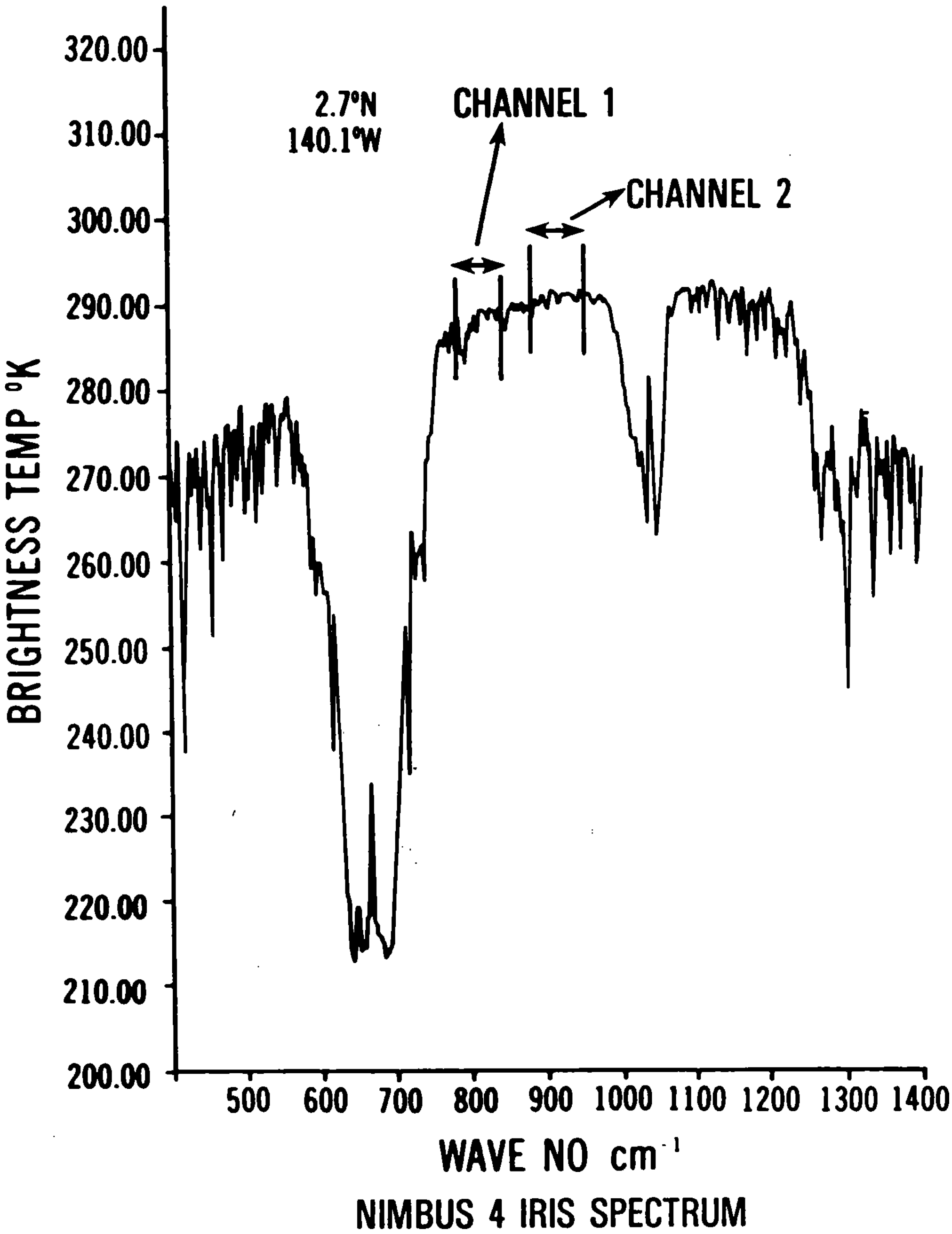


FIG. 9. Nimbus-4 Infrared Interferometer Spectrometer (IRIS) brightness temperature spectrum measured near Guam (2.7°N, 140.1°W) on 27 April 1970. The spectral position of the band centered at 12.6 and 10.8 $\mu$m are shown as channel 1 and 2.

the paper. This inference is in accord with the results of Heymsfield and Platt (1984) and Sassen et al. (1985). Furthermore, in an experimental study by Volkvitskiy et al. (1983) involving artificially generated ice crystal fog in a refrigerated chamber, it was observed that fine crystals of varying shape, with sizes less than 20 $\mu$m, produced spectrally dependent extinction in the window region similar to that reported in this study.

Theoretical calculations indicate that water droplets in the size range of a few microns can also produce infrared spectral effects analogous to that of ice crystals. It should be pointed out here that the results shown in Figs. 12a–d derived from the IRIS data (field of view of 95 km) do not arise from low-level water droplet clouds. The low-level convective clouds tend to be smaller in area and generally will be much heavier in liquid water content and, hence, are optically thick. On the other hand, low-level stratus clouds which can

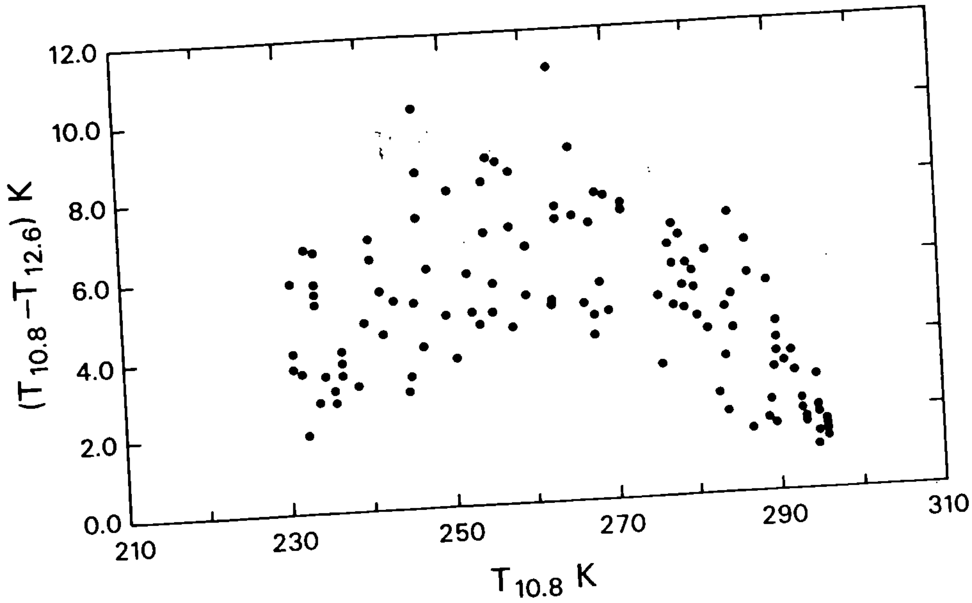


FIG. 10. The temperature difference, $\Delta T$, vs $T_{10.8}$ derived from the IRIS data over the tropical oceans (10°N to 10°S).

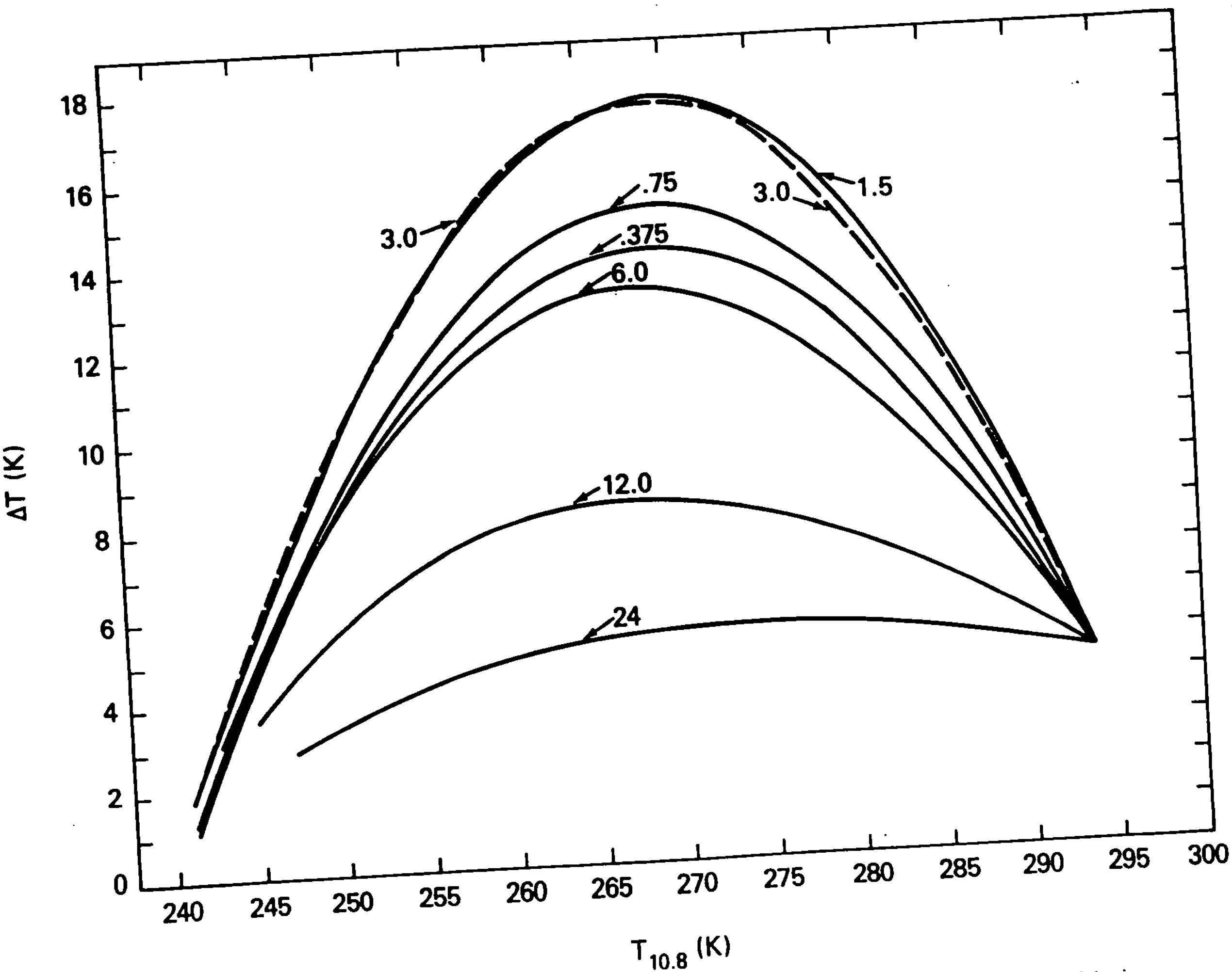


FIG. 11. Theoretical values of $\Delta T$ vs $T_{10.8}$ for high-level (cirrus) spherical ice crystal clouds as a function of particle size.

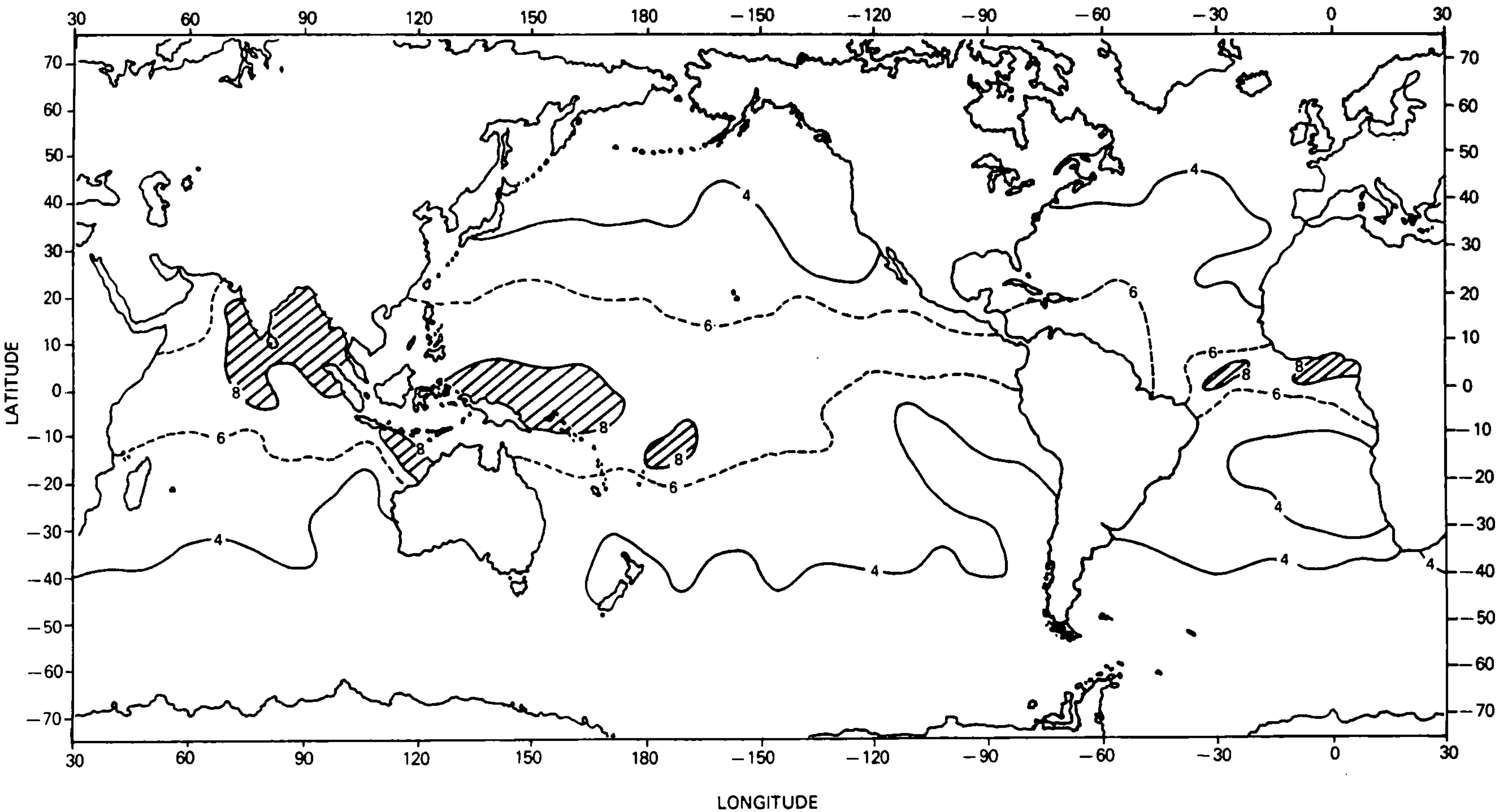


FIG. 12a. Distribution of maximum in $\Delta T$ (K), adopted as an index of the optically thin cirrus clouds, over the global oceans composited for the months April and May 1970.

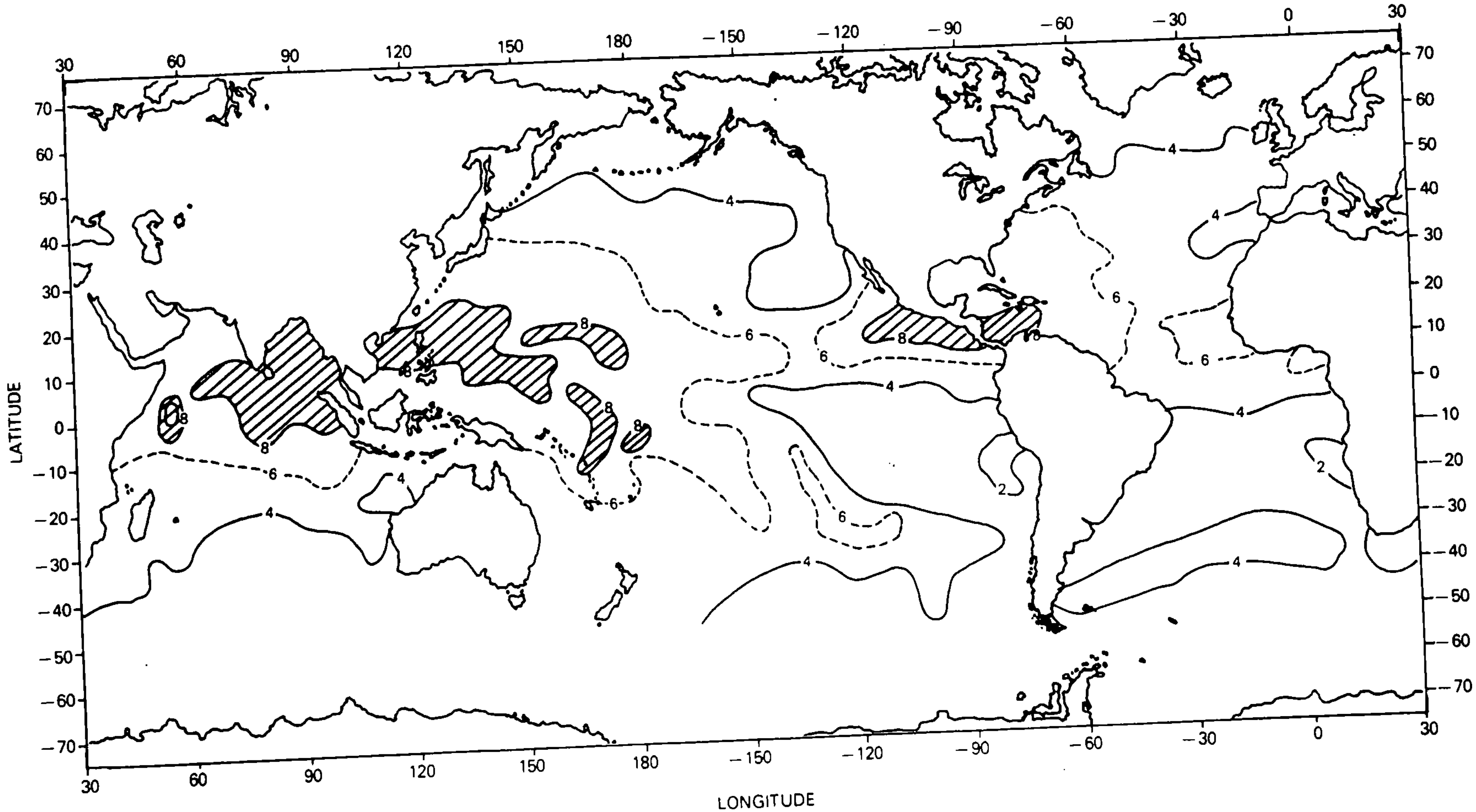


FIG. 12b. As in Fig. 12a but for June, July, and August 1970.

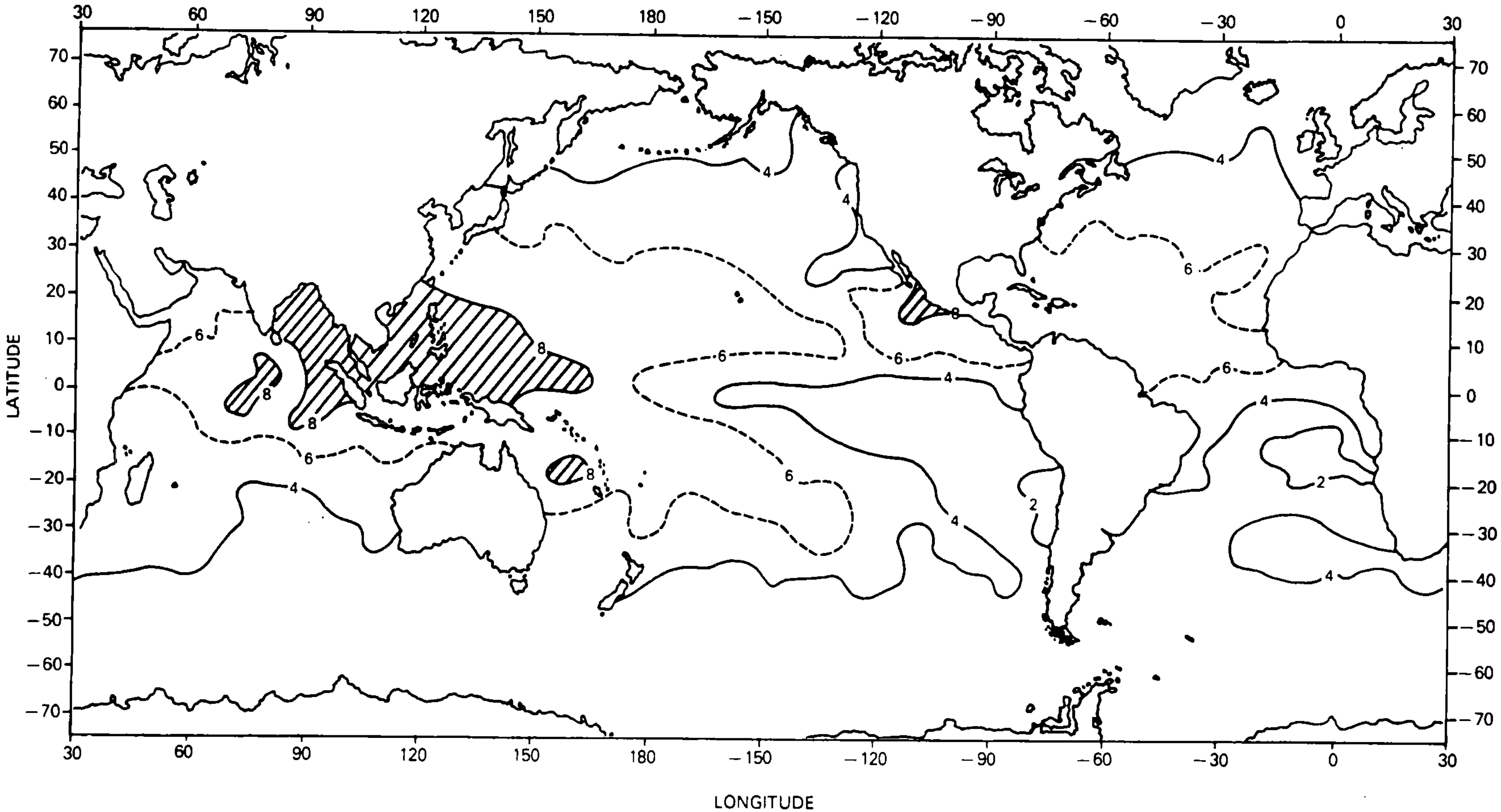


FIG. 12c. As in Fig. 12a but for September, October, and November 1970.

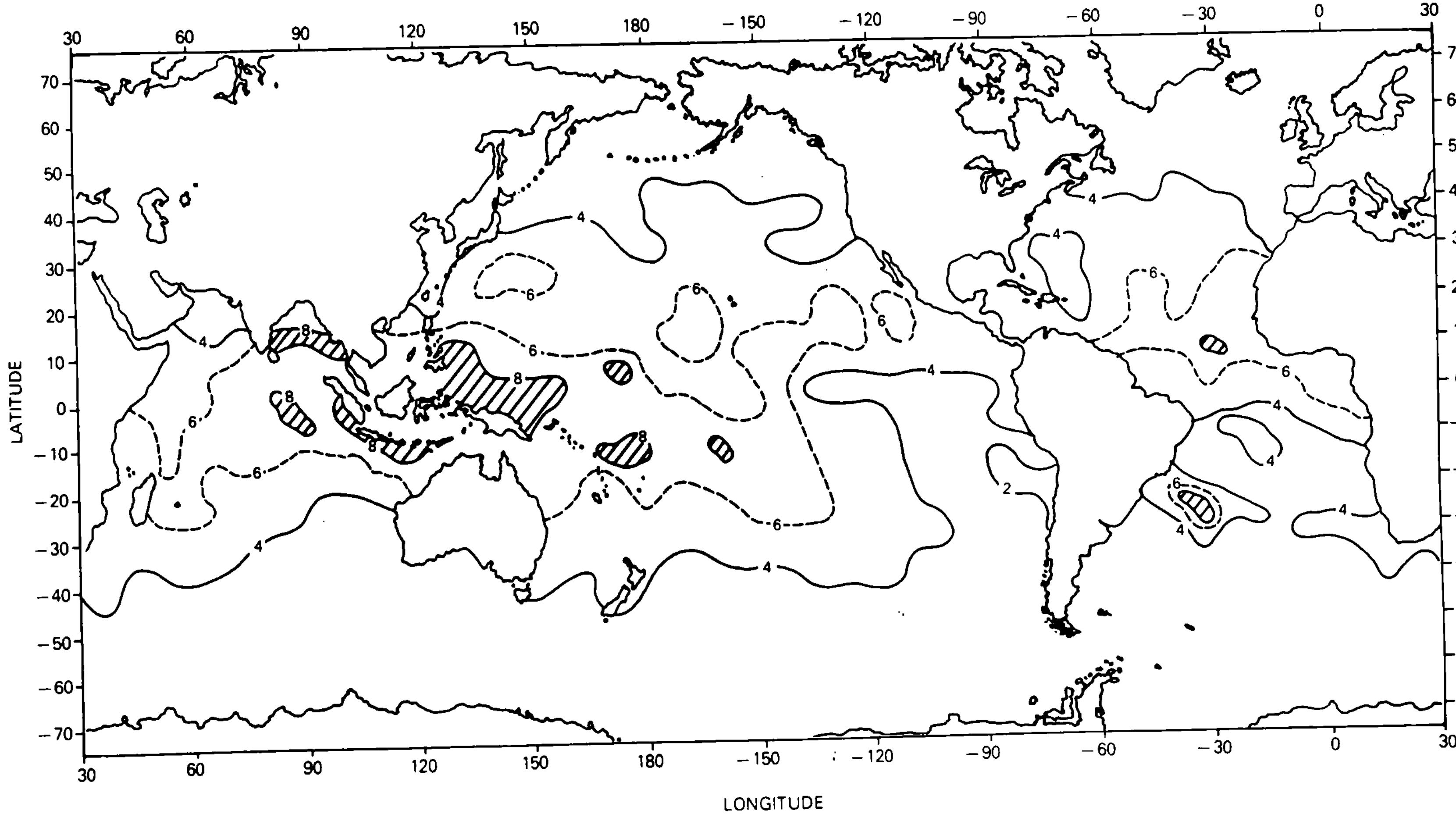


FIG. 12d. As in Fig. 12a but for December 1970 and January 1971.

be extensive in area are present in subsidence regions of the subtropical anticyclones over the oceans. Such stratus clouds could be optically thin. The $\Delta T$ deduced from IRIS data in such areas is not large as shown in Figs. 12a–d. For these reasons we believe that high-level clouds, most likely cirrus, fit the IRIS observations.

Optically thin cirrus clouds can interfere with remote sensing of the atmosphere and surface below them. Particularly the sea surface temperature (SST) sensing, from the split window channels near 11 and 13 $\mu$m (Prabhakara, et al., 1974) can be in error. During the daytime the visible reflectivity of the clouds may be helpful to screen out the cloud contaminated data (McClain et al., 1982). But at night when the infrared data is the principal means to sense SST, thin cirrus clouds can introduce errors.

Global information on optically thin clouds, which enhance the greenhouse effect, will be valuable for climate studies (Liou, 1986).

*Acknowledgments.* We are thankful to the late Mr. John Semyan for his help in obtaining the Ocean Temperature Scanner (OTS) data during the MASEX field experiment. We thank Mr. Lamdin R. Blaine for the helpful discussions pertaining to the calibration of OTS instrument and we are thankful to Mr. Robert Black of NOAA, Miami, for providing us the analysis and interpretation of the Knollenberg 2D probe data obtained during MASEX.

REFERENCES

Appleman, H. S., 1961: Occurrence and forecasting of cirrostratus clouds. World Met. Org., 109–47, Technical Note 40.

Arking, A., and J. D. Childs, 1985: Retrieval of cloud cover parameters from multi-spectral satellite images. *J. Climate Appl. Meteor.*, **24,** 322–333.

Barnes, W. L., 1977: Ocean temperature scanner experiment. NASA/Goddard Space Flight Center, Report No. X-941-77-94, p. 46.

Barton, I. J., 1983: Upper level cloud climatology from an orbiting satellite. *J. Atmos. Sci.*, **40,** 435–447.

Bohren, C. F., and D. R. Huffman, 1983: *Absorption and scattering of light by small particles.* John Wiley & Sons, p. 309.

Chandrasekar, S., 1960: *Radiative transfer.* New York, Dover, Inc.

Curran, R. J., 1972: Variation of cloud emissivity in the infrared. *Proc. of the Conference on Atmospheric Radiation,* Amer. Met. Soc., Fort Collins, Aug. 7-9, pp. 103–107.

Downing, H. D., and D. Williams, 1975: Optical constants of water in the infrared. *J. Geophys. Res.*, **80,** 1656–1661.

Hanel, R. A., B. J. Conrath, V. G. Kunde, C. Prabhakara, I. Revah, V. V. Salomonson and G. Wolford, 1972: The Nimbus 4 infrared spectroscopy Experiment 1. Calibrated thermal emission spectra. *J. Geophys. Res.*, **77,** 2629.

Hansen, J. E., and L. D. Travis, 1974: Light scattering in planetary atmospheres. *Space Science Reviews,* **16,** 527–610.

Heymsfield, A. J., and C. M. R. Platt, 1984: A parameterization of the particle size spectrum of ice clouds in terms of ambient temperature and the ice water content. *J. Atmos. Sci.*, **41,** 846–855.

Inoue, T., 1985: On the temperature and effective emissivity determination of semi-transparant cirrus clouds by bi-spectral measurements in the 10 $\mu$m window region. *J. Met. Soc. Japan.* **63,** 88–89.

Liou, K., 1980: *An introduction to atmospheric radiation.* Academic Press, 1-392.

——, 1986: Influence of cirrus clouds on weather and climate processes: A global perspective. *Mon. Wea. Rev.*, **114,** 1167–1199.

McClain, E. P., W. G. Pichel, C. C. Walton, Z. Ahmed and J. Sutten, 1982: Multichannel improvements to satellite-derived global sea surface temperatures. *Proc. of XXIV COSPAR,* Ottawa, Canada, May, pp. 22–29.

Melfi, S. H., J. D. Spinhirne, Shu-Hsien Chou and S. Palm, 1985: Lidar observations of vertically organized convection in the planetary boundary layer over the ocean. *J. Climate Appl. Meteor.*, **24,** 806–821.

Mugnai, A., and W. J. Wiscombe, 1986: Scattering from nonspherical chebyshev particles. I: Cross sections, single scattering albedo, asymmetry factor, and backscattered fraction. *Appl. Opt.*, **25,** 1235–1244.

Platt, C. M. R., 1981: The effect of cirrus of varying optical depth on the extra terrestrial net radiation flux. *Quart. J. Roy. Meteor. Soc.*, **107,** 671–678.

Prabhakara, C., G. Dalu and V. G. Kunde, 1974: Estimating of sea surface temperature from remote sensing in the 11 to 13 $\mu$m window region. *J. Geophys. Res.*, **79,** 5039–5044.

Sassen, K., K. N. Liou, S. Kinne and M. Griffin, 1985: Highly supercooled cirrus cloud water: Confirmation and climatic implications. *Science,* **227,** 411–413.

Volkovitskiy, O. A., V. V. Kuznetsov, L. N. Pavlova, A. G. Petrushin and G. F. Yaskevich, 1983: Investigation of the spectral transmission of a crystal fog. Izvestiya, Academy of Sciences. USSR, *Atmospheric and Oceanic Physics,* **19,** 368–372.

Warren, S. G., 1984: Optical constants of ice from the ultraviolet to the microwave. *Appl. Opt.*, **23,** 1206–1225.

Welch, R. M., S. K. Cox and J. M. Davies, 1980: Solar radiation and clouds. *Meteorological Monographs,* **17,** 39, Amer. Met. Soc., Boston, MA, p. 96.

Wiscombe, W. J., 1980: Improved Mie scattering algorithm. *Appl. Optics,* **19,** 1505–1507.

Woodbury, G. E., and M. P. McCormick, 1986: Zonal and geographic distribution of cirrus clouds determined from SAGE data. *J. Geophys. Res.*, **91,** 2775–2785.

# Clinton Presidential Records
# Digital Records Marker

This is not a presidential record. This is used as an administrative marker by the William J. Clinton Presidential Library Staff.

This marker identifies the place of a publication.

Publications have not been scanned in their entirety for the purpose of digitization. To see the full publication please search online or visit the Clinton Presidential Library's Research Room.

Reprinted from JOURNAL OF APPLIED METEOROLOGY, Vol. 29, No. 12, December 1990
American Meteorological Society

# Deep Optically Thin Cirrus Clouds in the Polar Regions. Part I: Infrared Extinction Characteristics

C. PRABHAKARA, JUNG-MOON YOO*, GIUSEPPE DALU** AND R. S. FRASER

*NASA/Goddard Space Flight Center, Greenbelt, Maryland*

(Manuscript received 12 September 1989, in final form 26 July 1990)

ABSTRACT

The spectral data obtained by the Infrared Interferometer Spectrometer (IRIS) flown on Nimbus 4 satellite in 1970 indicated the existence of optically thin ice clouds in the upper troposphere that probably extended into lower stratosphere, in the polar regions, during winter and early spring. The spectral features of these clouds differ somewhat from that of the optically thin cirrus clouds in the tropics. From theoretical simulation of the infrared spectra in the 8–25 $\mu$m region, we infer that these polar clouds have a vertical stratification in particle size, with larger particles ($\sim$12 $\mu$m) in the bottom of the cloud and smaller ones ($\leq$1 $\mu$m) aloft. Radiative transfer calculations also suggest that the equivalent ice-water content of these polar clouds is of the order of 1 mg cm$^{-2}$.

## 1. Introduction

Infrared Interferometer Spectrometer (IRIS) (Hanel et al. 1972) flown on Nimbus 4 satellite revealed spectral properties of the optically thin cirrus clouds in the upper troposphere. In the tropics the 10–13 $\mu$m infrared (IR) window region of the IRIS spectrum shows these properties quite vividly (Hanel et al. 1972; Curran 1972). Prabhakara et al. (1988) (called PFDWCS hereafter) accounted for these spectral features utilizing the extinction characteristics of small ice and/or supercooled water particles, present in the clouds, having an equivalent radius of about 5 $\mu$m. On the basis of the IRIS observations PFDWCS inferred that these thin cirrus clouds arise from the spreading of the anvil clouds associated with deep convective storms in the tropics. That study was limited to 50°N and 50°S excluding the polar regions.

Further examination of the IRIS data extending to its north and south limits, i.e., 80°N and 80°S, revealed unexpectedly the presence of optically thin upper tropospheric ice clouds with possible extension into the lower stratosphere in the polar regions. These clouds show infrared spectral features that are somewhat different from the tropical ones. In this investigation these spectral features are illustrated with the help of the IRIS observations and explained theoretically.

The polar stratospheric clouds (PSCs) have been studied extensively (see, McCormick et al. 1982; Steele et al. 1983). The possible role played by these PSCs and the ice particles associated with them in the formation of the ozone hole (Schoeberl and Krueger, 1986) is currently a subject of keen interest. Since the PSCs are observed approximately in the same seasonal time frame, winter and early spring, as the polar cirrus reported in this study one would like to know the connection between these two cloud systems.

The study of these apparently deep polar cirrus clouds is presented in two parts. In this part I the extinction properties of the clouds are examined with the help of radiative transfer theory. In a companion paper part II, the meteorological aspects of these clouds are presented.

## 2. IRIS observations

IRIS had a field of view of $\sim$100 km and covered the spectral region $\nu$ = 400 to 1500 cm$^{-1}$ with a resolution of 2.8 cm$^{-1}$. The noise in the data amounted to about $0.5 \times 10^{-7}$ W cm$^{-2}$ sr$^{-1}$ cm$^{-1}$. With this capability one could examine the spectral data of high altitude clouds which tend to be cold, within an accuracy of $\sim$2K in brightness temperature up to $\sim$1200 cm$^{-1}$. At higher frequencies this error increases. For this reason the data are not presented beyond 1200 cm$^{-1}$. IRIS is a nadir viewing instrument and not a scanner. The broad spectral coverage of the IRIS with fine resolution helps us considerably in the examination of the spectral properties of clouds over the global oceans including the polar regions in winter. To demonstrate this, in appendix A IRIS spectra attributable to clear sky, and optically thick and thin clouds, over oceans at widely

* Applied Research Corporation, Landover, Maryland.
** C.N.R. Istituto di Fisica dell' Atmosfera, Rome, Italy.

*Corresponding author address:* Dr. C. Prabhakara, Code 613, NASA/Goddard Space Flight Center, Greenbelt, MD 20771

# Optically Thin Cirrus Clouds over Oceans and Possible Impact on SST of Warm Pool in Western Pacific

C. Prabhakara, J.-M. Yoo[1], G. Dalu[2] and D. P. Kratz[3]

*Laboratory for Atmospheres*

*NASA/Goddard Space Flight Center*

*Greenbelt, Maryland 20771*

July 1991

[1]Applied Research Corporation, Landover, MD 20785

[2]C.N.R., Istituto di Fisica dell' Atmosfera, Rome, Italy

[3]Universities Space Research Association, Columbia, MD 21044

## Abstract

Over the convectively active tropical ocean regions, the measurements made from space in the infrared and visible have revealed the presence of optically thin cirrus clouds, which are quite transparent in the visible and nearly opaque in the infrared. The Nimbus-4 Infrared Interferometer Spectrometer (IRIS), which has a FOV of $\approx$100 km, has been utilized to examine the infrared optical characteristics of these cirrus clouds. From the IRIS data, it has been observed that these optically thin cirrus clouds prevail extensively over the 'warm pool' region of the equatorial western Pacific, surrounding Indonesia. It is found that the seasonal cloud cover due to these thin cirrus exceeds 50% near the central regions of the 'warm pool'. For most of these clouds the optical thickness in the infrared is $\leq 2$. It is deduced that the dense cold anvil clouds associated with deep convection spread extensively and are responsible for the formation of the thin cirrus. This is supported by the observation that the coverage of the dense anvil clouds is an order of magnitude less than that of the thin cirrus. From these observations together with a simple radiative-convective model, it is inferred that the optically thin cirrus can provide a greenhouse effect which can be a significant factor in maintaining the 'warm pool'. In the absence of fluid transports, it is found that these cirrus clouds could lead to a runaway greenhouse effect. The presence of fluid transport processess, however, act to moderate this effect. Thus, if a modest 20 W/m$^2$ energy input is considered to be available to warm the ocean, then it is found that the ocean mixed-layer of 50 meters depth will be heated by $\approx 1°$C in 100 days.

## 1. Introduction

The 'warm pool' area, located in the equatorial western Pacific, has sea surface temperatures which exceed about 28°C in all seasons. As revealed by satellite measurements, the 'warm pool' region is usually cloud covered (Garcia, 1985) and is characterized by low values of the outgoing longwave radiation (OLR), $\approx 200$ W/m$^2$. Moreover, in the 'warm pool' region the net radiation, the solar incoming minus OLR, at the top of the atmosphere is $\approx 80$ W/m$^2$ (Barkstrom et al., 1989). Another remarkable aspect of this region is that there is on the average about 10 mm/day of rain (Dorman and Bourke, 1979). By combining this salient information together with a knowledge of the transports prevailing in the atmosphere and the ocean up to a depth of the thermocline, it is possible to explain how the elevated temperatures in the 'warm pool' are maintained. The errors in the estimation of the various energy processes at present, however, are such that it is difficult to draw definitive conclusions. To resolve this situation, the TOGA COARE (World Climate Research Program, 1989) program will make extensive measurements to help improve our understanding of the energy budget.

The purpose of the present study is to introduce a new mechanism, namely the radiative effects of thin cirrus clouds, to explain the energy balance of the 'warm pool' region. The available evidence indicates that the impact of the thin cirrus clouds is to radiatively produce a local heat source which appears to be a significant factor in maintaining the 'warm pool'.

Several studies (e.g., Platt, 1989; Ramanathan et al., 1989; Stephens, 1980) have discussed the role of clouds in the atmosphere as regulators of the radiative energy balance. From observations, it has been deduced that clouds found primarily at low altitudes, such as stratiform clouds in the boundary layer, lead to a net cooling since they reflect a significant percentage of the incoming solar energy while radiating to space in the infrared at fairly warm temperatures (Stephens and Webster, 1981). The high altitude cirrus and cirrostratus clouds, however, radiate to space in the IR at a much cooler temperature which can result in a net warming. In the context of the global warming due to increase in $CO_2$ and other trace gases, the role of the clouds in the atmosphere must be understood and properly taken into consideration.

Satellite observations in the infrared and visible (e.g., Hanel et al., 1972; Prabhakara et al., 1988; Inoue, 1985; Stowe et al., 1989) have revealed some of the interesting properties of the cold high altitude cirrus clouds which prevail over the warm pool. Other studies (Stephens, 1980; Platt et al., 1987) have also discussed the nature of the optically thin cirrus clouds. Platt et al. (1987) suggest that in the cold upper tropospheric regions, where there are small amounts of water vapor, the optically thin cirrus clouds present tend to be fairly transparent to incoming solar radiation while being nearly opaque to the outgoing infrared. These optical properties of the thin cirrus clouds have the potential to lead to a greenhouse warming. To date, the extent to which such a greenhouse warming is affecting the earth has not been assessed because of the lack of data concerned with the geographic extent of the thin cirrus and their infrared optical depth. Based on a recent study (Prabhakara et al., 1988) it is now possible to derive the necessary information from the data obtained by the Infrared Interferometer Spectrometer (IRIS) that was flown on Nimbus 4 satellite in 1970.

A brief account of the IRIS and a method to estimate the thin cirrus information is presented in section 2. A simple radiative convective model that is applicable to the mesoscale convective systems in the 'warm pool' is developed in section 3. This radiative convective model, which does not explicitly take into account the transports, allows us to estimate the net heating in the presence of thin cirrus clouds.

## 2. Satellite observations of thin cirrus

The IRIS on board Nimbus 4 provided valuable data for about 10 months: April 1970 to January 1971. This spectrometer viewed the earth at nadir with a field of view of about 100 km and had a spectral resolution of 2.8 $cm^{-1}$ in the IR region, 7 to 25 $\mu$m (see Hanel et al., 1972 for more details on IRIS). In a study based on these high resolution IRIS data, Prabhakara et al. (1988) (hereafter called PFDWCS) inferred the presence of optically thin cirrus clouds over the convective areas of the oceans namely the 'warm pool' region, the ITCZ (Intertropical Convergence Zone) and the SPCZ (South Pacific Convergence Zone).

From the IRIS observations it is deduced that the thin cirrus clouds have a spatial scale of about a few hundred kilometers. Based on these observations, one can also infer that these thin cirrus clouds result from the spreading of the thick anvil clouds that have cold tops of $\approx$ 220 K. The scale of these complex cloud structures suggests that they are associated with mesoscale convective systems (MCS) that prevail in the convective areas.

In Fig. 1 a schematic picture of the MCS over the 'warm pool' area is shown with a mature cumulonimbus anvil and some cumulus clouds at low altitude in different stages of development. Under the outer reaches of the anvil there can be open ocean with no cumulus underneath. The IRIS spectra are well suited to distinguish the character of the cirrus clouds in the MCS. To demonstrate this point, a clear sky spectrum over the oceans, and a spectrum of an oceanic scene containing an optically thin cirrus (PFDWCS) over the ocean are displayed in Fig. 2a and 2b, respectively.

Unlike molecular absorption which exhibits fine spectral structure, clouds tend to produce broad spectral features. A very prominent cloud extinction feature, namely an enhanced difference between the brightness temperatures at 11 and 13 $\mu$m, can be readily identified and is located in the window region of the spectrum (see Fig. 2b) between the 9.6 $\mu$m $O_3$ band and the 15 $\mu$m $CO_2$ band. The range of this cloud extinction feature stretches from 980 to 750 $cm^{-1}$ (10.2 to 12.9 $\mu m$). In addition, cloud extinction inferred from the IRIS spectra for the wavelength region from 18 to 25 $\mu m$, where the water vapor rotation band is present, reinforces the conclusions drawn from the observations made in the window region.

Due to the presence of water vapor in the earth's atmosphere, especially in the first few kilometers above the sea surface, the brightness temperature in the window region, for clear sky conditions, decreases from 980 to 775 $cm^{-1}$. This decrease in brightness temperature from 11 to 13 $\mu m$, $\Delta T = T_{11} - T_{13}$, can be as large as 5° C in the humid 'warm pool' region. Under these conditions, the value of $T_{11}$ is about 293 K; however when there is an optically thin cirrus in the scene, $\Delta T$ is significantly greater than 5° C and $T_{11}$ is several degrees below 293 K. The brightness temperature in the rotation band region at 18 $\mu m$, $T_{18}$, is also reduced by thin cirrus. As shown in PFDWCS the $\Delta T$ in the optically thin cloud cases can be related to the cloud properties with the help of the radiative transfer theoretical calculations that take into account the absorption and scattering by the cirrus ice particles. Unlike the optically thin cloud whose absorption is wavelength dependent, the optically thick cloud emits like a blackbody and hence $\Delta T$ is small. If we assume this optically thick cloud top is around 11 km, the brightness temperature at 11 $\mu m$ is some 70 K below the SST.

The discussion of the cloud spectra presented above is applied to a large MCS complex observed over the 'warm pool' around local noon on October 16, 1970. In order to understand this case, twelve spectra observed by IRIS along one orbital track as the satellite passed northward from about 4° S, 167° E to 7° N, 164° E, are presented in Fig. 3. Each of these spectra show some degree of cirrus cloud contamination with the exception of the # 7 near 0.3° N, which has the largest values of $T_{11}$ and $T_{18}$ (292 K and 267 K, respectively), and the smallest value of $\Delta T$ (5.6 K). It is straightforward to see that the spectra # 3 and 4, where the 15 $\mu m$ $CO_2$ and the 9.6 $\mu m$ $O_3$ bands are weak and $T_{11} \approx 225$ K, correspond to high cold clouds in the center of the MCS complex. The spectra on either side of the MCS center, i.e., # 1 & 2 and 5 & 6 show a gradual warming and suggest a decrease in the effect of the dense clouds, and an increase in the effect of the optically thin clouds. This is evident from the values of $T_{11}$, $\Delta T$ and $T_{18}$ identified in these spectra.

Spectra # 8, 9, 10, 11, and 12 are influenced by some MCS that are outside the subsatellite track of the IRIS observations. The presence of the thin cirrus background in these spectra can be deduced, however, from their spectral characteristics (i.e. $T_{11}$, $\Delta T$ and $T_{18}$). This can be appreciated by contrasting these spectra with that of spectrum # 7. All of these cloud spectra give an indication of the massive aerial extent of thin cirrus over the 'warm pool'.

In the theoretical calculations, PFDWCS assumed the cirrus ice particles are spherical having a log normal size distribution with an effective radius $r_e$. The value of brightness temperature calculated from this theoretical model for the relatively narrow spectral intervals at 11 and 13 $\mu$m is shown to have the following functional dependence:

$$\begin{aligned} T_{11} &= f\left\{(T_s - T_c), m, k_{11}(r_e), \omega_{11}(r_e)\right\} \\ T_{13} &= f\left\{(T_s - T_c), m, k_{13}(r_e), \omega_{13}(r_e)\right\} \end{aligned} \tag{1}$$

where $T_s$ is the sea surface temperature, $T_c$ is the temperature of the cirrus cloud layer which is assumed to be isothermal, $m$ (g/cm$^2$) is the mass of the ice particles in a column of the cloud, and $k_{11}$ and $k_{13}$ (cm$^2$/g) are the extinction cross sections of the ice particles in the cloud whose effective radius is $r_e$, and $\omega_{11}$ and $\omega_{13}$ are the corresponding single scattering albedo values. It follows from Eq. 1 that for a given $(T_s - T_c)$ and $r_e$, $T_{11}$ and $T_{13}$ are dependent on $m$, the mass of the particles in the cloud. Hence the difference $\Delta T = T_{11} - T_{13}$ is also a function of $m$. Results of theoretical calculations (see PFDWCS) are illustrated in Fig. 4 for a family of cirrus clouds with particle sizes $r_e$ ranging between 1.5 $\mu$m to 24 $\mu$m and the total extinction optical depth, $\tau_{11}$, ranging from 0 to 20. Underneath the cirrus it is assumed there are no other clouds and the surface temperature, $T_s$, is 301 K, while the temperature of the cirrus clouds, $T_c$, is taken to be 230 K. In Fig. 4, $\Delta T$ is plotted as a function of the brightness temperature $T_{11}$ as both these quantities are measurable. It can be observed that the curves of $\Delta T$ versus $T_{11}$ for different values of $r_e$ have a maximum $\Delta T$ in the vicinity of $T_{11} \approx 270$ K. This maximum is quite pronounced for small ice particles whose $r_e \leq 6$ $\mu$m. The isolines of optical depth $\tau_{11}$ are shown in the Fig. 4. These isolines reveal that $\Delta T$ maximum is close to $\tau_{11} = 1$. An important result obtained from these theoretical calculations is that the extinction due to the thin cirrus clouds is mainly responsible for decreasing $T_{11}$ below 290 K and increasing $\Delta T$ above 5 K. Water vapor absorption alone can not explain such results.

In Fig. 5 the IRIS observations over the tropical ocean (10° S to 10° N) are plotted as a function of $\Delta T$ versus $T_{11}$ to illustrate the correspondence between theory and observations.

In Fig. 6 the theoretical frame work developed above is applied to the IRIS data over the equatorial Pacific. Here the IRIS observations, made during three months at four oceanic regions of 10° lat. ×10° long size, are presented in the form of frequency distribution in the space defined by the two variables $\Delta T$ and $T_{11}$. Two of these oceanic regions represent the 'warm pool' during the northern summer and fall seasons. The other two regions are chosen to reveal the character of the dry tropical eastern Pacific where the subsidence in the atmosphere and the oceanic upwelling are dominant. The IRIS data over the 'warm pool', Fig. 6 (a & b), when compared with the theoretical results, Fig. 4, show some gross similarities. It should be noted that in observations involving diverse natural situations, other clouds such as cumulus (see Fig. 1) may be present between the sea surface and cirrus, which can introduce a significant spread in the data presented in Fig. 6 (a & b). Thus, one has to take into consideration these variable conditions when comparing the theoretical results with the IRIS data. Despite these limitations one observes that the $\Delta T$ maximum in both the figures is close to $T_{11} \approx 270$ K. The magnitude of $\Delta T$ maximum of about 10 K in the data, when compared with that in Fig. 4, suggests that $r_e$ for such clouds is about 6 $\mu$m.

The percentage cloud cover due to thin cirrus and their optical depth can be estimated with the help of the analysis presented above. Based on the arguments presented earlier, if we assume the IRIS data shown in Fig. 6 (a & b) with $T_{11} < 290$ K and $\Delta T > 5$ K represent thin cirrus in the whole field of view, then we can get an estimate of their percentage. Such estimates over the 'warm pool' region are shown to reach $\approx 60\%$. On the contrary over the dry subsidence regions Fig 6 (c & d) the cirrus amount is negligibly small. Another important observation is that in the 'warm pool' events the high cold clouds $T_{11} < 225$ K constitute only a small fraction $\approx 5\%$ of the total number of cases.

Utilizing this technique the percentage of optically thin cirrus over the tropical oceans from 25°N to 25°S is deduced from IRIS measurements for four seasons as shown in Fig. 7 (a–d). In order to illustrate the significance of the inferred thin cirrus, the climatology of sea surface temperature (SST) is shown in Fig. 8 (a & b) for two seasons. The striking similarity between the distribution of thin cirrus clouds and the SST over the tropical oceans and in particular over the 'warm pool' region is clearly revealed. Note that the maxima of these two variables move poleward during the local summer season.

A weighted mean optical depth of these thin cirrus clouds can be assessed as follows. If one takes the population of clouds with $T_{11} < 290$ K and $\Delta T > 5$ K, it is found that the weighted mean $\overline{\tau}_{11}$ of such population is approximately 1.0 ($\overline{\tau}_{11} = \sum \tau_i f_i / \sum f_i$ where $f_i$ is the frequency of observations, also note from Figs. 4 and 6 that this population of cirrus clouds has $2 > \tau_{11} > 0$).

## 3. Energy balance model for the 'warm pool'

Optically thin cirrus clouds, which are more transparent in the visible than in the IR, are produced by MCS. They are present over an extensive area of the 'warm pool' and therefore should have important implications to the local energy balance. The thermal structure, the convective cloudiness and precipitation in the atmosphere, as well as the temperature in the ocean up to a depth of the thermocline could be impacted by this local energy balance. A comprehensive model that can explicitly take into account all the dynamical, physical and radiative processes pertaining to the coupled ocean-atmosphere system of the 'warm pool' is beyond the scope of this study. Instead, a simple energy balance model is developed which assumes implicitly the existence of convective transport, latent heating, and clouds which result from small scale and large scale dynamical processes in the 'warm pool'. Given these salient conditions, a radiative energy balance model, which will be discussed, is considered to estimate the surface temperature.

It is assumed that the large scale transport processes and convective motions in the tropics result in the formation of MCS's (see Fig. 1). In the MCS's, some of the cumulonimbus clouds form anvils whose optically thin cirrus covers the sky completely. The lower tropospheric convective cumulus are taken to have cloud tops which reach an average altitude of 5.5 km. If we take the surface temperature to be 301 K and the lapse rate to be 6.5 K/km, then the cumulus cloud tops will have a temperature of 265 K. The cumulus clouds are taken to be black bodies radiating at the cloud temperature. This means that the cumulus clouds emit 0.6 times the surface flux, $\sigma T_s^4$, where $\sigma$ is the Stefan-Boltzmann constant. The cirrus are located near 12 km and are taken to have a negligible thickness. As before, if we take the surface temperature to be 301 K and the lapse rate to be 6.5 K/km, then the thin cirrus have a temperature of 223 K. This implies that if these thin cirrus were to radiate with an emissivity, $\epsilon$, then their emission would be equal to $0.3\epsilon\sigma T_s^4$. The cumulus cloud cover, $C$, underneath the cirrus is an important parameter of the model and is allowed to vary. In our formulation the IR emissivity of the cirrus is related to its visible albedo, $\alpha$ , with the help of radiometer measurements obtained from aircraft flights (Spinherne and Hart, 1990) as shown in Table 1. The IR transmissivity of the cirrus is given by $(1-\epsilon)$ and its visible transmissivity is $(1-\alpha)$. In these calculations the visible reflectivity of the cumulus, $r$, is allowed to vary between 0.55 and 0.65 (e.g., Stowe et al., 1988), and the visible albedo is varied from 0.0 to 0.4, and the cumulus fraction from 0.0 to 0.9. A scheme for the radiative processes in the model is presented in Fig. 9. As shown by Eq. 2, the energy balance between the incoming solar radiation and the outgoing longwave radiation at the top of the atmosphere can be described by:

$$\begin{aligned} G_1\sigma T_s^4(\epsilon t' + A) + (1-\epsilon)\left[0.6CG_2\sigma T_s^4 + (1-C)G_3\sigma T_s^4\right] \\ = S(1-\alpha)\left[\{1-\alpha_s(1-\alpha)\}(1-C) + \{1-r(1-\alpha)\}C\right] \end{aligned} \tag{2}$$

where $S$ is the solar constant, and $\alpha_s$ is the albedo of the cloud free atmosphere and the ocean surface. The first term on the left hand side gives the IR emission from the cirrus and the overlying atmosphere containing $CO_2$, $O_3$ and $H_2O$. $t' = 0.94$ is the IR flux transmission of the atmospheric absorbing gases above the cirrus level. The constant, $A = 0.06$, arises because of the emission of the atmosphere above the cirrus. The constant, $G_1$, represents the ratio $(T_c/T_s)^4$ which is 0.30. The second term on the left hand side represents the IR radiation emerging through the cirrus. This term has two components: a) a part that corresponds to the emission from the cumulus, and the atmospheric gases between cumulus top and cirrus, and b) a part that represents the emission from the surface and the atmosphere underlying the cirrus. In here the emission from the cumulus region is weighted by the cumulus fraction, $C$, and the rest by $(1-C)$. The constants $G_2$ and $G_3$ are scaling constants which are meant to scale the emission from a) and b), respectively. This scaling is done to express the emission from these layers in terms of the blackbody radiation from the surface,

$\sigma T_s^4$. The values of $G_2$ and $G_3$ are 0.83 and 0.63, respectively. These constants, as well as $t'$ and $A$ are obtained from IR radiative transfer computations for a tropical atmosphere assuming $T_s = 301$ K, lapse rate of 6.5 K/km, 5 g/cm$^2$ of water vapor, a tropical ozone profile with 0.28 cm of $O_3$ and a tropopause temperature of 190 K at 17 km.

The term on the right hand side of Eq. 2 is an approximation for the incoming solar energy which is absorbed by the surface-atmosphere system. This absorption, for clear sky conditions within the tropics, leads to an effective radiative temperature at the top of the atmosphere near 270 K. This estimate of the effective radiative temperature in the tropics is consistent with that obtained in other studies (e.g., Stephens and Webster, 1981). From Eq. 2, one can solve for the surface temperature, $T_s$, as a function of $C$ and $\alpha$, given the magnitude of the other variables. For present purposes the diurnal mean insolation near the equator is taken to be $S = 405$ W/m$^2$. Based on satellite measurements, $\alpha_s$ is taken to be 0.10 (e.g., Gill, 1982). Eq. 2 may be simplified as follows:

$$\beta \sigma T_s^4 = (1 - \alpha_c) S$$

$$\text{where } \beta = [G_1(\epsilon t' + A) + (1 - \epsilon)\{0.6 C G_2 + (1 - C) G_3\}] \tag{3}$$

$$\text{and } \alpha_c = [\alpha_s((1 - C)(1 + \alpha^2) + 2\alpha C) + (1 - 2\alpha_s)\alpha + rC(1 - \alpha)^2]$$

In Eq. 3, $\alpha_c$ is equivalent to an effective albedo and $\beta$ is the effective emissivity of the earth atmosphere system. From Eq. 3 one notes that the ratio $(1 - \alpha_c)/\beta$ may be interpreted as a greenhouse amplification factor which takes into account not only the effect of the gases but also the strong interaction of clouds on IR and solar radiation.

Taking $r = 0.55$ in Eq. 2, $T_s$ is estimated for different values of $C$ and $\alpha$. These values of $T_s$ are presented in Table 2a. The corresponding values of $\alpha_c$ and $\beta$ as defined by Eq. 3 are listed in Tables 2b and 2c, respectively.

From Table 2a, one notes that in the absence of cumulus and cirrus clouds, the radiative-convective equilibrium leads to a surface temperature of 316.1 K. This warm temperature of the equatorial ocean results from the greenhouse effects of the atmospheric gases such as $CO_2$ and $H_2O$. It must be noted, however, that this assumes the absence of fluid transports. If the effects of clouds are taken into consideration, it is observed that as the cumulus cloud fraction is increased to 0.9 with no cirrus present, the surface temperature drops to 287.8 K. If optically thin cirrus clouds with $\alpha = 0.2$ (i.e., $\epsilon = 0.63$) are now included in the scene, the surface temperature is raised to a value of 307.7 K (see Table 2a). This example demonstrates the effect of the thin cirrus veil on the sea surface temperature.

When the incoming solar energy is not in balance with the OLR, there will be a net radiative energy input, $E_{net}$, at the top of the atmosphere. This input may be estimated by the following simple expression when $\alpha_c$, $\beta$ and $T_s$ are given:

$$E_{net} = S(1 - \alpha_c) - \beta\sigma T_s^4. \tag{4}$$

Taking the values of $\alpha_c$ and $\beta$ from Table 2b and 2c, and the surface temperature, $T_s = 301$ K from observations, of the 'warm pool' region, we have estimated the net energy input, $E_{net}$. The values of $E_{net}$ which are calculated from Eq. 4 are presented in Table 3. One notes that the maximum net input of energy into the ocean atmosphere system occurs when the cirrus visible albedo is about 0.2. Based on the approximations developed by Platt and Stephens (1980) we can relate this emissivity to a total optical depth of approximately one for the cirrus cloud. These optimal conditions of energy input are apparently present in the 'warm pool' region as evidenced by the IRIS observations (see Fig. 5 and 6) which show that the bulk of the cirrus clouds have optical depths around unity. One may also note from Table 1 that the cumulus clouds generally decrease the net energy input to the system.

Following the path of maximum net energy input, which corresponds closely to $\alpha = 0.2$, we find from Table 3 that when $C \approx 0.2$ the input energy is about 80 $W/m^2$. This combination of cirrus and cumulus yields $\alpha_c \approx 0.33$ (see Table 2b).

These estimates of the albedo, $\alpha_c$, and net energy input of $\approx 80$ W/m$^2$ are consistent with the ERBS observations reported by Barkstrom et al. (1989).

In Fig. 9, two curves are shown which illustrate the dependence of the sea surface temperature, $T_s$, on the cumulus cloud fraction, $C$, which is calculated according to Eq. 2. These curves correspond to a) $r = 0.55$, $\alpha = 0.2$ and b) $r = 0.65$, $\alpha = 0.3$. The first case is contained in Table 2. Although no table is presented for the second case, it is noted that when $\alpha = 0.2$ and $C = 0.2$, an increase in $r$ from 0.55 to 0.65, results in a drop of the net input energy from $\approx 80$ W/m$^2$ to $\approx 75$ W/m$^2$. This example demonstrates the sensitivity of $E_{net}$ to the value of $r$ while Table 3 gives the sensitivity of $E_{net}$ to $C$ and $\alpha$.

To convey the significance of the energy input, we take as an example a case where only 20 W/m$^2$ of the net radiative energy at the top of the atmosphere is available to heat the ocean water. We find that for these conditions, an ocean mixed layer of 50 meter depth will be heated by about 1°C in 100 days. Measurements of the surface energy balance over the 'warm pool' region from the TOGA COARE program will be valuable in validating our conclusions.

The radiative convective model adopted here may be scrutinized further. In particular, one may examine the parameterization of the cumulus and cirrus cloud temperatures which are scaled in terms of the surface temperature. This parameterization forces the cumulus and cirrus cloud temperatures to increase approximately by factors of 0.6 and 0.3, respectively, of the surface temperature increase. Thus, for small perturbations of $T_s$, taking a constant lapse rate, one can note that the altitude and the pressure level of the clouds remain virtually unchanged. In this coupled cloud temperature system, as the surface temperature increases, infrared loses to space increases both from the surface and the clouds. This has a moderating effect on $T_s$ variations. If, however, as a counter example we take the temperature of the cumulus and cirrus clouds to be constant, then the heights of the clouds will increase as $T_s$ increases. Moreover, the infrared loss to space will depend mainly on $T_s$, and thus as a consequence, for a given increase in infrared opacity (such as that due to an increase in the $CO_2$ abundance) of the atmosphere and clouds, $T_s$ will increase by a larger amount than that in the scaled cloud temperature case (see Table 3). This constant cloud temperature scenario leads to a runaway greenhouse effect more quickly than the scaled cloud temperature scenario. The two formulations considered here are anticipated to cover a reasonable range of conditions. Thus, from the results presented here we expect that the coupled surface and cloud temperature model, which we adopted, will yield conservative estimates of the surface temperature variations.

## 4. Discussion and conclusions

Satellite cloud pictures in the visible channel show almost perpetual cloudiness over the western Pacific equatorial regions around Indonesia. These clouds have the potential to block a significant amount of solar input energy. Furthermore, it is well known from climatology that the western equatorial Pacific is a region of heavy precipitation as well as being the area with the warmest sea surface temperature. The coexistence of these clouds and warm waters requires an explanation. The TOGA COARE program, in which several components of the energy balance pertaining to the 'warm pool' region will be measured, is attempting to explain this. The aim of this study is to show that optically thin cirrus clouds, which emanate from the anvils of convective storms in the 'warm pool' and cover the area extensively with sufficient optical depth in the IR, can account for a significant net solar energy input locally into this atmosphere-ocean system. This net input amounting to about 80 W/m$^2$ may be largely responsible for the maintenance of the 'warm pool' regime.

Another important factor is the rain water addition. The low density rain water in the top layers of the ocean (Lukas, 1988) together with weak wind stress helps to maintain stable stratification and promote heating. Thus the ocean atmosphere system in the 'warm pool' through a set of positive feedback mechanisms retains a significant amount of solar energy to keep itself operating. A schematic diagram of the various dynamic and physical processes that lead to the formation of the 'warm pool' system is presented in Fig. 10. The two physical processes namely the optically thin cirrus and the addition of fresh rain water in the top layer of the ocean, i.e., a freshwater lens, are coupled to the 'warm pool' and aid in its maintenance. A clear implication of this schematic figure is that the solar energy, through monsoonal scale interactions and by localized heating aided by the thin cirrus, is directly responsible for the maintenance of the 'warm pool'.

On a global scale, considerations of energy balance lead to the conclusion that although the sun is the ultimate source of energy, the greenhouse effect produced by gases such as $H_2O$, $CO_2$ and $O_3$ is important in maintaining the relatively warm surface temperatures for the earth. While the transport processes in the atmosphere and oceans are primarily responsible for reducing the thermal contrast between the tropics and polar regions, they have a relatively minor influence on the global mean temperature. For these reasons, a radiative convective equilibrium model (e.g. Arking, 1991; Ramanathan and Coakley, 1978) which does not consider the large scale fluid transports may be used to calculate the global mean surface temperature assuming a tropospheric temperature profile that follows a prescribed lapse rate.

In a localized region, the fluid transport processes can have a significant influence on heat and moisture. If these processes are very rapid then the effect of any local energy input due to radiative convective processes will be reduced to a negligible level. On the other hand, if these transports are not rapid then a discernable temperature rise will result. Based on the satellite observations pertaining to a net radiative energy input of $\approx 80$ W/m$^2$ and to the thin cirrus clouds, that can enhance the greenhouse effect, we have inferred that the 'warm pool' region has a source of net radiative input and has a directly driven circulation. This forms the basis for our simple radiative convective equilibrium model for the 'warm pool' region. The current model is self-consistent and yields an understanding of the radiative and dynamic interactions prevailing in this region along with an explanation for surface temperature.

## REFERENCES


Arking, A., 1991: The radiative effects of clouds and their impact on climate. Bull. Amer. Meteor. Soc., In press.

Barkstrom, B., E. Harrison, G. Smith, R. Green, J. Kibler, R. Cess, and the ERBE Science Team, 1989: Earth radiation budget experiment (ERBE) Archival and April 1985 results. Bull. Amer. Meteor. Soc., 70, 1254-1262.

Dorman, C.E., and R.H. Bourke, 1979: Precipitation over the Pacific Ocean, 30°S to 60°N. Mon. Wea. Rev., 107, 896-910.

Garcia, O., 1985: Atlas of highly reflective clouds for the global tropics: 1971-1983. U.S. Dept. of Commerce, NOAA, Environmental Research Lab., Boulder, Co.

Gill, A.E., 1982: Atmosphere-Ocean Dynamics. Academic Press, 662 pp.

Hanel, R.A., B.J. Conrath, V.G. Kunde, C. Prabhakara, I. Revah, V.V. Salomonson, and G. Wolford, 1972: The Nimbus 4 infrared spectroscopy experiment 1. Calibrated thermal emission spectra. J. Geophys. Res., 77, 2629.

Inoue, T., 1985: On the temperature and effective emissivity determination of semi-transparent cirrus clouds by bi-spectral measurements in the 10 $\mu$m window region. J. Met. Soc. Japan, 63, 88-89.

Lukas, R., 1988: On the role of western Pacific air-sea interaction in the El Nino/Southern Oscillation Phenomenon. In Proceedings of the U.S. TOGA Western Pacific Air-Sea Interaction Workshop Honolulu, 16-18 September, 1987. R. Lukas and P. Webster, eds., U.S. TOGA Rept. USTOGA-8, U. Corp. Atmos. Res., 43-69.

Platt, C.M.R., 1989: The role of cloud microphysics in high-cloud feedback effects on climate change. Nature, 341, 428-429.

_____________, and G.L. Stephens, 1980: The interpretation of remotely sensed high cloud emittances. J. Atmos. Sci., 37, 2314-2322.

_____________, J.C. Scott, and A.C. Dilley, 1987: Remote sensing of high clouds. Part VI: Optical properties of midlatitude and tropical cirrus. J. Atmos. Sci., 44, 729-747.

Prabhakara, C., R.S. Fraser, G. Dalu, Man-Li C. Wu, R.J. Curran and T.L. Styles, 1988: Thin cirrus clouds: Seasonal distribution over oceans deduced from Nimbus 4 IRIS. J. Appl. Meteor., 27, 379-399.

Ramanathan, V., R.D. Cess, E.F. Harrison, P. Minnis, B.R. Barkstrom, E. Ahmad, and D. Hartmann, 1989: Cloud-radiative forcing and climate: Results from the earth radiation budget experiment. Science, 243, 57-63.

_____________, and J.A. Coakley, Jr, 1978: Climate modeling through radiative-convective models. Rev. Geophys. Space Phys., 16, 465-489.

Spinhirne, J.D., and W.D. Hart, 1990: Cirrus structure and radiative parameters from airborne lidar and spectral radiometer observations: The 28 October 1986 FIRE study. Mon. Wea. Rev., 118, 2329-2343.

Stephens, G.L., 1980: Radiative properties of cirrus clouds in the infrared region. J. Atmos. Sci., 37, 435-446.

_____________, and P.J. Webster, 1981: Clouds and climate: Sensitivity of simple systems. J. Atmos. Sci., 38, 235-247.

Stowe, L.L., C.G. Wellemeyer, T.F. Eck, H.Y.M. Yeh, and the Nimbus-7 Cloud Data Processing Team, 1988: Nimbus-7 global cloud climatology. Part I: Algorithm and validation. J. Climate, 1, 445-470.

_____________, H.Y.M. Yeh, T.F. Eck, C.G. Wellemeyer, H.L. Kyle and the Nimbus-7 Cloud Data Processing Team, 1989: Nimbus-7 global cloud climatology. Part II: First year results. J. Climate, 2, 671-709.

World Climate Research Programme, 1989: A coupled ocean-atmosphere response experiment for the warm pool regions of the western Pacific. Scientific plan for the TOGA coupled ocean-atmosphere response experiment (COARE). Draft July 1989, 111 pp.

Table 1. Relationship between the visible albedo and infrared emissivity of cirrus.

| $\alpha$ | $\epsilon$ |
|---|---|
| 0.0 | 0.00 |
| 0.1 | 0.36 |
| 0.2 | 0.63 |
| 0.3 | 0.78 |
| 0.4 | 0.88 |
| 0.5 | 0.94 |

Table 2. Results obtained from Eq. 3 as a function of the cirrus albedo $\alpha$ and the cumulus fraction C (Note: in Eq. 3 the cumulus and cirrus temperatures are coupled to the surface temperature). (a) Surface temperature $T_s$ . (b) Effective albedo $\alpha_e$ . (c) Effective emissivity $\beta$.

(a)

| $\alpha$ \ C | 0.0 | 0.1 | 0.3 | 0.5 | 0.7 | 0.9 |
|---|---|---|---|---|---|---|
| 0.0 | 317.8 | 315.4 | 310.1 | 303.9 | 296.7 | 288.1 |
| 0.1 | 327.1 | 324.7 | 319.5 | 313.7 | 307.1 | 299.4 |
| 0.2 | 334.1 | 331.7 | 326.6 | 321.0 | 314.9 | 307.9 |
| 0.3 | 334.2 | 332.0 | 327.3 | 322.2 | 316.7 | 310.7 |
| 0.4 | 330.0 | 328.0 | 323.8 | 319.3 | 314.6 | 309.5 |

(b)

| $\alpha$ \ C | 0.0 | 0.1 | 0.3 | 0.5 | 0.7 | 0.9 |
|---|---|---|---|---|---|---|
| 0.0 | 0.10 | 0.15 | 0.24 | 0.33 | 0.42 | 0.51 |
| 0.1 | 0.18 | 0.22 | 0.29 | 0.36 | 0.44 | 0.51 |
| 0.2 | 0.26 | 0.29 | 0.35 | 0.41 | 0.47 | 0.52 |
| 0.3 | 0.35 | 0.37 | 0.42 | 0.46 | 0.50 | 0.55 |
| 0.4 | 0.44 | 0.45 | 0.49 | 0.52 | 0.55 | 0.58 |

(c)

| $\alpha$ \ C | 0.0 | 0.1 | 0.3 | 0.5 | 0.7 | 0.9 |
|---|---|---|---|---|---|---|
| 0.0 | 0.63 | 0.62 | 0.59 | 0.57 | 0.54 | 0.51 |
| 0.1 | 0.51 | 0.50 | 0.49 | 0.47 | 0.45 | 0.44 |
| 0.2 | 0.42 | 0.42 | 0.41 | 0.40 | 0.39 | 0.38 |
| 0.3 | 0.37 | 0.37 | 0.36 | 0.36 | 0.35 | 0.35 |
| 0.4 | 0.34 | 0.34 | 0.34 | 0.33 | 0.33 | 0.33 |

Table 3. Net energy input at the top of the atmosphere ($E_{net}$) calculated according to Eq. 4 as a function of cirrus albedo $\alpha$ and cumulus fraction C when the surface temperature $T_s$ is a constant ($T_s$ = 301 K).

| $\alpha$ \ C | 0.0 | 0.1 | 0.3 | 0.5 | 0.7 | 0.9 |
|---|---|---|---|---|---|---|
| 0.0 | 71.0 | 58.8 | 34.5 | 10.1 | -14.2 | -38.5 |
| 0.1 | 93.5 | 82.6 | 60.9 | 39.1 | 17.3 | -4.4 |
| 0.2 | 101.4 | 92.0 | 73.2 | 54.3 | 35.5 | 16.6 |
| 0.3 | 90.1 | 82.5 | 67.3 | 52.1 | 36.9 | 21.7 |
| 0.4 | 70.2 | 64.4 | 52.7 | 41.0 | 29.4 | 17.7 |

Table 4. Same as Table 2a except the cumulus and cirrus temperature are not coupled to the surface and are given a constant value of 265 K and 223 K respectively. Reflectivity r of cumulus is 0.55.

| $\alpha$ \ C | 0.0 | 0.1 | 0.3 | 0.5 | 0.7 | 0.9 |
|---|---|---|---|---|---|---|
| 0.0 | 317.8 | 316.6 | 313.1 | 306.4 | 288.7 | * |
| 0.1 | 333.0 | 332.5 | 331.1 | 328.5 | 322.2 | 283.1 |
| 0.2 | 354.9 | 355.3 | 356.2 | 358.0 | 361.9 | 379.8 |
| 0.3 | 374.3 | 375.3 | 377.9 | 382.5 | 392.7 | 434.4 |
| 0.4 | 395.7 | 396.9 | 400.2 | 406.1 | 419.0 | 470.1 |

* The case where $\alpha = 0$ and C = 0.9 is physically unrealistic since the incoming solar energy is insufficient to balance the outgoing IR when the cumulus cloud temperature is 265 K.

Figure Captions

Fig. 1. Schematic figure of the mesoscale convective system containing optically thin cirrus produced by spreading of deep convective cumulonimbus anvil. Depicted in the figure are a) weak cumulus underlying the cirrus, b) radiative processes at the sea surface and within the atmosphere including cumulus and thin cirrus, and c) energy transports in the atmosphere and the ocean.

Fig. 2. IRIS spectra observed over the tropical oceans.
(a) Cloud free tropical ocean spectrum.
(b) Maritime tropical spectrum contaminated by optically thin cirrus.

Fig. 3. IRIS spectra observed along one orbital track as the satellite passed northward from about 4°S, 167°E to 7°N, 164°E on October 16, 1970. The spectra are numbered 1 to 12 starting with 7°N as 1 and ending with 4°S as 12. Each spectrum is identified with its location and spectral details pertaining to $T_{10.8}$, $\Delta T$ and $T_{18}$. The spectra are compacted along the ordinate with separate ordinate values.

Fig. 4. Theoretical values of $\Delta T$ vs $T_{10.8}$ for high-level (cirrus) spherical ice crystal clouds as a function of particle size and optical depth. The solid isolines of particle size $r_e$ and dashed isolines of optical depth $\tau$ are identified (Note: isoline of $r_e$ = 3 $\mu$m is also dashed.).

Fig. 5. The temperature difference, $\Delta T$, vs $T_{10.8}$ derived from the IRIS data over the tropical oceans (10°N to 10°S).

Fig. 6. Frequency distributions of seasonal IRIS data as a function of $\Delta T$ and $T_{10.8}$ over the 10° lat X 10° long oceanic regions for different seasons. Dashed vertical and horizontal lines delineate the thresholds on $\Delta T$ and $T_{10.8}$. Both total frequency and cirrus percentage are also shown.
(a) June, July, and August (5°N-5°S, 130°E-140°E).
(b) June, July, and August (5°N-5°S, 90°W-100°W).
(c) September, October and November (5°N-5°S, 100°E-110°E).
(d) September, October and November (5°N-5°S, 120°W-130°W).

Fig. 7. Seasonal percentage cloud cover due to optically thin cirrus in the tropics between 25°N and 25°S. The numbers should be multiplied by 10 to get % cloud cover.
(a) April and May.
(b) June, July and August.
(c) September, October and November.
(d) December, January.

Fig. 8. Climatological sea surface temperature °C (from World Climate Research Programme, 1989) for
(a) June, July and August and
(b) November, December and January.

Fig. 9. (Left panel) Schematic diagram showing the energy balance model and its vertical structure in this study.
(Right panel) Surface temperature $T_s$ computed according to Eq. 3. The curve with the symbol 'o' is for cumulus reflection r = 0.55 and cirrus visible transmission = 0.8 (i.e. $\mathcal{L}$ = 0.2). The curve with the symbol '□' stands for r = 0.65 and cirrus visible transmission = 0.7 (i.e. $\mathcal{L}$ = 0.3).

Fig.10. Flow diagram for physical processes in the convectively active oceanic regions responsible for maintaining the warm pools.

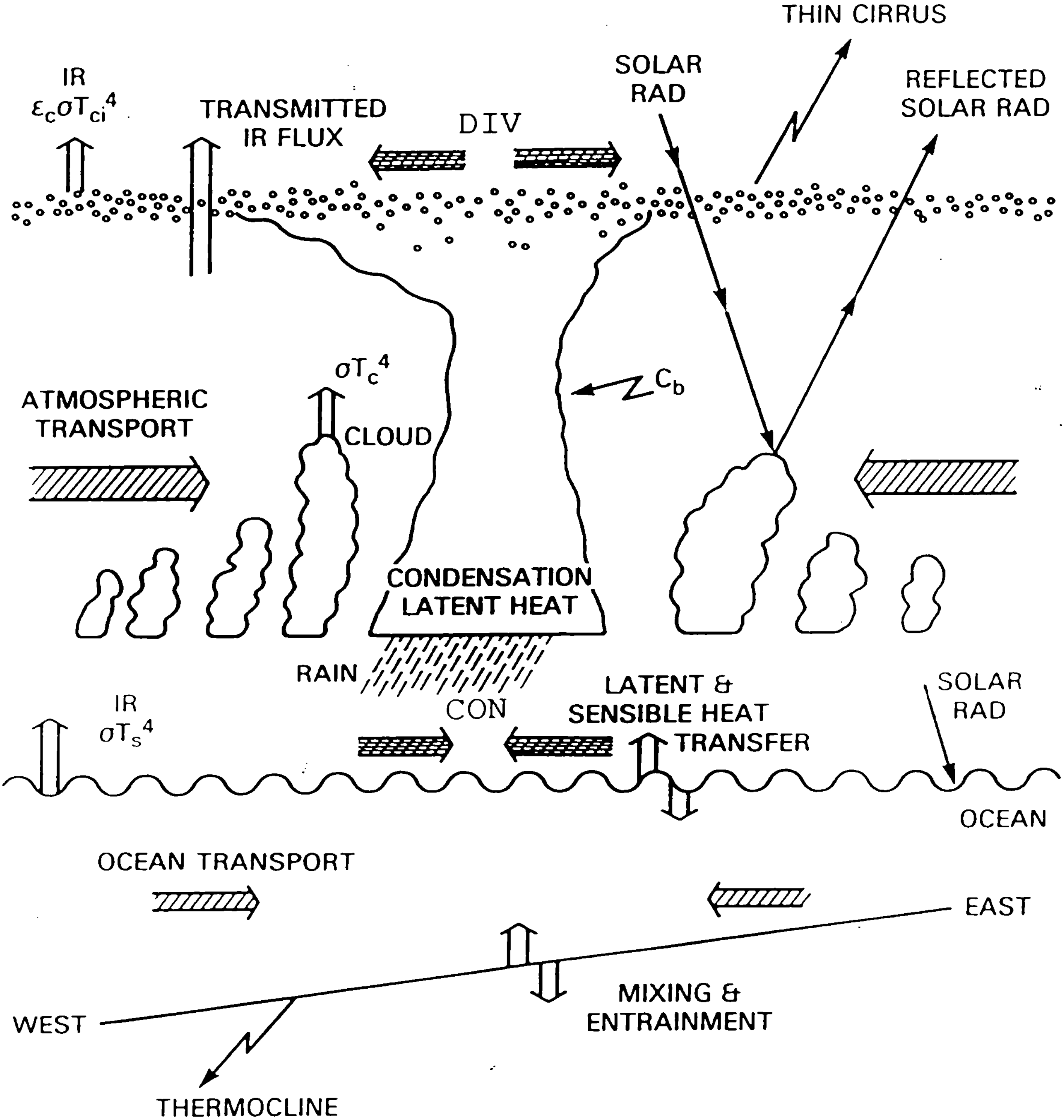

THIN CIRRUS
SOLAR RAD
REFLECTED SOLAR RAD
IR $\epsilon_c \sigma T_{ci}^4$
TRANSMITTED IR FLUX
DIV
$\sigma T_c^4$
$C_b$
ATMOSPHERIC TRANSPORT
CLOUD
CONDENSATION LATENT HEAT
RAIN
LATENT & SENSIBLE HEAT TRANSFER
SOLAR RAD
IR $\sigma T_s^4$
CON
OCEAN
OCEAN TRANSPORT
EAST
MIXING & ENTRAINMENT
WEST
THERMOCLINE

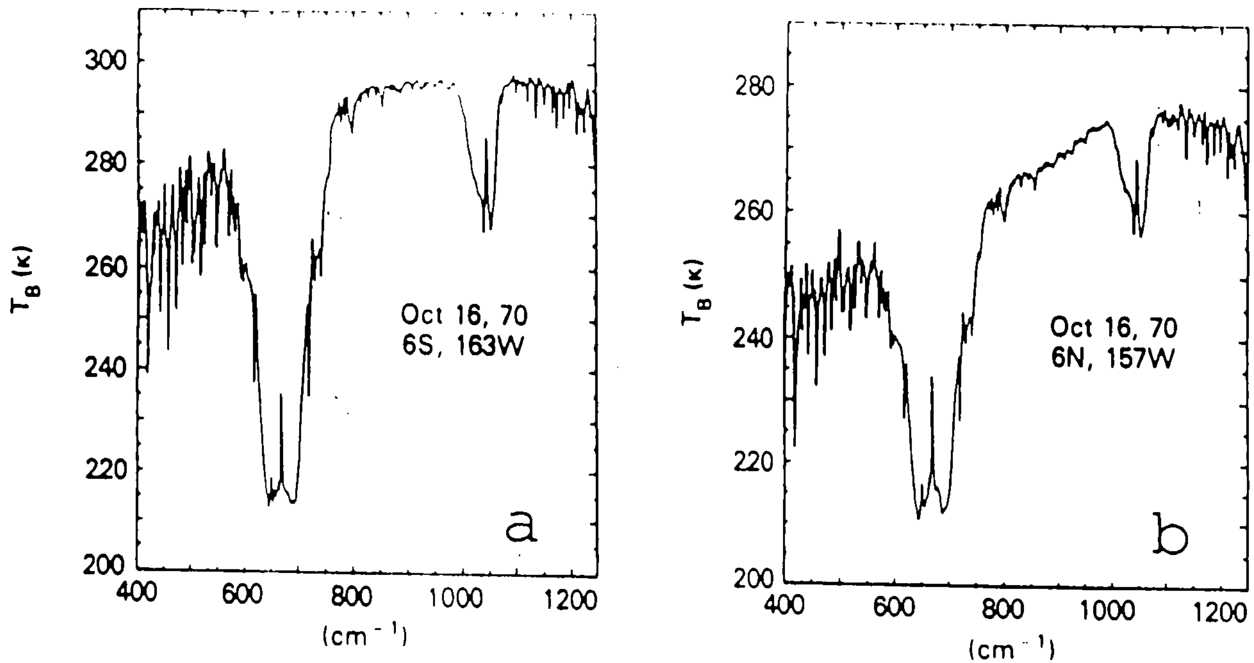

300
280
260
240
220
200
$T_B$ (K)
400
600
800
1000
1200
(cm$^{-1}$)
Oct 16, 70
6S, 163W
a
280
260
240
220
200
$T_B$ (K)
400
600
800
1000
1200
(cm$^{-1}$)
Oct 16, 70
6N, 157W
b

OCT 16. 70

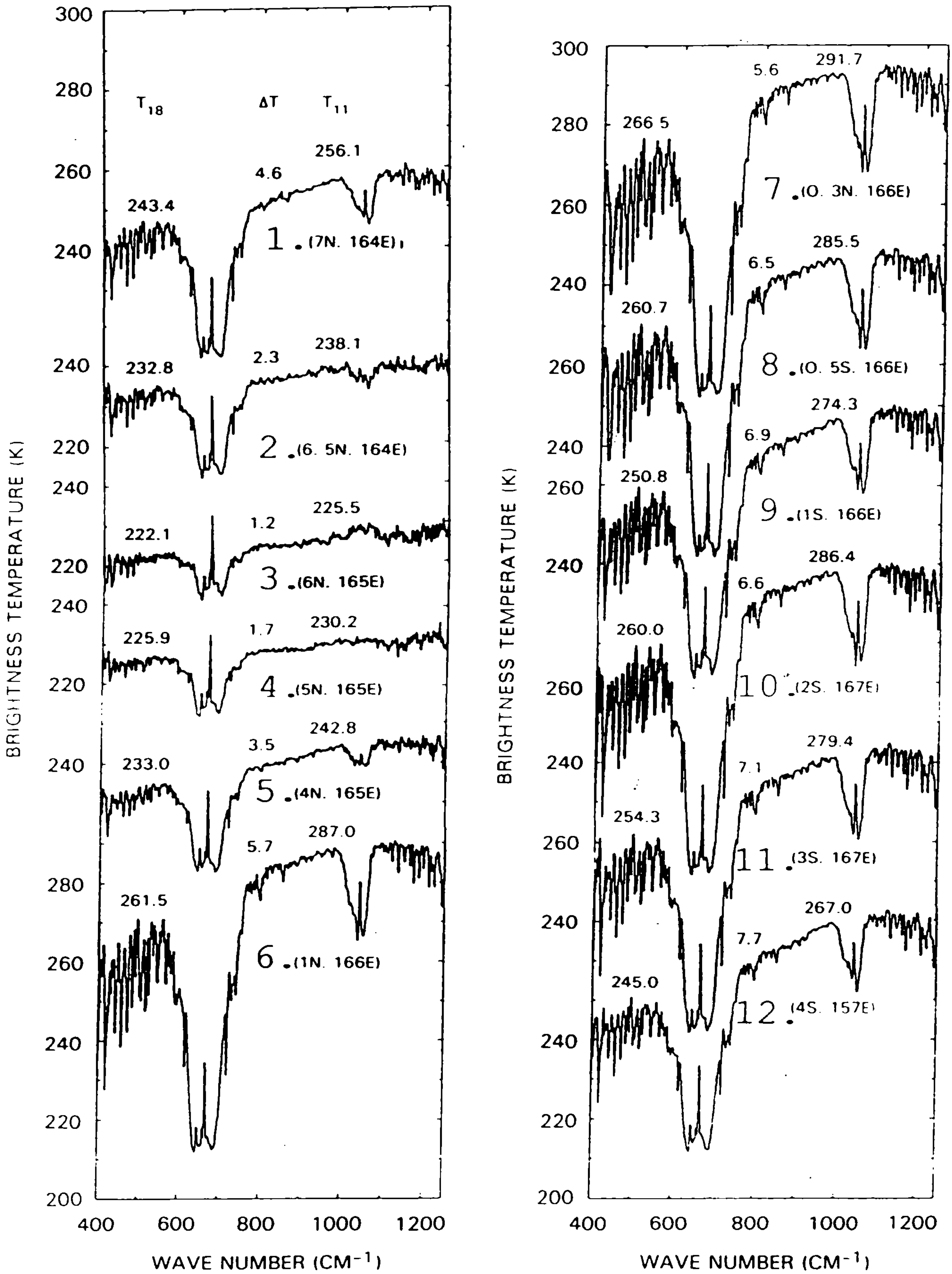

$T_{18}$
ΔT
$T_{11}$
243.4
4.6
256.1
1 .(7N. 164E)
232.8
2.3
238.1
2 .(6. 5N. 164E)
222.1
1.2
225.5
3 .(6N. 165E)
225.9
1.7
230.2
4 .(5N. 165E)
233.0
3.5
242.8
5 .(4N. 165E)
261.5
5.7
287.0
6 .(1N. 166E)
266 5
5.6
291.7
7 .(O. 3N. 166E)
260.7
6.5
285.5
8 .(O. 5S. 166E)
250.8
6.9
274.3
9 .(1S. 166E)
260.0
6.6
286.4
10 .(2S. 167E)
254.3
7.1
279.4
11 .(3S. 167E)
245.0
7.7
267.0
12 .(4S. 157E)
BRIGHTNESS TEMPERATURE (K)
WAVE NUMBER (CM⁻¹)
400
600
800
1000
1200
200
220
240
260
280
300

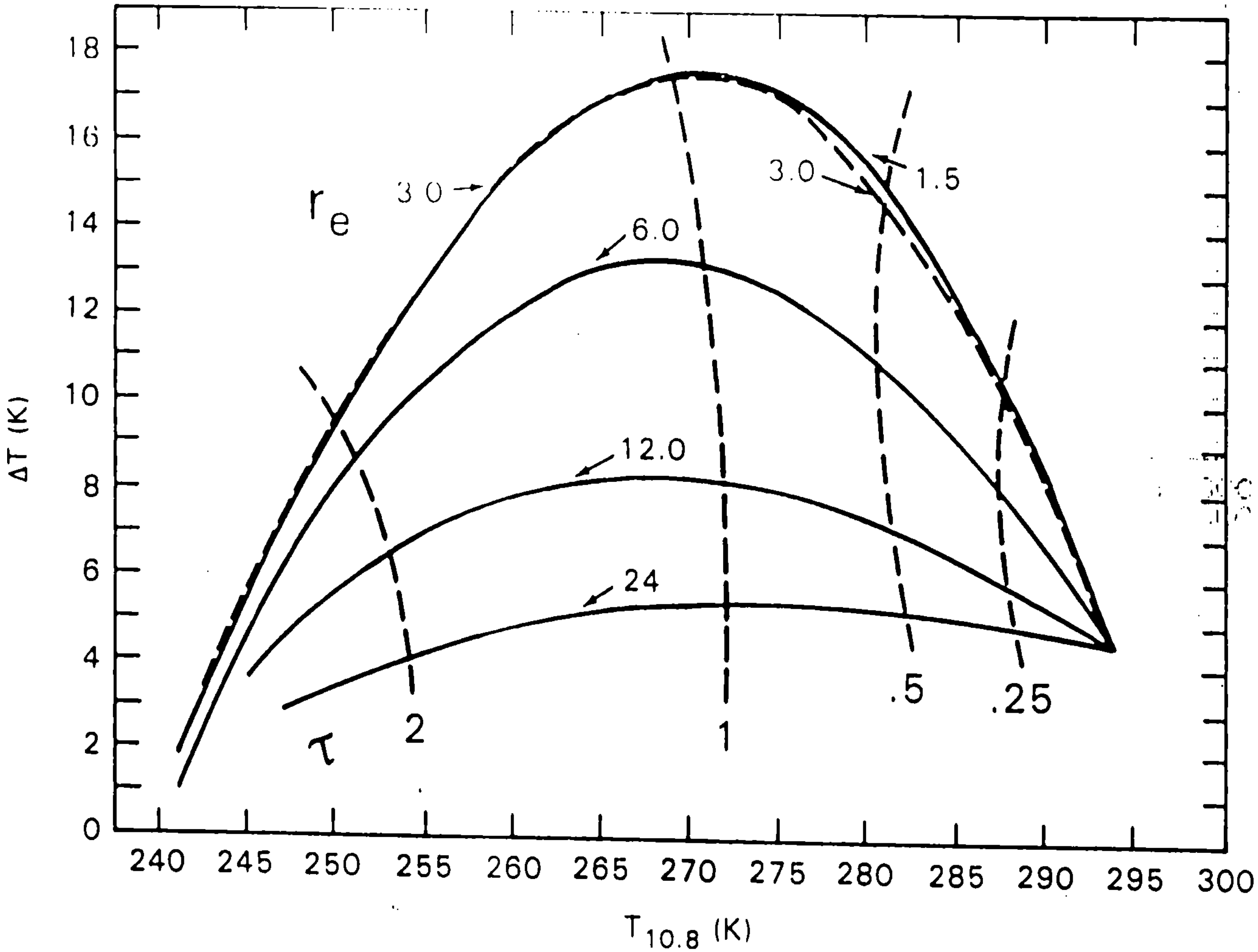

18
16
14
12
10
8
6
4
2
0
ΔT (K)
240
245
250
255
260
265
270
275
280
285
290
295
300
T 10.8 (K)
r e
3.0
6.0
12.0
24
3.0
1.5
τ
2
1
.5
.25

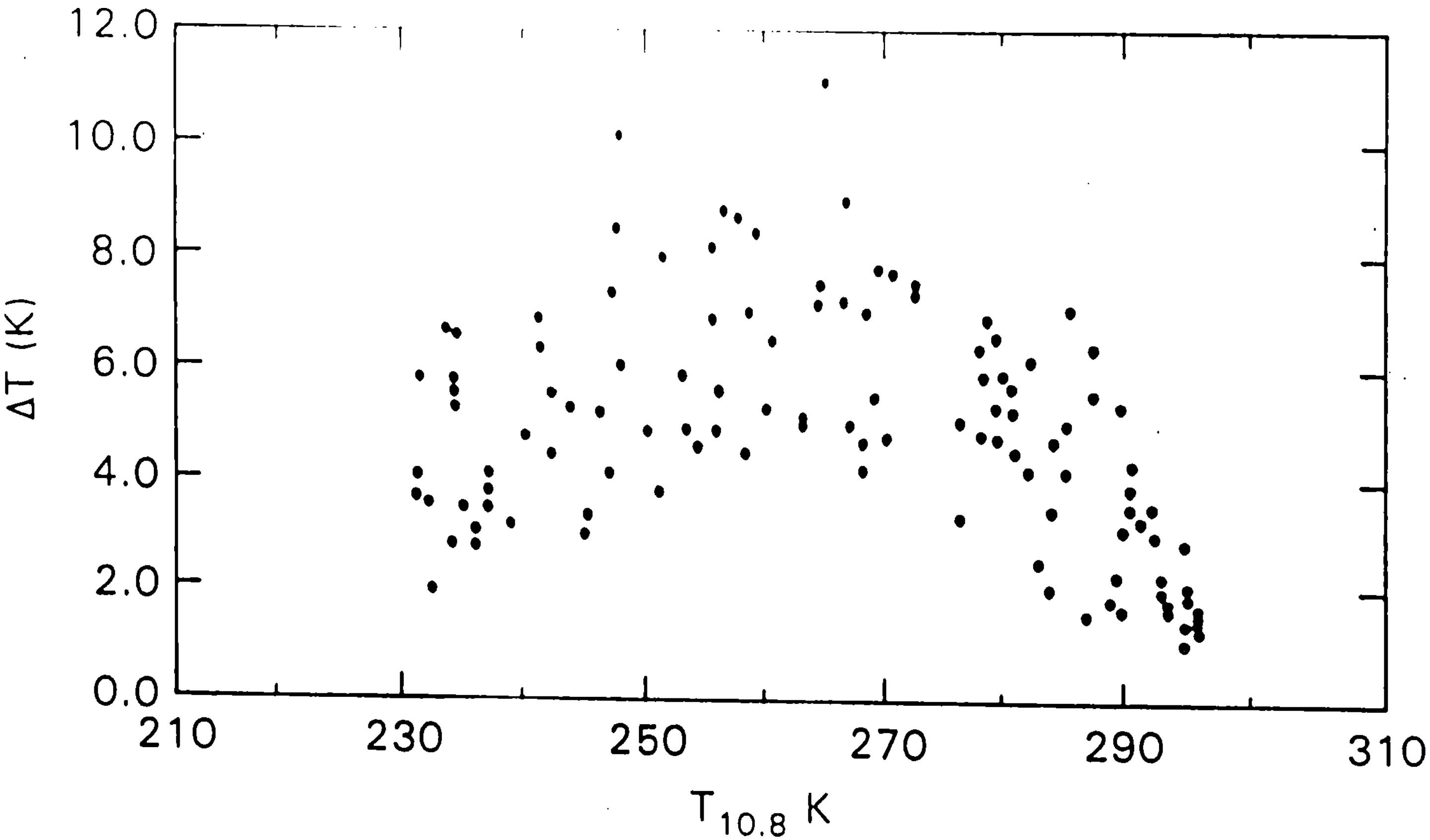
12.0
10.0
8.0
6.0
4.0
2.0
0.0
ΔT (K)
210
230
250
270
290
310
T10.8 K

# SUMMER

**Latitude: 5°N ~ 5°S, Longitude: 130°E ~ 140°E**

| $T_{11}$ | $T_{11}-T_{13}$: 1 | 0 | 1 | 2 | 3 | 4 | 5 | 6 | 7 | 8 | 9 | 10 |
|---|---|---|---|---|---|---|---|---|---|---|---|---|
| 295 300 | | | | | | 2 | | 1 | | | | |
| 290 295 | | | | 1 | 1 | 9 | 8 | 7 | 1 | | | |
| 285 290 | | | | | 1 | 5 | 8 | 21 | | | | |
| 280 285 | | | | | 1 | 3 | 10 | 17 | 4 | | | |
| 275 280 | | | | | 1 | 12 | 11 | 8 | 1 | 1 | | |
| 270 275 | | | | 3 | 6 | 4 | 8 | 17 | 2 | 2 | | |
| 265 270 | | | | 1 | 7 | 2 | 6 | 7 | 3 | | | |
| 260 265 | | | | 4 | 4 | 6 | 6 | 5 | | | | |
| 256 260 | | | | 2 | 2 | 4 | 8 | 3 | 1 | | | |
| 250 256 | | | | 1 | 4 | 2 | 4 | 2 | 1 | | | |
| 245 250 | | | | 2 | 2 | 2 | 2 | 2 | | | | |
| 240 245 | | | | 1 | 4 | 3 | 2 | 1 | | | | |
| 235 240 | | | | 1 | 1 | | | | | | | |
| 230 235 | | | | | 2 | 1 | | | | | | |
| 225 230 | | 2 | 1 | | 1 | | | | | | | |
| 220 225 | | 2 | 3 | 2 | | | | | | | | |
| 215 220 | 1 | | | | | | | | | | | |
| 210 215 | | 2 | | | | | | | | | | |
| 205 210 | | | | | | | | | | | | |
| 200 205 | | | | | | | | | | | | |
| 195 200 | | | | | | | | | | | | |

a

Total frequency = 305
Cirrus 44%

**Latitude: 5°N ~ 5°S, Longitude: 90°W ~ 100°W**

| $T_{11}$ | $T_{11}-T_{13}$: 1 | 0 | 1 | 2 | 3 | 4 | 5 | 6 | 7 | 8 | 9 | 10 |
|---|---|---|---|---|---|---|---|---|---|---|---|---|
| 295 300 | | | | | | | | | | | | |
| 290 295 | | | 2 | 14 | 24 | 5 | | | | | | |
| 285 290 | | 11 | 97 | 134 | 43 | 9 | | | | | | |
| 280 285 | | 9 | 31 | 18 | 7 | 4 | | | | | | |
| 275 280 | | | 1 | | 2 | 3 | 4 | | | | | |
| 270 275 | | | | | 3 | 2 | | 1 | | | | |
| 265 270 | | | | | 3 | 1 | | | | | | |
| 260 265 | | | | 1 | 1 | | | | | | | |
| 256 260 | | | | | | | | | | | | |
| 250 255 | | | | | | | | | | | | |
| 245 250 | | | | | | | | | | | | |
| 240 245 | | | | | | | | | | | | |
| 235 240 | | | | | | | | | | | | |
| 230 235 | | | | | | | | | | | | |
| 225 230 | | | | | | | | | | | | |
| 220 225 | | | | | | | | | | | | |
| 215 220 | | | | | | | | | | | | |
| 210 215 | | | | | | | | | | | | |
| 205 210 | | | | | | | | | | | | |
| 200 205 | | | | | | | | | | | | |
| 195 200 | | | | | | | | | | | | |

b

Total frequency = 430
Cirrus = 1%

# FALL

**Latitude: 5°N ~ 5°S, Longitude: 100°E ~ 110°E**

| [illegible] | $T_{11}-T_{11}$: [illegible] | [illegible] | [illegible] | 2 | 3 | 4 | 5 | 6 | 7 | 8 | 9 | 10 |
|---|---|---|---|---|---|---|---|---|---|---|---|---|
| 295 300 | | | | | | 1 | | | | | | |
| 290 295 | | | | | | 3 | 3 | 3 | 3 | | | |
| 285 290 | | | | | | | 3 | 8 | 6 | | | |
| 280 285 | | | | | 1 | | 5 | 12 | 9 | 1 | | |
| 275 280 | | | | | 1 | 1 | 4 | 9 | 8 | | 1 | |
| 270 275 | | | | | | | 4 | 5 | 8 | 1 | | |
| 265 270 | | | | | | 3 | 2 | 6 | 5 | 2 | | |
| 260 265 | | | | | | 4 | 5 | 4 | 3 | 1 | 1 | 1 |
| 256 260 | | | | | | 2 | 1 | 1 | | 1 | | |
| 250 255 | | | | | 2 | 1 | 6 | 2 | 1 | | 1 | |
| 245 250 | | | | | 3 | 2 | 1 | 1 | 1 | | | |
| 240 245 | | | | | 2 | | 1 | | | | | |
| 235 240 | | | | | 3 | | | 1 | | 1 | | |
| 230 235 | | | | | 1 | 3 | | | | | | |
| 225 230 | | | | 1 | 2 | | 1 | | | | | |
| 220 225 | | | | 2 | 1 | | | | | | | |
| 215 220 | | | 2 | | 1 | | | | | | | |
| 210 215 | | | 1 | 1 | | | | | | | | |
| 205 210 | | | | | | | | | | | | |
| 200 205 | | | | | | | | | | | | |
| 195 200 | | | | | | | | | | | | |

c

Total frequency = 197
Cirrus = 59%

**Latitude: 5°N ~ 5°S, Longitude: 120°W ~ 130°W**

| $T_{11}$ | $T_{11}-T_{11}$: 1 | 0 | 1 | 2 | 3 | 4 | 5 | 6 | 7 | 8 | 9 | 10 |
|---|---|---|---|---|---|---|---|---|---|---|---|---|
| 295 ~ 300 | | | | | | | | | | | | |
| 290 ~ 295 | | | 4 | 89 | 46 | 2 | | | | | | |
| 285 ~ 290 | | | 19 | 58 | 12 | | | | | | | |
| 280 ~ 285 | | 1 | 6 | 2 | 3 | | | | | | | |
| 275 ~ 280 | | | | | | | | | | | | |
| 270 ~ 275 | | | | | | | | | | | | |
| 265 ~ 270 | | | | | | | | | | | | |
| 260 ~ 265 | | | | | | | | | | | | |
| 256 ~ 260 | | | | | | | | | | | | |
| 250 ~ 255 | | | | | | | | | | | | |
| 245 ~ 250 | | | | | | | | | | | | |
| 240 ~ 245 | | | | | | | | | | | | |
| 235 ~ 240 | | | | | | | | | | | | |
| 230 ~ 235 | | | | | | | | | | | | |
| 225 ~ 230 | | | | | | | | | | | | |
| 220 ~ 225 | | | | | | | | | | | | |
| 215 ~ 220 | | | | | | | | | | | | |
| 210 ~ 215 | | | | | | | | | | | | |
| 205 ~ 210 | | | | | | | | | | | | |
| 200 ~ 205 | | | | | | | | | | | | |
| 195 ~ 200 | | | | | | | | | | | | |

d

Total frequency = 242
Cirrus = 0%

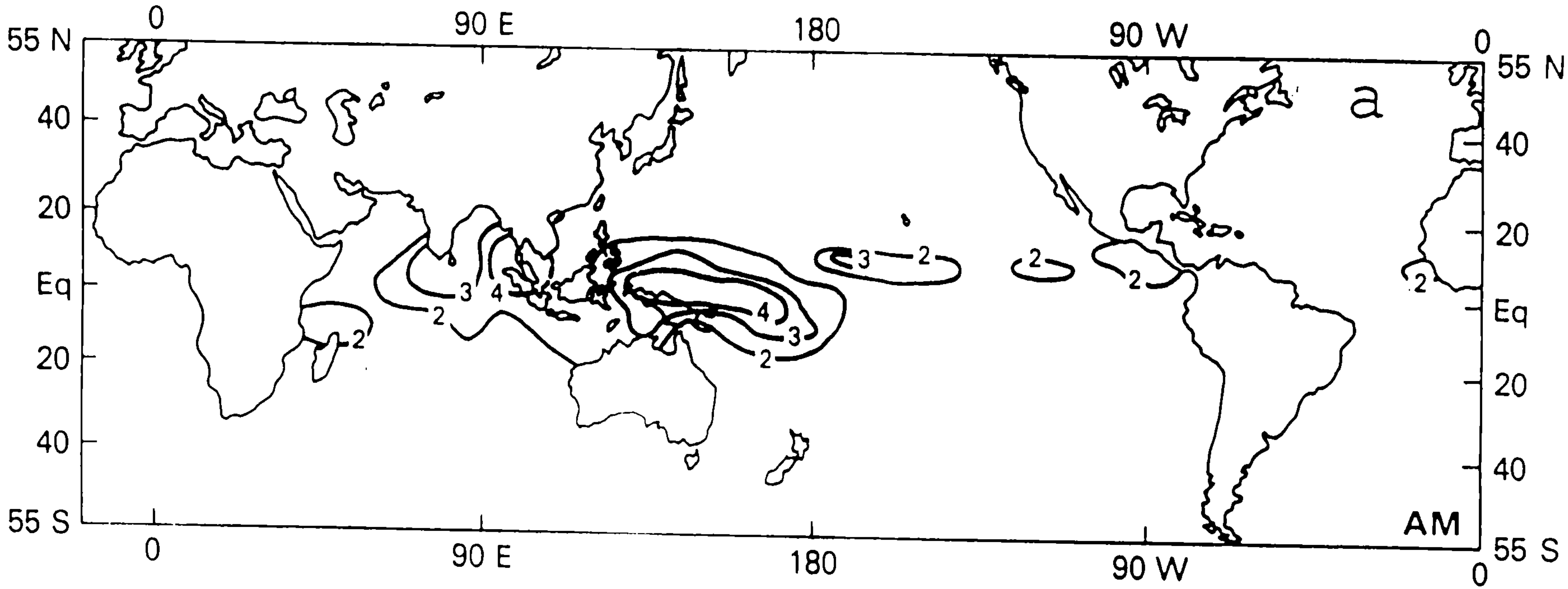


Fig. 7a

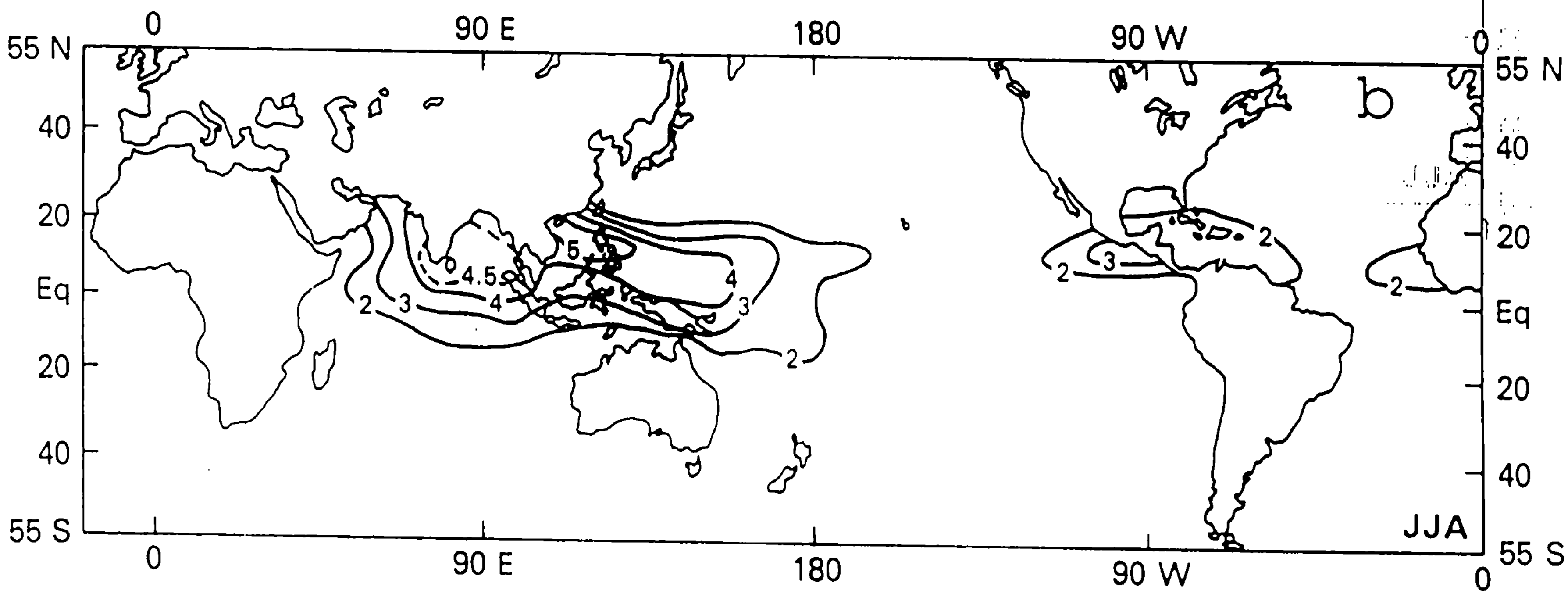


Fig. 7.

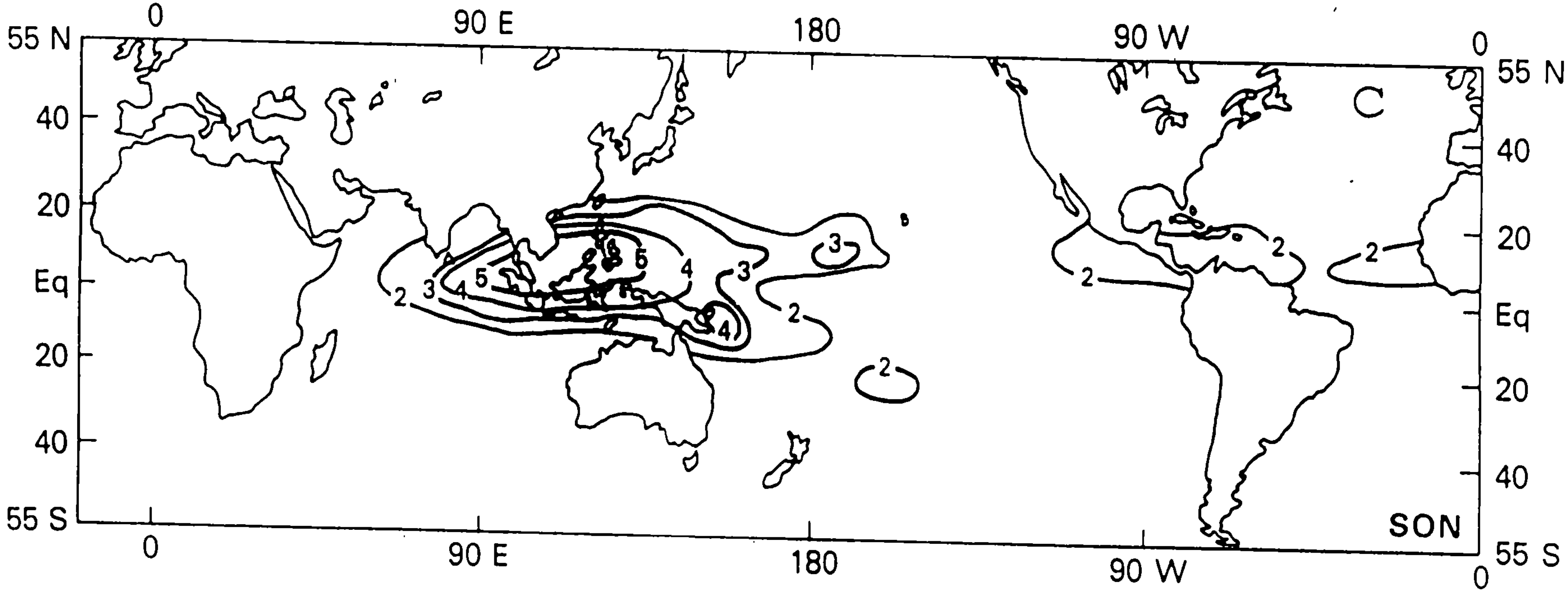


Fig. 7c

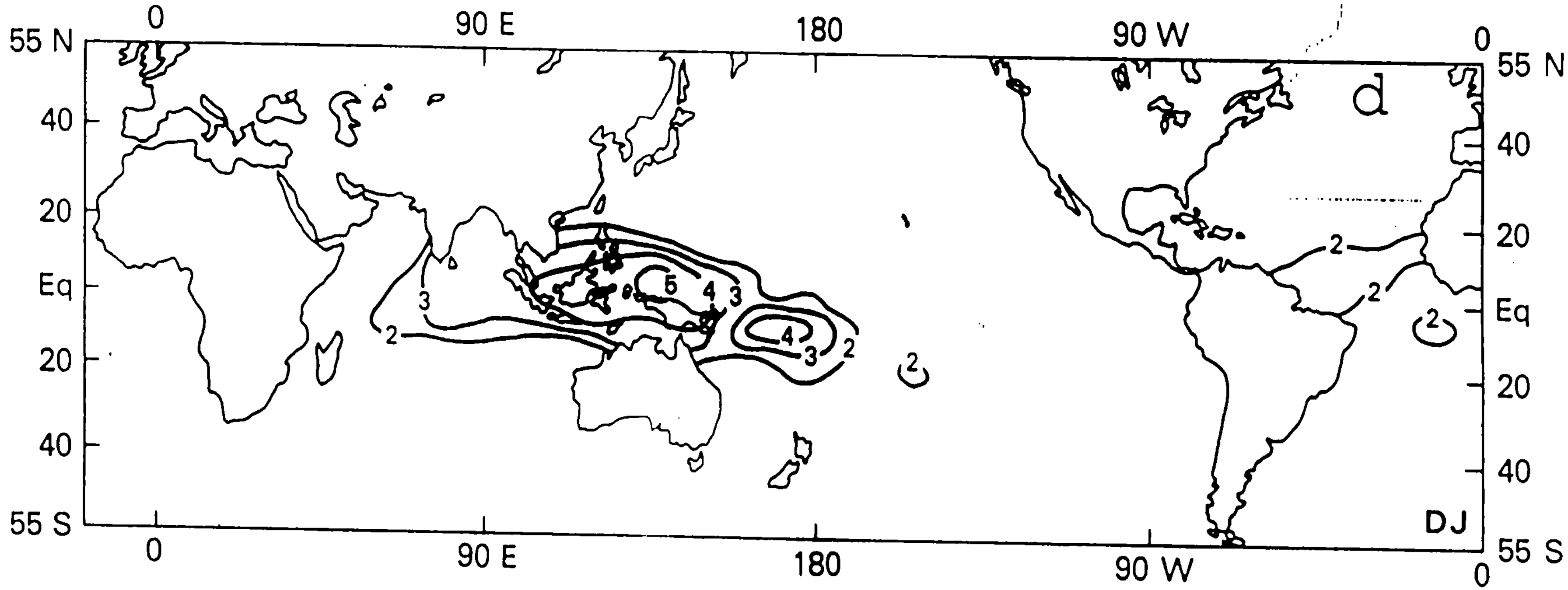


Fig. 7d

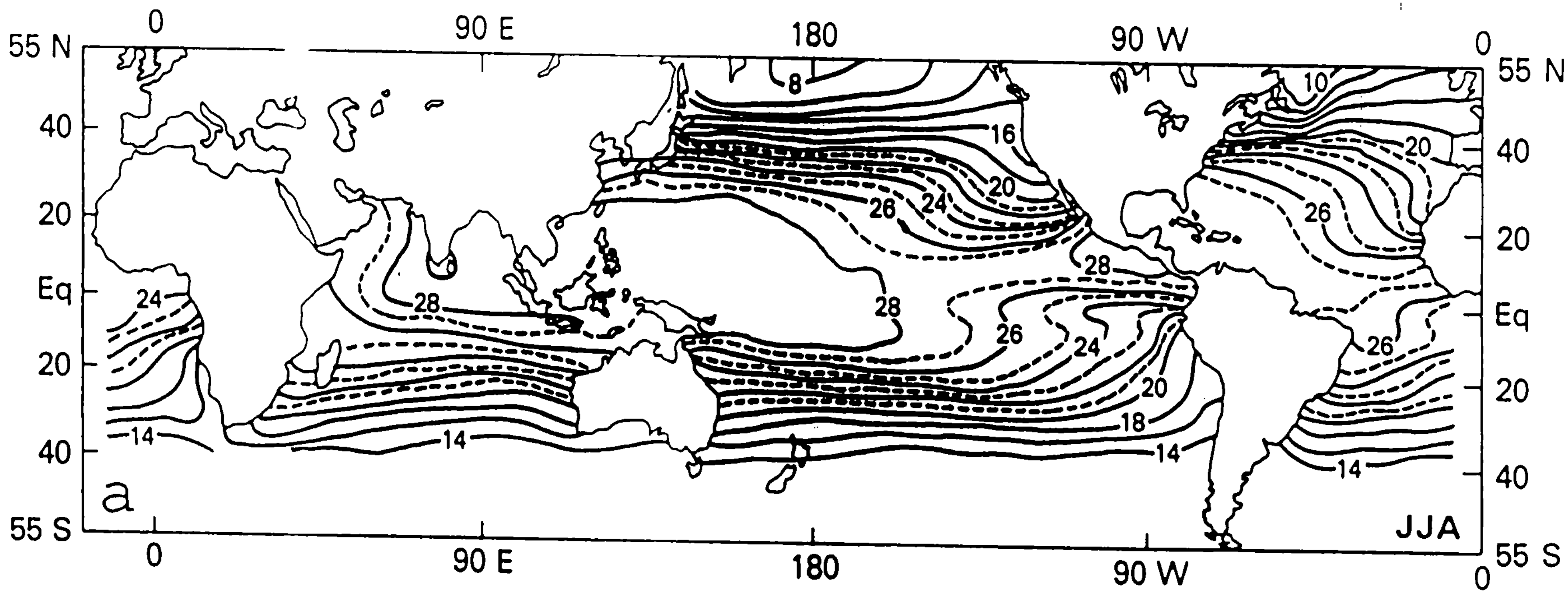
0
90 E
180
90 W
0
55 N
40
20
Eq
20
40
55 S
8
10
16
20
24
26
28
14
18
a
JJA

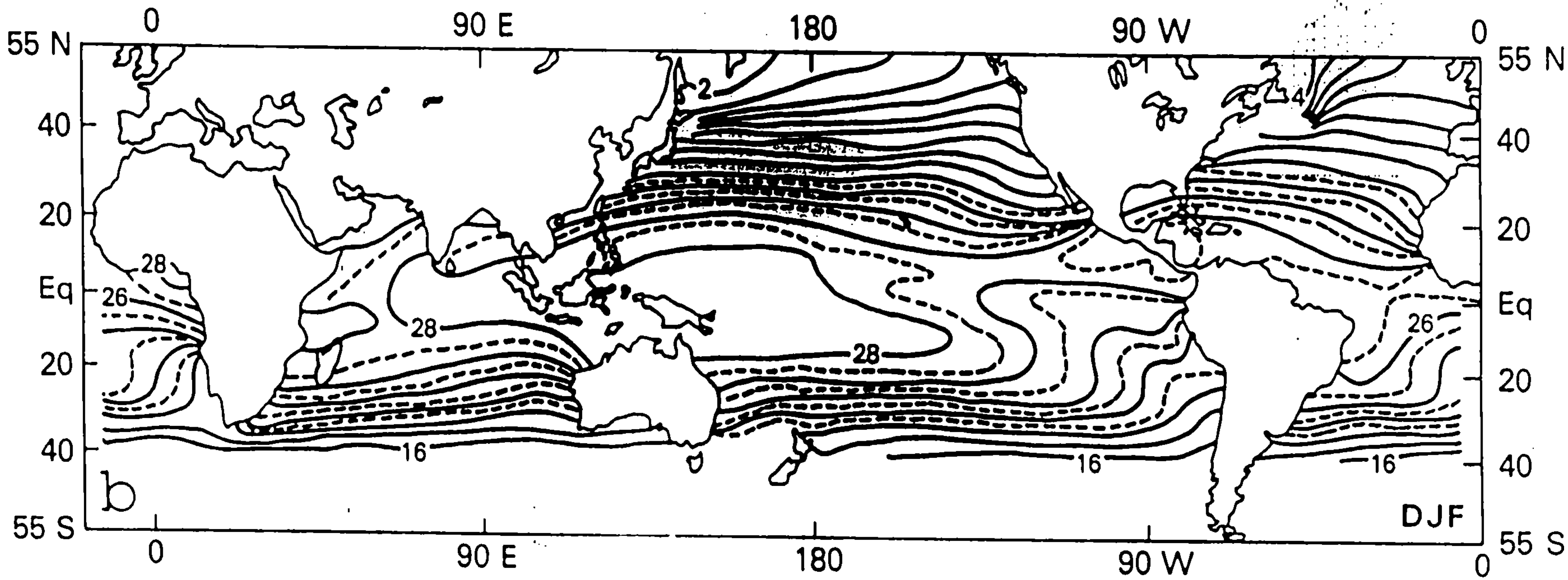


Fig. 8b

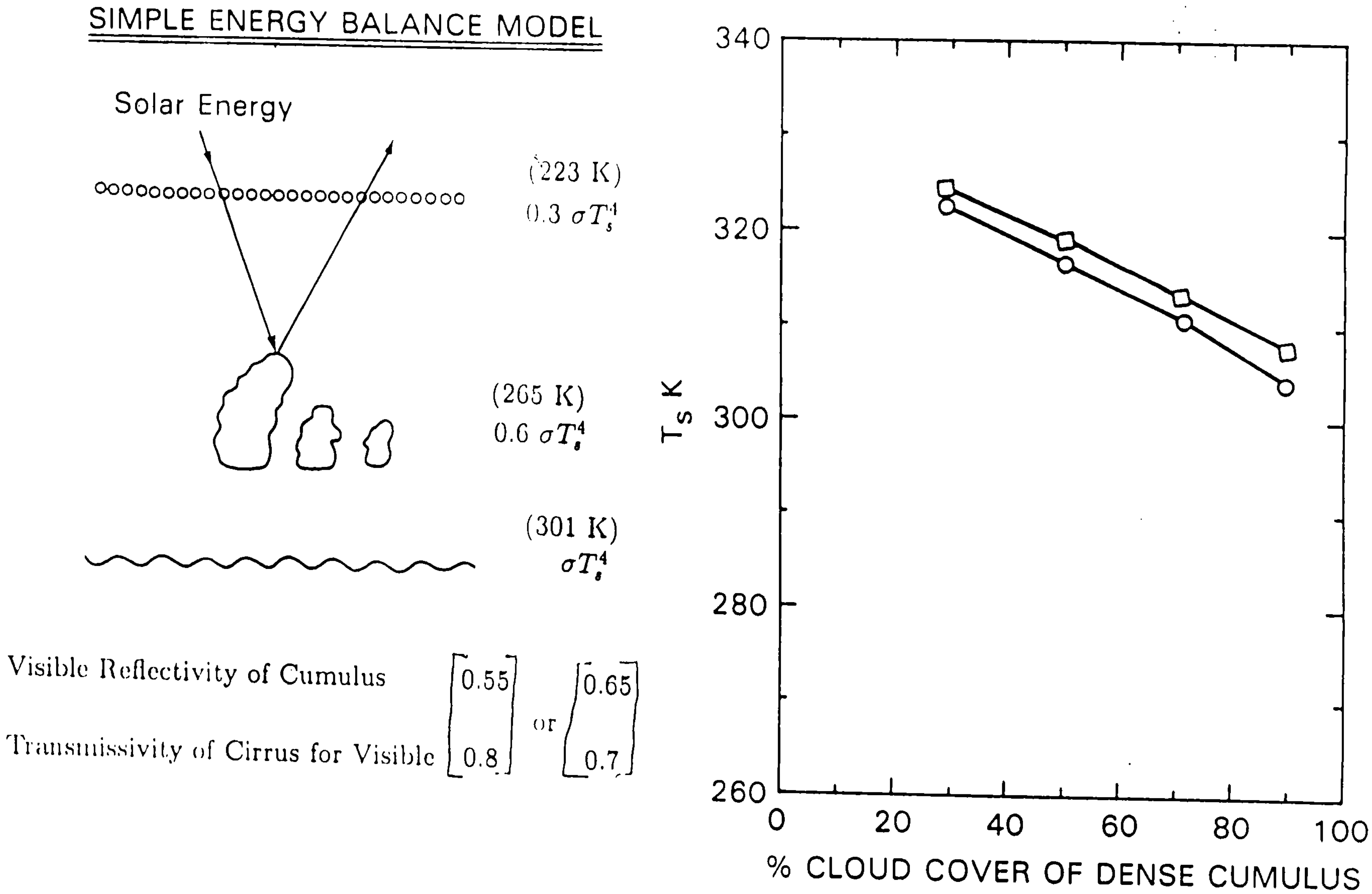
SIMPLE ENERGY BALANCE MODEL
Solar Energy
(223 K)
$0.3\ \sigma T_s^4$
(265 K)
$0.6\ \sigma T_s^4$
(301 K)
$\sigma T_s^4$
Visible Reflectivity of Cumulus
Transmissivity of Cirrus for Visible
0.55
0.8
or
0.65
0.7
$T_s$ K
340
320
300
280
260
0
20
40
60
80
100
% CLOUD COVER OF DENSE CUMULUS

Fig. 9

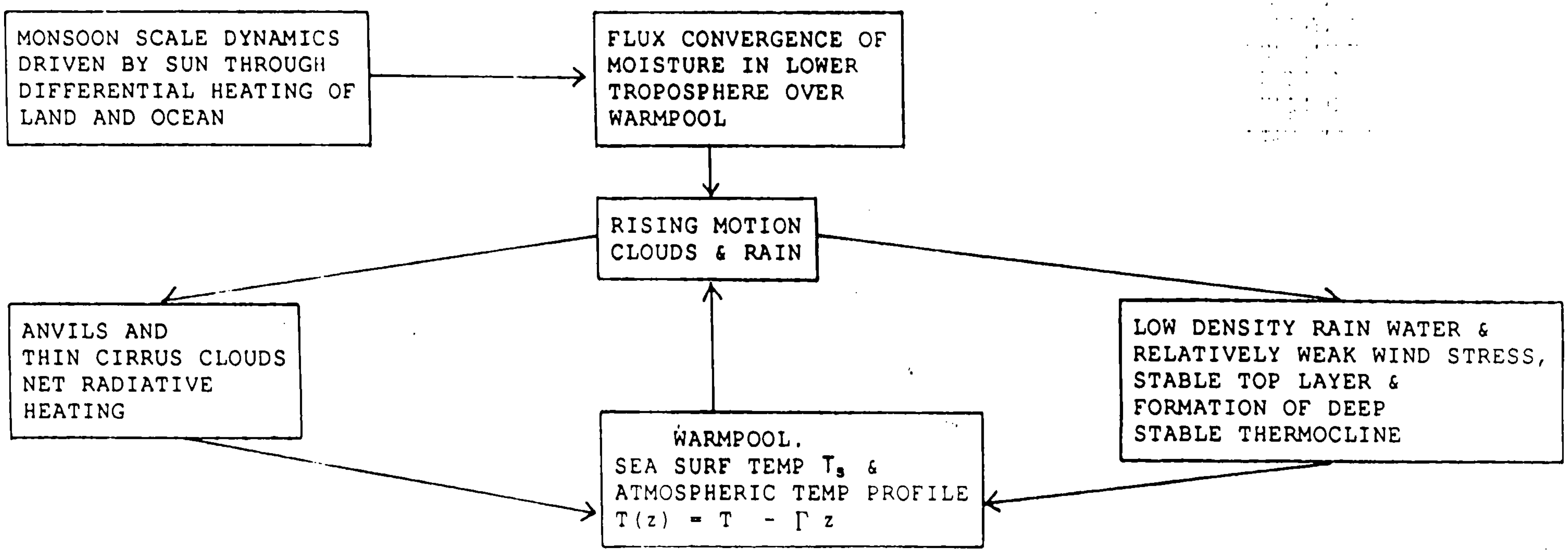
MONSOON SCALE DYNAMICS DRIVEN BY SUN THROUGH DIFFERENTIAL HEATING OF LAND AND OCEAN
FLUX CONVERGENCE OF MOISTURE IN LOWER TROPOSPHERE OVER WARMPOOL
RISING MOTION CLOUDS & RAIN
ANVILS AND THIN CIRRUS CLOUDS NET RADIATIVE HEATING
LOW DENSITY RAIN WATER & RELATIVELY WEAK WIND STRESS, STABLE TOP LAYER & FORMATION OF DEEP STABLE THERMOCLINE
WARMPOOL.
SEA SURF TEMP $T_s$ &
ATMOSPHERIC TEMP PROFILE
$T(z) = T - \Gamma z$

Fig. 10